STUDIES ON CRYSTAL GROWTH OF SOME PURE AND MIXED RARE-EARTH FUMARATES AND THEIR CHARACTERISTICS

THESIS

Submitted to the

UNIVERSITY OF KASHMIR

For the award of the degree of

DOCTOR OF PHILOSOPHY *in* PHYSICS

by

MAIRAJ UD DIN SHAH

Under the Supervision of

Dr. BASHARAT AHMAD WANT
Associate Professor
Department of Physics, University of Kashmir,
Hazratbal, Srinagar, 190006

May, 2015

Post Graduate Department of Physics, University of Kashmir, Srinagar.

Certificate

This is to certify that the thesis entitled "**Studies on crystal growth of some pure and mixed rare-earth fumarates and their characteristics**" submitted by ***Mairaj ud din Shah***, in partial fulfillment for the award of the **degree of Doctor of *Philosophy*** in ***Physics***, is the original research work carried out by him under my supervision and guidance. It is further certified that the thesis has not been submitted for the award of Ph.D or any other degree to this university or any other university and the scholar has attended the department for statutory period as required under rules.

Dr. Basharat Ahmad Want (*Supervisor*)

Prof. Manzoor Ahmad Malik (*Head of the Department*)

Acknowledgements

I am heartily thankful to the **Almighty Allah** for the abundant blessings and the special providence that came through his work, **Who** blessed me with knowledge and potential to plan my research work. I offer my humblest words of thanks to **His** most noble messenger **Muhammad** (S.A.W), who is forever, a torch of guidance and knowledge for all humanity. I would like to express my deep sense of gratitude and deepest appreciation to my supervisor, **Dr. Basharat Ahmad Want** (Associate Professor, Department of Physics, University of Kashmir, Srinagar) for his guidance, encouragement and support during the research. He has always been ready to offer his help, whenever needed. May Allah bless him Iman and prosperous life. (Aameen!).

I wish to thank all the scholars/group members of solid state research laboratory, particularly Miss Rubiya Samad, Mr. Zahoor Ahmad Bhat, Mr. Bilal Hamid Bhat, Mr. Feroz Ahmad Dar and Mr. Mairaj ud din Rather for being so supportive to me in difficult moments, their help in conducting experimental work and nice friendship.

A deep sense of appreciation goes towards all of my family for providing me with the endless love and support I needed to pursue and achieve my goals in life. Special appreciation goes to my son Shah Tavseef Mairaj for guiding me to use different softwares meant for research work. A very special thanks goes to my brother-in-law Prof. Dr. Yaseen Ahmad Shah (Principal S.P. College Srinagar), who motivated and encouraged me in pursuing the research programme under FIP programme.

I am highly indebted to **Prof. Manzoor Ahmad Malik** Head, Department of Physics, (University of Kashmir) for providing the necessary facilities in the department. I also extend my thanks to the whole teaching faculty of the department for their moral support.

I am also thankful to former Head, Department of Physics Prof. Farooq Ahmad, for his help and constant encouragement.

I also express gratitude to Syeed Shafiq Ahmad (Associate Professor Govt, Degree College Pulwama), Nadia Shah (Assistant Professor S.P.College Srinagar), Mr. Feroz Rafique (Research Scholar) and Parveez Ahmad Bhat (Assistant Professor) for their kind help.

I would fail in my duty if I do not acknowledge the moral support of all the scholars, library staff, non-teaching staff and Mr. Manzoor Ahmad Shah, formerly scientific officer of the Department of Physics University of Kashmir.

I am also highly thankful to the UGC, New Delhi and Department of Higher Education, Government of Jammu and Kashmir for providing and facilitating me the teacher fellowship from Govt; Degree College Pulwama. I would like to acknowledge the magnanimity, kind co-operation, encouragement and support of the Principal, teachers and management of Govt, Degree College Pulwama.

Mairaj ud-din Shah

Dedicated

To

My Parents

(At Whose Feet My Heaven Lies)

Preface

Crystal growth and its characterization has become valuable branch of science due to the growing demand of scientifically and technologically important crystals for different applications. Rare-earth based crystals of metal organic coordination compounds have an important role from both academic and technological point of view due to their outstanding physical, magnetic and luminescent properties. The compounds of rare-earths have also gained importance for their dielectric, ferroelectric, ferroelastic and conductivity behaviour. Due to the large applicability of rare-earth coordination compounds, it was thought worthwhile to investigate growth and characterization of tebium fumarate, gadolinium fumarate and mixed gadolinium-terbium fumarate heptahydrate single crystals for scientific investigations.

The work presented in this thesis was carried out at the Solid-State Research Laboratory, Department of Physics, University of Kashmir, Srinagar. The thesis entitled "**Studies on crystal growth of some pure and mixed rare-earth fumarates and their characteristics**" is a comprehensive report on the growth of single crystals of terbium, gadolinium and mixed gadolinium-terbium fumarate heptahydrates in hydro silica gel and their detailed characterization. It also includes the results of dielectric, ac conductivity, thermal, luminescent and magnetic moment measurements of the grown crystals. The thesis is divided into two sections, Section-A pertaining to growth and characterization of crystals, consists of four chapters and section-B including the physical properties of as-grown crystals consists of five chapters.

Section-A

Chapter- 1 gives a general introduction of the crystal growth of rare-earth coordination compounds. The chapter is subdivided into three sections with regard to the introduction of crystals, significance of co-ordination compounds and significance of the present work.

Chapter-2 gives the concept of crystallization with an overview of crystalization techniques in general and the gel growth technique in particular. In this chapter, nucleation in gels, gel structures, gelling mechanism, gel properties and different types of gel growth methods are briefly discussed. Apart from this, the advantages and disadvantages of gel growth technique are also incorporated.

Chapter-3 gives an overview of experimental techniques used for the characterization of samples, such as an Optical Electron Microscopy, Scanning Electron Microscopy (SEM), X-ray diffraction analysis (XRD), Carbon Hydrogen Nitrogen (CHN) analysis, Energy-Dispersive Analysis of X-rays (EDAX), Thermo-gravimetric analysis (TGA, DTA), Fourier Transform Infrared Spectroscopy (FTIR), Ultraviolet and Visible Spectroscopy (UV-Vis), Electric Impedance Spectroscopy, Photoluminescence (PL) and Vibrating Sample Magnetometery (VSM).

Chapter-4 describes the growth of terbium fumarate, gadolinium fumarate and mixed gadolinium-terbium fumarate heptahydrate single crystals by silica gel diffusion technique. A series of experiments are carried out for optimising the growth conditions for growing good quality single crystals. The effect of various growth parameters such as gel pH, gel density, concentration of reactants and effect of temperature on the growth kinetics are studied in detail.

Section-B

Chapter-5 describes the dependence of dielectric polarization on the frequency of applied field. An overview of dielectric dispersion with regard to different theories of dielectrics is also discussed in this chapter. The effect of frequency and temperature on the dielectric constant and ac conductivity of the grown materials is discussed. Also, a comparative study of dielectric and conductivity behaviour of pure and mixed rare-earth fumarate heptahydrate crystals is discussed in this chapter.

Chapter-6 describes a comparative study of thermo analytical behaviour of terbium, gadolinium and mixed gadolinium-terbium fumarate heptahydrate compounds. A non-isothermal kinetics of these compounds is also discussed in this chapter.

Chapter-7 gives UV-Vis and Photoluminescence measurements of terbium fumarate and mixed gadolinium-terbium fumarate heptahydrate crystals. The increase in photoluminescence of mixed rare-earth fumarate compound is also reported.

Chapter-8 describes a comparative study of magnetic susceptibility measurements of terbium fumarate, gadolinium fumarate and mixed gadolinium-terbium fumarate heptahydrate compounds. The diamagnetic correction of various molecules is also calculated by using Pascal's constants.

Chapter-9 describes a general conclusion of under taken work and its future scope.

The Bibliography of all the nine chapters is given at the end of the thesis.

List of publications

1. B. Want and M.D. Shah, Growth and characterization of terbium fumarate heptahydrate single crystals, J. Crystal Growth, 389, 39–46 (2014).

2. M.D.Shah and B. Want, Dielectric characteristics and thermal behaviour of terbium fumarate heptahydrate crystals, Current Applied Physics, 15, 64-70 (2015).

3. M.D.Shah and B. Want, Growth, characterization and dielectric studies of gadolinium fumarate heptahydrate single crystals Bull. Mater. Sci., 38, 73-81 (2015).

4. M.D.Shah and B. Want, Effect on luminescence of rare-earth Tb (III) by mixing of Gd (III) in a fumarate complex and intra-molecular energy transfer, Materials Science Poland. (Accepted) ISSN: 2083-1331 (Print) 2083-134X (Online).

5. M.D.Shah and B. Want, Dielectric and conducting behaviour of gadolinium-terbium fumarate heptahydrate crystals, Journal of Advanced Dielctrics. (Accepted) DOI: 10.1142/S2010135X15500204.

6. B.Want and M.D. Shah, Magnetic susceptibility measurements of pure and mixed gadolinium-terbium fumarate heptahydrate crystals (Communicated to journal of magnetism and magnetic materials).

List of papers presented at various conferences

1.	Growth and characterization of terbium fumarate heptahydrate single crystals	**J & K Science Congress in (2012)**
2.	Dielectric studies of terbium fumarate heptahydrate	**J & K Regional Science Congress in (2013)**
3.	Dielectric studies of pure and mixed rare-earth fumarate crystals	**National Seminar "Towards new horizons with interplay between physics and computer science" at Amar Singh College, Srinagar, J&K.**

Abstract

The overall aim of the work described in this thesis was to undertake the growth and characterization of pure and mixed rare-earth fumarates i.e. terbium fumarate, gadolinium fumarate and gadolinium-terbium fumarate heptahydrate single crystals. These crystals were grown by using silica gel diffusion technique. The effect of various growth parameters on the nucleation rate of these crystals was studied and was found in conformity with the classical nucleation theory. The grown crystals were characterized by different physico-chemical techniques of characterization. Powder X-ray diffraction pattern showed that the compounds are crystalline in nature. The single crystal X-ray diffraction results showed that terbium fumarate heptahydrate has monoclinic structure belonging to the space group $P2_1/n$. The cell parameters are a = 9.4495Å, b =14.6561Å, c =14.7272Å, $\alpha = \gamma = 90^o$ and $\beta = 91.318^o$. Well matching of d-values and the cell parameters of gadolinium fumarate and mixed gadolinium-terbium fumarate crystals with that of the terbium fumarate showed that the crystals grown in the present work are isomorphous to each other.

The comparative studies of thermal analysis and non isothermal kinetic measurements of the grown compounds were carried out. Mixed gadolinium-terbium fumarate crystals were found to be thermally more stable than the pure rare-earth fumarate crystals.

Dielectric and conductivity behaviour of the compounds were carried out. In general, the investigation based on measurements of the dependence of dielectric constant (ε'), dielectric loss (tanδ) as well as ac conductivity (σ_{ac}) of the crystals was studied as a function of applied frequency and temperature. The dielectric anomaly was found due to the dehydration of the compounds and not due to their ferroelectric phase transition. AC conductivity of the crystals obeyed Johnscher power law equation. UV-Vis and photoluminescence of the crystals were also carried out. From UV-Vis data, the band gap of the grown crystals was calculated and the spectra suggested the suitability of the crystals for laser use. The photoluminescent intensity of mixed fumarate complex was found to get enhanced than that of the pure terbium fumarate complex. From the magnetic susceptibility measurements, the experimental values of effective magnetic moments of the grown materials are in good agreement with the theoretical values of the free tripositive rare-earth ions.

Table of Contents

1. General Introduction 1

1.1 Introduction to crystals 1

1.2 Significance of co-ordination compounds 3

1.3 Significance of the present study 6

2. An overview of crystallization and crystal growth techniques 9

2.1 Introduction 9

2.2 Crystal growth techniques 10

2.2.1 Growth from solid phase 10

2.2.2 Growth from vapour phase 11

2.2.3 Growth from solution phase 11

2.3 Nucleation in gel 14

2.3.1 Classical theory of nucleation 16

2.3.2 Nucleation control in gel 18

2.3.3 Mechanism of gelling 19

2.4 Crystal growth methods in gels 20

2.4.1 Chemical reaction method 20

2.4.2 Chemical reduction method 22

2.4.3 Solubility reduction method 22

2.4.4 Electrolytic method 22

2.5 Crystal habit 23

2.6 Advantages and drawbacks of gel growth technique 23

3. Techniques of materials characterization- A brief review 25

3.1 Introduction 25

3.2. Characterization techniques 25

3.2.1 Optical microscopy 25

3.2.2 Scanning electron microscopy 26

3.2.3 Powder X-ray diffraction 26

3.2.4 Single crystal X-ray diffraction 27
3.2.5 Energy dispersive X-ray analysis 28
3.2.6 Carbon Nitrogen and Hydrogen analysis.....29
3.2.7 Thermal analysis.....29
3.2.8 Fourier transformation infra-red spectroscopy 30
3.2.9 Ultraviolet and Visible spectroscopy.....31
3.2.10 Photoluminescence spectroscopy 32
3.2.11 Vibrating sample magnetometery.....32
3.2.12 Electric impedance spectroscopy.....33
4. Growth and characterization of terbium, gadolinium and mixed gadolinium-terbium fumarate heptahydrate single crystals. 34
4.1 Introduction 34
4.2 Experimental Procedure 36
4.3 Nucleation rate of gel grown crystals.....37
4.3.1 Effect of various growth parameters on nucleation rate of terbium fumarate heptahydrate single crystals.....38
4.3.2 Effect of growth parameters on nucleation rate of gadolinium fumarate heptahydrate crystals 44
4.3.3 Effect of growth parameters on nucleation rate of mixed gadolinium-terbium fumarate heptahydrate single crystals 44
4.4 Super-saturation as the cause of nucleation 44
4.5 Characterization 47
4.5.1 General morphology 47
4.5.2 Powder X-ray diffraction results 50
4.5.3 Comparative study of X-ray diffraction results.....53
4.5.4 Single Crystal X-ray diffraction of terbium fumarate heptahydrate.....55
4.5.5 Elemental analysis 61
4.5.6 Thermal analysis.....63
4.5.7 FTIR spectroscopy.....68
Conclusions 71
5. Dielectric and conducting behaviour of terbium, gadolinium and mixed gadolinium-terbium fumarate heptahydrate single crystals.....73

5.1 Introduction 73

5.2 Dielectric polarization and its frequency dependence 74

5.3 Dielectric dispersion: An overview 76

5.4 Experimental procedure 80

5.5 Dielectric characteristics 81

5.5.1 Dependence of dielectric constant and dielectric loss on temperature 81

5.5.2. Dependence of dielectric constant and dielectric loss on frequency 87

5.6. Conducting behaviour 91

5.6.1. Temperature dependent ac conductivity 91

5.6.2. Frequency dependent ac conductivity 95

Conclusions 99

6. Thermal behaviour of terbium, gadolinium and mixed Gd-Tb fumarate heptahydrate single crystals 101

6.1 Introduction 101

6.2 Experimental Procedure 102

6.3 Results and discussions 102

6.3.1 Comparative study of thermal behaviour 102

6.4 Non–isothermal decomposition kinetics 104

6.4.1 Non-Isothermal decomposition kinetics of terbium fumarate crystals 108

6.4.2 Non-isothermal decomposition kinetics of gadolinium fumarate crystals 110

6.4.3 Non-isothermal decomposition kinetics of mixed Gd-Tb crystals 113

Conclusions 115

7. Luminescence properties of terbium and mixed Gd-Tb fumarate heptahydrate single crystals 117

7.1 Introduction 117

7.2 UV-Vis spectral analysis 119

7.2.1 UV-Vis spectral analysis of terbium fumarate 119

7.2.2 UV-Vis spectral analysis of gadolinium-terbium fumarate 120

7.3 Photoluminescence spectroscopy 121

7.3.1 Photoluminescence spectrum of terbium fumarate crystals 121
7.3.2 Photo luminescence spectrum of mixed Gd-Tb fumarate 123
7.4. Energy transfer mechanism 124
Conclusion 125
8. Magnetic susceptibility measurements of pure and mixed rare-earth fumarate crystals 126
8.1 Introduction 126
8.2 Experimental 127
8.3 Results and discussions 127
8.3.1 Theoritical magnetic moments of free tripositive rare-earth ions 127
8.3.2 Calculation of diamagnetic correction 129
8.3.3 Experimental magnetic moments of pure and mixed Gd-Tb fumarate single crystals 130
Conclusions 133
9. Summary and Future Scope 134
9.1 Summary of the present work 134
9.2 Future scope of the work 137
Bibliography 138

List of Figures

Figure 2.1: Free energy diagram for nucleation. 17

Figure 2.2: Gel structure 19

Figure 2.3: Schematic representation of single gel diffusion process. 21

Figure 2.4: Crystal growth by double gel diffusion method. 21

Figure 4.1: Variation of crystal count with upper reactant concentration 39

Figure 4.2: Variation of crystal count with the gel age. 39

Figure 4.3: Variation of crystal count with gel concentration at room temperature ... 40

Figure 4.4: Variation of crystal count with gel pH at room temperature 42

Figure 4.5: Photograph showing increase in nucleation rate with increase in pH for $5.0 \leq pH < 6.0$. 42

Figure 4.6: Photograph showing increase in nucleation rate with temperature. 43

Figure 4.7: Variation of crystal count with temperature at a gel pH of 5.0 43

Figure 4.8: (a) Optical micrograph (b) SEM micrograph at a magnification 65X. (c) SEM micrograph of (100) face at a magnification 8500X illustrating the two dimensional layered growth and (d) Schematic diagram illustrating the general morphology, of a typical terbium fumarate heptahydrate single crystal. 48

Figure 4.9: (a) SEM micrograph at a magnification 60X and (b) Schematic diagram depicting the general morphology, of a typical GFH single crystal. 49

Figure 4.10: SEM micrograph of a mixed Gd-Tb fumarate single crystal at a magnification 65X. 49

Figure 4.11: Optical micrograph of some typical single crystals of mixed Gd-Tb fumarate. 50

Figure 4.12: PXRD of terbium fumarate heptahydrate crystals with inset graph showing its phase matching with simulated pattern of samarium fumarate. 51

Figure 4.13: PXRD pattern of gadolinium fumarate single crystals. 52

Figure 4.14: PXRD pattern of mixed gadolinium-terbium fumarate crystals.....52

Figure 4.15: Assymmetric unit of terbium fumarate heptahydrate. 57

Figure 4.16: ORTEP diagram showing presence of water molecules in terbium fumarate heptahydrate crystals.....57

Figure 4.17: Unit cell of terbium fumarate heptahydrate crystal. 58

Figure 4.18: Packing diagram of terbium fumarate heptahydrate crystal. 59

Figure 4.19: Three distinct bonding modes of fumarate ligand in terbium fumarate. 59

Figure 4.20: EDAX spectrum of TFH crystals. 62

Figure 4.21: EDAX pattern of GFH crystals. 62

Figure 4.22: EDAX spectrum of GTFH crystals. 63

Figure 4.23: TGA/DTA curves of terbium fumarate heptahydrate crystals. 65

Figure 4.24: TGA/DTA curves of gadolinium fumarate heptahydrate crystals.....66

Figure 4.25: TGA/DTA curves of mixed Gd-Tb fumarate heptahydrate crystals. 66

Figure 4.26: FTIR spectrum of terbium fumarate heptahydrate single crystals. 69

Figure 4.27: FTIR spectrum of gadolinium fumarate heptahydrate single crystals....69

Figure 4.28: FTIR spectrum of mixed Gd-Tb fumarate heptahydrate single crystals.70

Figure 5.1: Variation of total polarizability with frequency 76

Figure 5.2: Variation of dielectric constant (ε') with temperature of terbium fumarate heptahydrate compound at the frequencies 1 kHz, 100 kHz and 3 MHz. 83

Figure 5.3: Variation of dielectric constant with temperature of gadolinium fumarate heptahydrate crystals at different frequencies and the inset of the graph showing this variation after dehydration of the compound at a frequency of 1kHz. 83

Figure 5.4: Variation of dielectric constant (ε') with temperature of GTF heptahydrate compound at the frequencies 1 kHz,100 kHz and 3 MHz. 84

Figure 5.5: Graph between dielectric constant (ε') and temperature of dehydrated compound of terbium fumarate at 1 kHz. 84

Figure 5.6: Graph between dielectric constant (ε') and temperature of dehydrated compound of mixed Gd-Tb fumarate at 1kHz. 85

Figure 5.7: Variation of dielectric loss (tanδ) with temperature of pure rare-earth (TFH) crystals at frequencies 100 kHz, 1MHz and 3MHz. 86

Figure 5.8: Variation of dielectric loss (tanδ) with temperature of mixed rare-earth fumarate (GTFH) crystals at frequencies 1kHz, 100kHz and 1MHz. 86

Figure 5.9: Variation of dielectric constant (ε') with frequency of pure TFH crystals with the inset graph showing variation of dielectric loss with frequency at temperatures 15 ^{o}C, 50 ^{o}C and 100 ^{o}C. 88

Figure 5.10: Variation of dielectric constant (ε') with frequency of pure GFH crystals with the inset graph between dielectric loss and frequency at temperatures 30 ^{o}C,70 ^{o}C and 100 ^{o}C. 88

Figure 5.11: Variation of dielectric constant (ε') and dielectric loss with frequency of mixed GTFH crystals at a temperatures 30 ^{o}C. 89

Figure 5.12: Variation of susceptibility with frequency of terbium fumarate heptahydrate crystals. 90

Figure 5.13: Variation of susceptibility with frequency of mixed GTFH crystals. 90

Figure 5.14: Variation of a.c conductivity with temperature of TFH crystals at frequencies 10 kHz and 100 kHz with the inset graph at 3 MHz. 92

Figure 5.15: Variation of ac conductivity of GFH crystals as a function of temperature at frequencies 1 kHz, 100 kHz and 3 MHz. 92

Figure 5.16: Variation of a.c conductivity with temperature of GTFH crystals at frequencies 10 kHz and 100 kHz with the inset graph at 3 MHz. 93

Figure 5.17: Graph between conductivity (σ_{ac}) and 1000/T of terbium fumarate heptahydrate crystals at 1 kHz. 94

Figure 5.18: Graph between conductivity (σ_{ac}) and 1000/T of mixed GTHF crystals at 1 kHz. 94

Figure 5.19: Variation of ac conductivity with temperature of the dehydrated sample of terbium fumarate heptahydrate at 1 kHz. 95

Figure 5.20: Graph between conductivity ($\sigma_{a.c}$) and frequency (ω) of terbium fumarate heptahydrate crystals at 50 ^{o}C.....97

Figure 5.21: Variation of ac conductivity with frequency of TFH crystals at 50 ^{o}C. .97

Figure 5.22: Variation of ac conductivity with frequency of GFH at 50 ^{o}C**……...**98

Figure 5.23: Variation of ac conductivity with frequency of mixed GTFH crystals at 50 ^{o}C.....98

Figure 5.24: Variation of ac conductivity with frequency of mixed GTFH crystals at 50 ^{o}C.....99

Figure 6.1: XRD pattern of terbium oxide (Tb_2O_3). 104

Figure 6.2: Arrhenius plot of the best fitting of dehydration step (100- 150 ^{o}C) of terbium fumarate crystals.....109

Figure 6.3: Arrhenius plot of the best fitting of decomposition step (410- 650 ^{o}C) of terbium fumarate crystals.....110

Figure 6.4: Arrhenius plot of the best fitting of dehydration step (100- 150 ^{o}C) of gadolinium fumarate crystals.....112

Figure 6.5: Arrhenius plot of the best fitting of decomposition step (420- 650 ^{o}C) of gadolinium fumarate crystals.....112

Figure 6.6: Arrhenius plot of the best fitting of dehydration step (100- 150 ^{o}C) of mixed gadolinium-terbium fumarate crystals 113

Figure 6.7: Arrhenius plot of the best fitting of decomposition step (450- 700 ^{o}C) of mixed gadolinium-terbium fumarate crystals. 115

Figure 7.1: UV-Vis spectrum of TFH crystals. 120

Figure 7.2: UV-Vis spectrum of mixed GTFH crystals. 121

Figure 7.3: Photo luminescence spectra of terbium fumarate crystals.....122

Figure 7.4: Photoluminescene spectra of mixed GTFH crystals.....123

Figure 8.1: Graph between molar susceptibility and magnetizing field of GFH, TFH and GTFH single crystals.....133

List of Tables

Table 4.1: The effect of different parameters on the nucleation kinetics of gadolinium fumarate heptahydrate single crystals 45

Table 4.2: Observed d-values, 2θ values and miller indices from X-ray diffraction data of pure and mixed rare-earth fumarate heptahydrate crystals. 54

Table 4.3: Lattice parameters of TFH, GFH and GTFH single crystals 55

Table 4.4**:** Selected bond lengths of terbium fumarate single crystals.....56

Table 4.5: Crystal structure and refinement data for TFH single crystals. 60

Table 4.6: Comparative quantitative EDAX data of TFH, GFH and GTFH crystals. 61

Table 4.7: CHN analysis of TFH, GFH and GTFH crystals. 63

Table 4.8: FTIR data of pure and mixed fumarate crystals.....70

Table 6.1: Thermal analysis of pure and mixed rare-earth fumarate crystals 103

Table 6.2: Solid-state rate expressions for different reaction models 107

Table 6.3: Kinetic and statistical parameters values for the analysed models of terbium fumarate heptahydrate from TG experiment 108

Table 6.4: Kinetic and statistical parameters values for the analysed models of terbium fumarate heptahydrate from TG experiment 111

Table 6.5: Kinetic and statistical parameters for the analysed models of mixed GdTb fumarate heptahydrate from TG experiment.....114

Table 8.1: Theoretical magnetic moment of tripositive rare-earth ions 128

Table 8.2: Representative Pascal constants.....129

Table 8.3 Diamagnetic corrections of grown compounds……129

Table 8.4: Magnetic susceptibility measurements ……131

Table 8.5: Molar susceptibility / magnetic moments of pure and mixed crystals.....132

CHAPTER-1

General Introduction

1.1 Introduction to crystals

Matter consisting of one or more elements and their chemical compounds, can exist in nature in solid, liquid or gaseous states. The crystalline solids have a regular and periodic arrangement of atoms or molecules. The energy released during the formation of an ordered structure is more than that of the energy released during the formation of disordered structure. The crystalline state is, therefore, a low energy state and is preferred by most of the solids. Crystals are the vital pillars of the world of modern technology [1, 2]. For the technological importance the crystals with quality, purity, and defect-free nature is a prerequisite. It has attracted human civilization from prehistoric times owing to their beauty and rarity. The crystals have much importance in photonic industry, electronic industry or optical fibre communications. The ability to grow good quality crystals has become an essential criterion for the competitiveness of nations. The dimensions of the crystals cover a wide range from micrometer up to millimetre in ceramics and thin film arrangements and centimetre scale in electronics and optics and in special cases up to meter scale in silicon single crystals, natural ice and quartz crystals.

Crystal growth includes the systematic study of the growth and properties of the crystals. It can be both natural as well as artificial. A number of crystals of different variety in the crust of earth are grown in Mother Nature by freezing the molten state. These crystals include diamond, quartz and some precious stones. Some other crystals such as the ice crystals can be formed directly from a gas (water vapours) without passing through a liquid state. During the eruption of gases around volcanoes some mineral substances in the form of sulphur and ammonium chloride crystals are formed. The crystal growth is certainly an interdisciplinary subject. It covers the collaboration of the people from physics, chemistry, materials science, metallurgy,

chemical engineering, crystallography, mineralogy, etc. Since the growth processes for the crystallization of salt and sugar has been practicing since 1500 BC, therefore, the growth can be treated as an ancient scientific activity. Their large-scale applications for devices have been realized only from the last quarter of 19^{th} century. Today, the crystal growth has become a well advanced technique and does not remain the phenomena confined to nature only. Moreover, the crystals that do not grow in nature can be grown in laboratory for scientific and technological use. Now as far as Gibb's phase equilibrium concept is concerned, some driving force is required for the growth of crystals to occur. The conditions of a system change in accordance with the laws of thermodynamics in such a manner that the free energy in the whole of the system decreases. A decrease in free energy (driving force) associated with the crystallization process works to promote the ordered arrangement of atoms or molecules in the form of the growth of crystals. Basically, crystal growth is a delicate process of re-arranging the units of a substance such as atoms, molecules, ions or molecular assemblies into a regular three dimensional periodic arrays. However, the arrangement of perfect regularity has never been found in real crystals because of the presence of different kinds of local disorder and long-range imperfections such as dislocations. The field of crystal growth being an inter-disciplinary subject involves a variety of research fields. It is a three tier process i.e. (i) to grow good quality single crystals (ii) to study their physical and structural characteristics and (iii) to find their applications in science and technology. For the history of crystal growth, one can get the useful information from the works of *Scheel* [3, 4].

In recent years, the different growth and characterization techniques have advanced much. The formations of some materials of different sizes which are technologically important have been found. As such, the growth covers the crystals from bulk to small and even to fine, ultrafine, and nano-scale sizes. The concept of size becomes even more important with the progress achieved in nanotechnology in which the size effect explains the changes in the physical properties of crystalline materials. The process of characterization has become an important part of crystal growth for knowing their properties. Therefore, the characteristics of the materials can be found by using different characterization techniques, as only one characterization does not give the complete understanding of the materials. The crystalline solids may be categorised into single crystals and polycrystalline solids. The crystals, in which

the atomic arrays are periodic in three dimensions with repeated distances are called the single crystals. The materials consisting of an aggregate number of small crystallites with random orientations separated by well defined boundaries are polycrystalline in nature. It is rather more difficult to grow a single crystal than a poly-crystalline material and for this an extra effort is justified to achieve the outstanding advantages of single crystals. The reason for growing single crystals lies in the fact that many physical properties of solids are complicated or obscured by the effect of grain boundaries. Therefore, there has been always a requirement of good quality crystals for various applications. Good quality single crystals are essential for a variety of scientific and commercial purposes. In the modern world, there is a great demand for good quality single crystals in every branch of science and technology because many sophisticated instruments use different types of crystals, either as sensors or detectors.

After the crystal growth with tailored physics and chemistry it becomes necessary to do their characterization with more advanced instruments such that their conversion into useful devices play vital role in science and technology. In the present study, the growth of pure and mixed rare-earth coordination compounds (rare-earth fumarate single crystals) was carried out by a simple gel diffusion technique. The grown crystals were then characterized by various characterization techniques and some of their physical properties were studied. Before highlighting the significance of rare-earth fumarates it is worthwhile to throw some light on the significance of co-ordination compounds.

1.2 Significance of co-ordination compounds

Metal-organic coordination compounds consist of metal ions coordinated to organic linkers in the form of one-, two- or three dimensional structures [5]. The pores created within these structures make them ideal for uses such as catalysis, ion exchange, gas adsorption and separations. The choice of metal and the organic linker dictates the structure and hence properties of these compounds. In principle, through the wide choice of metal and an infinite choice and design of ligands, different structural, magnetic, electrical, optical, and catalytic properties may be incorporated into the co-ordination compounds. Since early 1990s, the research in the materials with polymeric structures with metal ions and organic bridging ligands has increased much

[6]. The rich possibility of new material structures and properties offered by these coordination compounds is reported in the literature [7-9]. The advantage of a metal-organic hybrid system is the structural variability and tenability as the compounds can be grown from both inorganic and organic building blocks such as metal ions and organic ligands. For the growth of metal-organic co-ordination compounds, carboxylates are used as one of the most common types of linkers. Carboxylates are considered to be hard ligands which form strong bonds with hard metal centres. In addition to transition metals, there are also numerous examples where carboxylates coordinate to lanthanide metals, with coordination numbers typically between eight and twelve. These linkers may be classified in accordance with the number of donor atoms they contain. A monodentate ligand donates a single electron pair and a bidentate ligand donates two electron pairs to the metal ion.

As far as the physical properties of metal-organic co-ordination compounds are concerned, their unusual dielectric, ferroelectric and second order non-linear optical (NLO) properties are currently considered as one of the important issues [10, 11]. These properties find applications in the areas of optical communication, signal processing, light modulators, random access memories and switch-able NLO devices. Ferroelectric and multiferroic behaviour has also been reported recently by many researchers in metal-organic compounds [12-15]. Recently, another potential property of metal organic coordination compounds, conductivity behaviour and in particular proton conductivity has begun receiving attention. This attention comes in part from fundamental scientific interest in ionic conductivity [16, 17].

In the class of metal-organic coordination compounds, the rare-earth coordination compounds are potential candidates which besides showing ferroelectric properties have the ability to incorporate both photoluminescent centers and magnetic properties, thus, making them ideal for developing new multifunctional materials [18-20]. They find wide applications such as in high temperature superconductors, lasers, high strength permanent magnets etc [21]. An important modification in structural and magnetic properties can be obtained in the co-ordination compounds by the addition of small amount of larger ions such as rare-earth ions in them [22]. The photoluminescent properties of rare-earth compounds have been fascinating researchers for decades [23-27]. The important thing to be noted is that the emission colour depends on the rare-earth ion and is highly independent of the environment of

a given lanthanide ion. So, the rare-earth compounds can be meant for promising light-emitting materials. For example, the devices emitting blue light are based on Tm compounds [28], the devices emitting reddish-orange are based on Sm compounds [29, 30], the devices emitting white are based on Dy compounds [31], and the devices emitting near-infrared are based on Er [32], Nd [33], and Yb [34] compounds. The metal organic coordination compounds of rare-earths have been expected to show some new properties for the functional materials in contrast to those simple inorganic coordination compounds. For example, some compounds containing Eu or other rare-earth ions can absorb excitation energies due to the co-ordinated ligands, and the energy transfer process from the ligand will excite rare-earth-ions to give the anticipated luminescence emission [35]. The luminescence in the visible domain has been reported as a result of an energy transfer between the ligand and the rare-earth ion [36, 37]. The near-infrared (NIR) luminescence studies from lanthanide ions have been greatly influenced by two significant applications for telecommunication and imaging of biomedical assays due to the development of optical fibers [38- 43]. Among the rare-earth compounds, rare-earth oxides are interesting materials for their significant physical and chemical properties [44, 45]. The most important functional materials based on rare-earth oxides are phosphors [46], catalysts [47] etc. The oxides of mixed rare-earth coordination compounds constitute a wide and very important class of materials due to their huge technological significance in several fields like optical [48] and superconductive applications [49], as well as for solid oxide fuel cells [50, 51].

As far as the theoretical investigations of metal-organic coordination compounds are concerned, the structural, electronic and magnetic properties of two dimensional metal organic coordination networks have been studied by abinitio methods like density functional theory (DFT) calculations [52]. For isnstance, lattice dynamics of metal organic framework has been investigated by first principles calculations [53]. The study of dipole layer formation at the metal-organic interface using first principles DFT calculations is also reported in the literature [54]. The first principle theoretical investigation of spin-polarized quantum transport in organic magnetic tunnel junction is reported [55], in which two different magnetic tunnel junctions are formed by sandwitching the organic radicals between two Ni-electrodes. On the basis of DFT calculations, existence of linear magnetism in the metal organic

framework materials is also reported [56]. Exotic magnetic properties have received much attention in experimental and theoretical studies [57-59].

1.3 Significance of the present study

Keeping in view the physical properties of rare-earth coordination compounds it was thought worth while to study the growth and characterization of pure and mixed rare-earth fumarates. The crystals were grown by a very simple silica gel technique. The grown crystals were found to be thermally more stable than transition metal compounds and were found to have the ability for developing new multifunctional materials. Since the choice of metal and the linker dictates the structure and the properties of the compounds, therefore, in the present study, fumaric acid was used as a ligand for the growth of pure and mixed rare-earth co-ordination compounds. The dicarboxylate groups of fumaric acid can act as both monodentate and multidentate ligands. In the present study, fumaric acid acted as mono and bidentate ligand which can allocate as much donor atoms as possible to facilitate a high degree of chelatization or bridiging with the metal ions and can be used to achieve luminescence quenching. A study of literarture reveals that the dicarboxylates of rare-earth and transition metals have emerged as an important class of materials possessing novel properties such as magnetic, optical and electrical conductivity [60-62]. Besides, the fumaric acid as well as its isomer, maleic acid, have been used for the production of polymers and in the construction of 3D framework structures [63-66]. Some of the fumarate compounds have shown to exibit luminescent [64], magnetic [67] and dielectric properties [68]. In past few years, there has been a considerable interest in growing the coordination compounds of mixed metals. In principle, such materials might exhibit novel physical properties such as protonic conductivity, ferroelectricity, luminescence and interesting magnetic behaviour resulting from interactions between two different magnetic elements [69-72].

So far as Eu^{3+} and Tb^{3+} ions are concerned, a class of efficient light conversion molecular devices (LCMD) has been formed by the compounds of these ions. These compounds contain one or more ligands which can absorb strongly in the near UV region and were first invoked by Wiessman [73] to describe the strong luminescence of certain organo-europium compounds. Later on, such a phenomenon was observed and studied by several other authors [74-76]. In the present study, fumaric acid which

was used as an organic ligand has also strong absorption band in it. Therefore, more light can be absorbed by it than by the lanthanide ion itself, the energy absorbed by the ligand can effectively transfer to Tb^{3+}, thus the luminescence efficiency of Tb^{3+} ions is enhanced [77]. The ligand to metal ion (Tb^{3+}) energy transfer can take place by the antenna effect as also reported in the literature [36, 37]. The intensity of energy transfer could increase manifold in case of hetero lanthanide compounds. As such, in the present study, mixed gadolinium-terbium fumarate heptahydrate was grown to improve terbium emission. In this way second rare-earth ions are expected to be introduced into the compounds and more luminescent materials could be obtained. The maximum transmission of the grown crystals in their visible part of the spectrum suggests their suitability for laser and luminescent materials. For the grown materials, the maximum absorption shown near-UV range was observed and therefore, for the physics point of view, their band gap energy was calculated.

As far as the dielectric study of the grown crystals is concerned, it is an important part of materials characterization, because it does not only throw light on the materials behaviour under the influence of applied electric field but also on its applications. The crystals grown in the present study have shown dielectric anomaly with temperature. Torres et al [78] have observed two phase transitions in the cadmium tartrate crystals, one due to structural changes and the other due to loss of water molecules. Very interestingly, some metal organic frame works that contain interconnected nanopores or tunnels where movable polar molecules are loosely bound have reported to show interesting dielectric behaviour [79, 80]. The dielectric constant and dissipation factor of a material is one of the key parameters for device design in nearly all fields of modern electronics, particularly for the engineers in their design of microelectronic equipments. The physicists, on the other hand, are more interested in the microscopic processes responsible for the dielectric relaxation. For studying the polymer structure, the study of dielectric constant and dielectric loss factor, as a function of temperature and frequencies is one of the most convenient and sensitive methods [81]. The dielectric properties (dielectric constant and dielectric loss) of a number of polymers have been investigated in last two decades [82-87]. In the field of opto-electronics and micro-electronics, very recently, a great deal of interest has been shown in the study of the dielectric and conduction behaviour of materials [88-90].

During the last few years, a number of efforts were made by researchers to find out new solids with high ionic conductivity for industrial applications, such as solid state batteries, fuel cells, sensors, etc [91]. The materials grown in the present work in addition to dielectric behaviour have also shown protonic conductivity. The ac conductivity of as-grown crystals obey the Jonscher's power law relation; $\sigma(\omega) = \sigma_o + A\omega^s$, with the temperature dependent power exponent $s < 1$, [92]. As far as the electrical conductivity in solids is concerned, there are generally two types of carries: ions and electrons. Ions are relatively massive and their transport is often described by a "hopping" mechanism of the ion from site to site. The incorporation of carboxylic, sulfonic, or phosphonic acid species act as channel-accessible functionalities on framework linkers [93]. Owing to the use of electrolyte for low and intermediate temperature fuel cells, proton conducting materials are currently attracting significant interest. The proton being the only ion, may be expected to form and be mobile in molecular organic solids and may play an important role in intramolecular biological processes. The direct application of solid state proton conduction occurs in the situations where there is a requirement to transmit hydrogen across some intervening barrier. Such a phenomenon occurs in fuel-cell technology with $H_2 \mid O_2$ cells where the materials with good proton-conducting ability, however, blocking the electrons and insoluble in water, would be of great value [94]. The literature survey unfolds the proton transfer in photosynthesis, where a primary process involves proton liberation and migration across a membrane in a number of specific biological processes [95-97].

The magnetic properties of the rare-earth metals can be understood in the angular momenta of the 4f level of the atoms. The magnetic properties of the rare-earth metal ions are given by the ground state; therefore, their magnetic moments are essentially not influenced by their chemical environment. As for as the crystals grown in the present work are concerned, their magnetic susceptibility was found to be consistent with many lanthanide complexes as reported in the literature [98-101].

In the present work, growth and characterization of pure and mixed rare-earth fumarate heptahydrate single crystals is reported. The crystals grown in the present work have shown dielectric, conducting behaviour, good thermal stability, non-isothermal kinetics, magnetic and optical behaviour which are being discussed in different chapters of the thesis.

CHAPTER- 2

An overview of crystallization and crystal growth techniques

2.1 Introduction

Crystal growth is either a homogeneous or heterogeneous chemical process involving solid, liquid or gas, whether individually or together, to form a homogeneous solid substance with three dimensional atomic arrangements. For the growth of crystals, some driving force is required and therefore a number of techniques have been developed and employed for it. The conditions in any given system change according to the laws of thermodynamics in such a manner that the free energy in the whole of the system decreases. As a result of decrease in free energy associated with the crystallization process arrangement of atoms or molecules is promoted in the form of the growth of crystals. The difference $\Delta \mu = \mu_m - \mu_c$, between the chemical potential μ_m of a melt, solution, or a vapour phase (the growth medium) and the chemical potential μ_c of the crystalline phase becomes a driving force for the crystal growth.

If the growth medium is a melt, the molten and crystalline phases co-exist in a stable state if the system is at the melting point T_m. And, if the temperature falls below T_m, crystals begin to grow. Thus, the level of super cooling $\Delta T = T_m - T$, becomes the driving force for the crystals to grow. The relationship between the level of super cooling ΔT and Δ_μ can be expressed as follows:

$$\Delta \mu = L \Delta T / T_m \qquad (2.1)$$

Here, L is the latent heat of melting.

In case, where the growth medium is a vapour, the crystals will grow when the vapour pressure p is higher than the equilibrium or saturated vapour pressure p_e, and then the level of supersaturation $\sigma = (p - p_e) / p_e$ becomes the driving force for the crystal

growth. The difference in chemical potential between the vapour phase and the crystal phase based on vapour pressure can be expressed as follows:

$$\Delta \mu = k\ T \log (p/p_e) \qquad (2.2)$$

The relationship between $\Delta \mu$ and the level of supersaturation σ can be expressed as follows:

$$\Delta \mu = k\ T \log (1+ \sigma) \approx k\ T\ \sigma \qquad (2.3)$$

Here, k is Boltzmann's constant.

When the growth medium is a solution, the threshold concentration of solutes that can be dissolved into the liquid is used as the criterion. The level of supersaturation $\sigma = (C - C_e) / C_e$, can be defined as the driving force, where C_e is the concentration of saturated solution and C is the actual solute concentration. The relationship of the chemical potential differences between the solution phase and the crystal phase can be expressed as follows:

$$\Delta \mu = k\ T \log (C / C_e) \qquad (2.4)$$

$$\Delta \mu = k\ T \log (1+ \sigma) \approx k\ T\ \sigma \qquad (2.5)$$

For a typical crystal growth experiment, the supersaturation σ becomes positive by lowering the system temperature to decrease the concentration C_e of the saturated solution instead of increasing the concentration C.

2.2 Crystal growth techniques

Different methods of crystal growth classified on the basis of their phase transformation [102-104], are as follows:

Growth from solid phase involves solid-solid phase transformation.

Growth from melt phase involves liquid-solid phase transformation.

Growth from vapour phase involves gas-solid phase transformation.

Growth from solution phase involves liquid-solid phase transformation.

2.2.1 Growth from solid phase

In this technique, the single crystals can be grown from the polycrystalline mass of a particular matter. Normally, the straining of the material and its subsequent annealing is done for crystallization. The large sized metallic crystals have been grown by this method [105]. The main advantage of this technique is that the growth can take place

at a temperature without the presence of any additional component. But, it is difficult to control nucleation as the growth takes place in the solids where the density of nucleation sites is high.

2.2.2 Growth from vapour phase

This technique of crystal growth is usually employed for the materials of which suitable solvents are not readily available and have high vapour pressure at ambient conditions. It primarily involves three stages: vaporization, transport and deposition. The deposition of vapour can occur by condensation or chemical reaction. This method was initially used to grow bulk crystals but with the enormous importance of thin films in electronic and metallurgical applications, the method is now widely used to grow thin films particularly in the field of semiconductor technology [106].

2.2.3 Growth from solution phase

This technique can be further classified as:

(i) Melt growth

(ii) Solution growth

(iii) Gel growth

2.2.3.1 Melt growth technique

This technique is certainly the most popular technique of growing large single crystals at relatively high growth rates (~ cm/hr). The basic conditions required for the growth of crystals by this method are:

1. The material must melt congruently i.e. there should be no change in composition during melting.
2. The material must not decompose before melting.
3. The material must not undergo a solid state phase transformation between melting point and room temperature.

A number of techniques have been developed for the growth of crystals of a material from its melt. These techniques include Verneuil, Czochralski, Bridgman etc. Out of these the earliest melt technique used to grow crystals was described by Verneuil in 1902, [107].

2.2.3.2 Solution growth technique

This is one of the oldest crystal growth techniques in which crystallization takes place when the solution becomes critically supersaturated. The supersaturation can be achieved either by lowering the temperature of the solution or by slow evaporation. In this method the crystals grow from a solution well below its melting point. This may help in growing crystals even at room temperature and will turn to be more advantageous [108].

2.2.3.3 Gel growth technique

Though, there are so many methods for growing crystals, none of them can be called as an ideal method. For instance, yttrium iron garnet (YIG) does not melt congruently, $CaCO_3$ and SiC decompose before they melt and SiO_2 undergoes a solid state phase transformation between the melting point and room temperature, thus, the single crystals of these materials can not be grown from the melt. Crystallization of substances having low solubility cannot be achieved by conventional slow-cooling, solvent evaporation or temperature differential methods. In these cases extremely high super-saturation develops readily which results in the formation of microcrystalline or amorphous precipitates. As such, gel diffusion technique using the chemical reaction at a controlled rate is the most suitable technique for growing these crystals. The rare-earth fumarates showing very poor solubility in water (solubility of fumaric acid is just 6.3 g/l) can, therefore, be grown by gel diffusion technique. They decompose before melting and do not vaporize or sublime. The necessary precise control over the super saturation in gels is goverened by controlling the flux of the inter diffusion pair i.e. by varying temperature, concentration gradient and solvent viscosity. This is the basic principle of gel growth technique for the growth of crystals of virtually insoluble materials [104]. Gel growth method is well described by Henisch [109, 110], Arora [111], and Patel and Venkateswara Rao [112] as well as by Lefaucheux and Robert [113].

The crystal growth has been correctly quoted in a different manner by Gilman [114] in his famous book “The Arts and Science of Growing Crystals” as, “*The Systematic production of artificial Crystals* might be viewed as a new *agriculture* that has began flourish. The new agriculture consists of *growing* solid crystals from a *nutrient* phase (gas, liquid or solid). To start the growth process, the nutrient is often

'seeded' with small crystal to be grown, and some workers speak of *reaping the harvest* after a certain length of time." There are some other well written books available on the subjects like, fundamentals of crystal growth [115]; different crystal growth techniques, their theories, characterization, applications [116-120] and understanding the growth mechanism [121]. Very recently, a handbook of crystal growth was also published [122]. Even some books are available with wonderful photographs of crystals [123].

Since, in the present work the growth of pure and mixed rare-earth fumarates was accomplished by gel diffusion technique; therefore the details of other growth technique are avoided hereby. The gel growth technique is relatively simple, in expensive and a versatile technique. It is an alternative technique to solution growth with controlled diffusion and the growth process is free from convections. Crystal growth in gels has recently gained the interest because of its suitability to grow crystals of biological macromolecules and in the studies involving bio mineralization. Fisher and Simons made an early claim to the effect that "*gels form an excellent media for the growth of crystals of almost any substance, under absolutely controlled conditions"* [124].

The subject of crystal growth in gels is not new but has become more popular since the beginning of 1900, when the famous *Liesegang Rings* formed the main subject of interest for the works of Liesegang [125], Bradford [126] and Holmes [127]. This has attracted the attention of a well known German chemist Ostwald [128] and Lord Rayleigh [129]. Among the earlier workers, Hatscheck [130] has worked primarily with (5-20 %) gelatin and (1-5 %) agar gels. Later on, Henisch et al. [131] described a method for growing single crystals from silica gels and also explained all aspects of gel growth techniques in detail in his book [132].

It is pertinent to mention here that the gel growth technique has attracted the attention of various workers for different reasons. Gel growth technique has been used to grow steroid crystals [133], to mimic the growth of urinary stone crystals *in vitro* and study inhibition and dissolution behaviour in presence of herbal extracts and some juices as well as crystals responsible to arthritis. It has been used to grow the crystals at ambient temperature for technologically important non-linear optical material crystals [134]. The crystal growth methods differ with the nature and properties of the materials. Among the various crystal growth methods, the gel growth technique draws

considerable interest because of its simplicity. This method is based on controlled diffusion of reagents in the gel. The gel growth method offers a significant advantage for the materials with poor solubility in water and which decompose before melting and do not vaporise or sublime on heating [135]. The gel technique has been used by several researchers to grow materials of great interest in the form of single crystals and polycrystals in solid state science for technological point of view and to determine the effect of suitable substitution on their characteristics [136-139].

2.3 Nucleation in gel

Free energy barrier is a major burden,
Transformation cannot happen without aid.
The question is what can we do to make it happen?
The answer is something has to nucleate.

In the beginning there was incubation.
The question is "when we will get to steady state?"
Patience will lead to further fluctuations.
Then nuclei will show and grow at a steady rate.

-L.I. Preston (2002)

The process of crystallization occurs basically in two steps, namely, nucleation and crystal growth. Nucleation is the step where the solute molecules dispersed in the solvent start to gather into clusters on the nanometer scale, as a result of which the solute concentration in a small region gets elevated. The stable clusters of critical size constitute the nuclei called the crystal nuclei and if the clusters are not stable, they get re-dissolved. For the stability of crystal nuclei, the clusters should reach a critical size 'r_c' [105]. At the stage of nucleation, the next step is the crystal growth where nuclei grow larger by the deposition of solute molecules or growth units, which break whatever bonds they have with the crystallizing or super-saturated solution and make new bonds with the crystals. The atoms arrange in a defined and periodic manner resulting the formation of crystal structure. The growth of crystals means a regular

addition of solute molecules or growth units from a supersaturated solution onto the crystal faces, which subsequently grow to visible size. Therefore, the solution concentration is depleting while the size and weight of the crystals increases. The nucleation and growth are only possible when the solution is either supersaturated or super cooled. Nucleation may occur spontaneously or it may be induced artificially. The nucleation which occurs spontaneously is called the homogenous nucleation and the nucleation which is induced artificially is called the heterogeneous nucleation.

Homogenous nucleation rarely occurs in practice. It occurs in a crystallizing solution in the absence of solute crystals or seed crystals and takes place at relatively very high super saturation. A super saturated solution is not in equilibrium and there are fluctuations in local concentrations which give rise to the formation of small and unstable molecular aggregates. These molecular aggregates are called the clusters which are continuously forming and falling apart. It is assumed that the clusters are formed by addition mechanism of growth units. As the addition continues, the cluster grows until a critical size is reached. Clusters of critical size can be formed in supersaturated solutions wherein the size is inversely dependent on the level of super-saturation. Higher the super-saturation smaller is the critical size of the cluster. The homogeneous nucleation requires a very high level of super saturation, therefore, its occurrence is practically rare and in most situations heterogeneous nucleation takes place before reaching conditions suitable for homogenous nucleation.

Heterogeneous nucleation usually takes place on small particles, like dust, impurity molecules or any foreign substrate. Under heterogeneous conditions, due to the presence of some foreign bodies, the formation of nucleus takes place at a less energy than that under homogeneous conditions. It has been postulated that the difference in energy requirements for both the two cases is related to the wetting angle 'θ' between foreign surface and the nucleus by the relationship as:

$$\Delta G_{\text{Homogeneous}} = \frac{[(2+\cos\theta)(1-\cos\theta)2]}{4} \Delta G_{\text{Heterogeneous}} \quad (2.6)$$

The above = n. implies that:

1. For complete non wetting of liquid–solid system, $\theta=180^{o}$, the overall free energy of nucleation is the same as that required for homogeneous or spontaneous nucleation.

2. For partial wetting of solid-liquid system $0 < \theta < 180^{o}$, the nucleation is easier to achieve because the overall excess free energy required is less than that for homogeneous nucleation.
3. For complete wetting, $\theta=0$, the free energy of nucleation is zero, which means that spontaneous nucleation could take place.

2.3.1 Classical theory of nucleation

The classical nucleation theory was put forward by Volmer and Weber [140] by considering the total free energy for a group of atoms. The embryos which are small clusters of molecules are formed as a result of fluctuations in a supersaturated solution. The change in free energy causes these embryos to grow into stable nuclei. If ΔG is the free energy change between the solid and liquid, the free energy of the system decreases by this amount for each unit volume of the solid created. But at the same time the free energy is increased by an amount equal to the interfacial energy σ, for each unit area of the solid-liquid interface formed. Therefore the change in Gibbs free energy associated with the formation of a spherical embryo of radius 'r' is given by the relation:

$$\Delta G = 4\pi r^2\sigma - \frac{4}{3}\pi r^3 \Delta G_v \qquad (2.7)$$

Fig. 2.1 shows the graphical representation of the formula in which the contribution due to surface and volume to the free energy changes are represented. The surface energy term increases with r^2 and the volume energy term decreases with r^3. The net free energy change increases with the increase in size, attains a maximum and decreases for further increase in nuclear size. The size of the nucleus corresponding to the maximum free energy change is known as the critical nucleus. If the size of the nucleus formed is below the critical dimension, there is no further growth possible and it will re-dissociate into the mother system. This maximum value of the free energy, ΔG^*, corresponds to the critical nucleus of radius, r*, which is obtained by maximizing equation 2.7, setting $\frac{d}{dr}\Delta G = 0$, that is

$$\frac{d}{dr}\Delta G = \frac{d}{dr}(4\pi r^2\sigma - \frac{4}{3}\pi r^3 \Delta Gv) = 0 \qquad (2.8)$$

Hence, the radius of the critical nucleus is expressed as $r^* = \frac{2\sigma}{\Delta G_v}$ (2.9)

It is worth noticing that, r* decreases with increase of ΔG_v, i.e., with supersaturation or supercooling. The activation energy necessary for nucleation can be calculated by substituting r* in equation (2.7).

$$\Delta G^* = \frac{16\pi\sigma 3}{3\Delta G_v^2} \qquad (2.10)$$

Using Gibbs-Thomson relation $\Delta G_v = \frac{kTlnS}{\Omega}$ in the equation (2.10), we get

$$\Delta G^* = \frac{16\pi\sigma^3\Omega^2}{3(kTlnS)^2} \qquad (2.11)$$

where, Ω is the molar volume, k is Boltzmann's constant, T is the temperature and S is the degree of supersaturation.

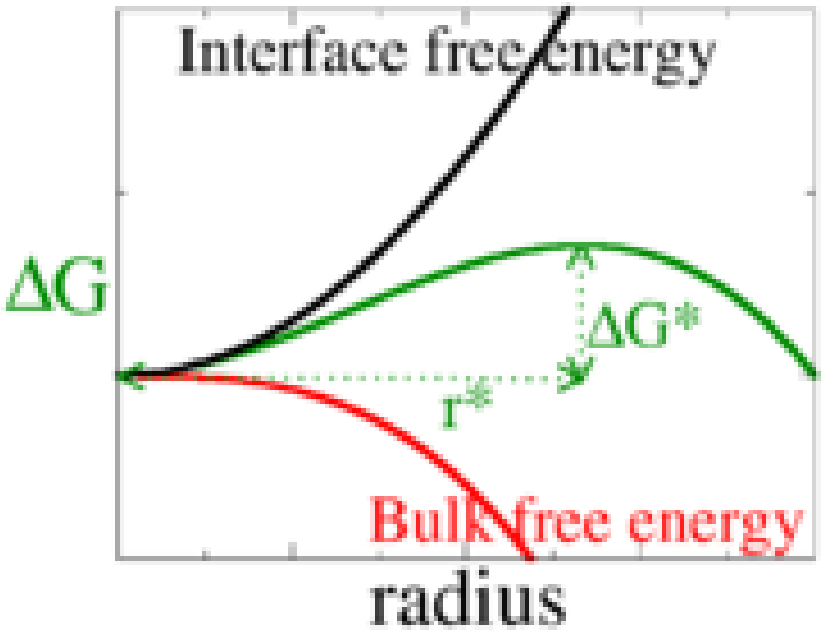

Figure 2.1: Free energy diagram for nucleation explaining the existence of a critical nucleus.
(Courtesy: Wikipedia, the free encyclopedia)

The number of nuclei formed per unit volume per unit time is called the rate of nucleation, and it can be expressed as:

$$J = J_0 \exp\left[\frac{-\Delta G^*}{kT}\right] \qquad (2.12)$$

By substituting = n. (2.11) in = n. (2.12), we get

$$J = J_0 exp\left[\frac{-16\pi\sigma^3\,\Omega^2}{3(kTlnS^2)kT}\right]$$

Or $$J = J_0 exp\left[\frac{-16\pi\sigma^3\,\Omega^2}{3k^3T^3(lnS)^2)}\right] \quad (2.13)$$

where, J_o is a pre-exponential numerical factor. Equation (2.13) shows that the temperature, degree of supersaturation and the interfacial energy govern the nucleation rate.

2.3.2 Nucleation control in gel

In a gel system, it is desirable to suppress nucleation so that only few crystals will grow. There are some methods which control nucleation in gel to some extent, which are:

1. Using suitable reactants of various concentrations
2. Optimization of gel density and ageing of gel
3. Concentration programming
4. Changing of temperature
5. Use of a neutral gel

Out of the different combinations used for obtaining the product crystals only a few are found to be suitable to achieve controlled nucleation. It is reported that nucleation rate is reduced using different combination of reactants to produce various crystals [141, 142]. It is possible to change the gel structure and reduce the nucleation rate by changing the gel density, gel pH and gel ageing [143]. The increased gel density and gel pH decreases the nucleation rate, but the final crystals are of poor quality. However the gel ageing also reduces the nucleation rate without affecting their quality. For the neutral gel we use a U-shaped tube and pour the two reactants in the two limbs of the tube. The neutral gel will slow down the reaction between the reactants and hence reduce the number of nuclei. This method was first used to grow single crystal like lead and thallous and cuprous oxide [144]. And in concentration programming, the concentration of the diffusing reactant is initially kept below the level at which nucleation just occurs and is then increased gradually in small steps. With very dilute reactants the amount of material diffused through the gel is small and hence smaller is the super-saturation rate. Under these circumstances, a few nuclei are formed. As the concentration is increased further the growth of the existing nuclei is

preferred to the formation of additional ones. Crystals grown by this method are more perfect and larger than those grown otherwise [145].

2.3.3 Mechanism of gelling

Gels are two component media with water molecules soaking a porous flexible polymer network and the gelation process corresponds to the setting of a polymeric cluster stretching over the whole volume of the solution. This process is irreversible for the chemical gels such as silica gel but reversible for physical gels, like gelatine or agar gels. The gelation time may vary from few minutes to many days, depending on the nature of the material, its temperature [146], history and the pH of the gel solution [145]. Among different gels, silica and agar gels have been commonly used because their porous network permits the diffusion of several ions and even some large polymers. In case of silica gels, when sodium meta-silicate is dissolved in water, mono silicic acid and sodium hydroxide are produced as per the following reaction in which the mono silicic acid polymerize with the liberation of water.

$$Na_2SiO_3 + 3H_2O \rightarrow H_2SiO_4 + 2NaOH$$

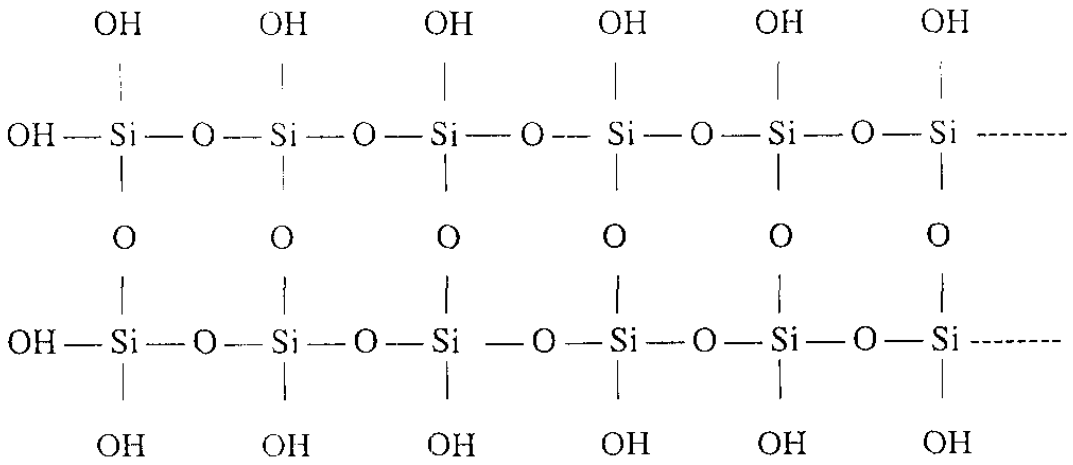

Figure 2.2: Gel structure

The hydrogen ion concentration i.e the pH plays a vital role for the process of gellation. During polymerization two types of ions are produced, viz. $H_3SiO_4^-$ and $H_2SiO_4^+$, whose relative amounts depend on pH. The formation of more reactive $H_2SiO_4^+$ is favoured at high pH values. However, higher charge implies a greater

degree of mutual repulsion. $H_3SiO_4^-$ is favoured at low pH values and is responsible for the sharp increase in viscosity. The process of polymerization continues, until a three-dimensional network of Si-O links is established as shown in Fig. 2.2.

2.4 Crystal growth methods in gels

Based on the nature of the chemical reactions and physical changes involved during the growth process crystal growth methods in gels fall into the following classes [147]:

- Chemical reaction method
- Chemical reduction method
- Complex dilution method
- Solubility reduction method
- Electrolytic Method

2.4.1 Chemical reaction method

The chemical reaction method is particularly used for the growth of materials which are insoluble in water and decompose before melting. Here, two soluble reactants are allowed to react inside the gel medium by incorporation of one of the reactants (lower) in the gel, whereas the other reactant (upper), which is used as the supernatant, diffuses into the gel medium as shown in Fig. 2.3. The simplest method is to incorporate one component in the gel prior to gel setting [148]**.** The reaction inside the gel leading to the formation of an insoluble or sparingly soluble crystalline product can be represented as:

$$AX_1 + BX_2 \rightarrow AB + X_1X_2$$

where, AX_1 and BX_2 are two water soluble compounds which on reaction give rise to AB the insoluble substance and X_1X_2 as the waste product which should be well soluble in water. When the concentration of the reaction products AB exceeds the solubility product (K_{sp}) homogeneous nucleation takes place. Gel method is used to provide an environment that is advantageous for growth by reaction because K_{sp} need only be exceeded in a local region where it is desired.

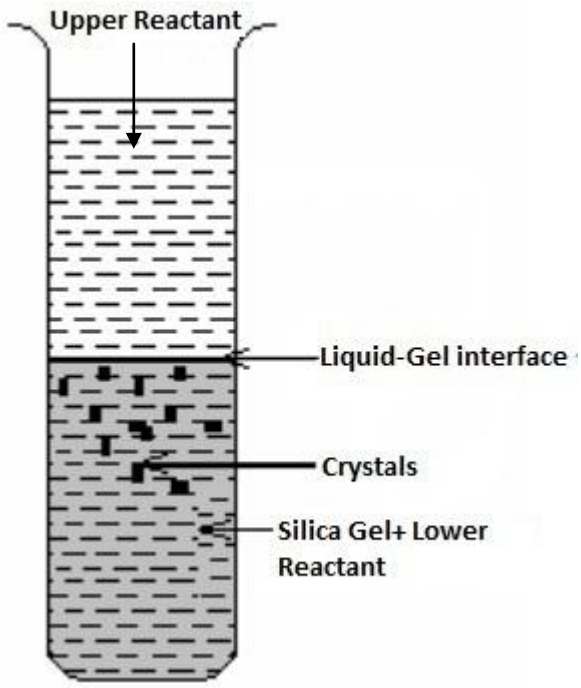

Figure 2.3: Schematic representation of single gel diffusion process.

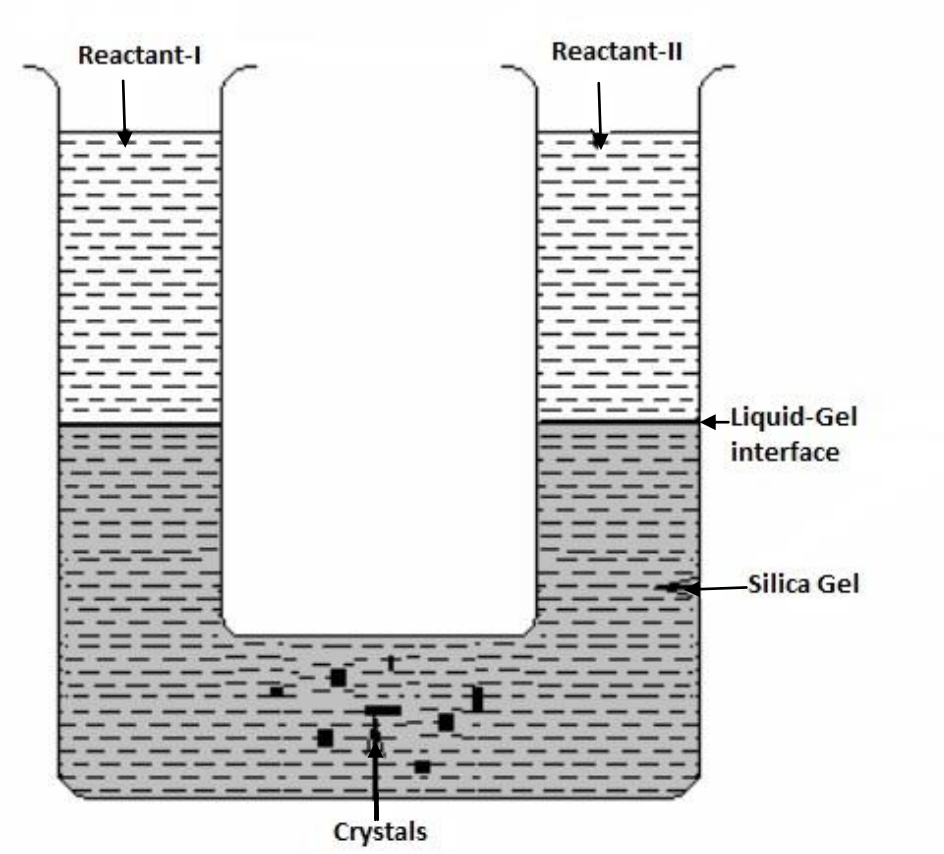

Figure 2.4: Crystal growth by double gel diffusion method.

One of the alternative methods is the use of neutral gel. The simplest technique for this is to employ U-tube method. Here the neutral gel is formed in the horizontal portion of the U-shaped glass tube as shown in Fig. 2.4. The two solutions AX_1 and BX_2 are poured over the set gel in the two limbs of U-tube. The two solutions, after diffusing slowly into the gel medium, react chemically and subsequently result into the formation of crystals in the horizontal portion of gel column. This technique can also be adopted to crystallize compounds which have poor aqueous and organic solubility (uric acid and cystine) using the displacement reaction method [149, 150].

2.4.2 Chemical reduction method

The metallic crystals, such as Cu, Au, Co and Ni are particularly grown by this method. In this method an aqueous solution of a reducing agent is slowly allowed to diffuse through the gel incorporated in a metallic salt, where the chemical reduction takes place and the formation of metallic crystals take place [112].

2.4.3 Solubility reduction method

Generally in this method the crystallization of highly water-soluble substances take place. The material to be grown is incorporated in the gel before gelation and then a supernatant solution to induce the crystallization is used to reduce the solubility of the substance (solute). Compounds which have low aqueous solubility can also be crystallized using this technique. The compounds having low aqueous solubility (Steroids) have been crystallized using this technique by reducing the water content in the gel by incorporating an organic solvent [112]. During this process of crystallization, crystals can be observed in the supernatant solution above the gel due to the reverse diffusion of the precipitating solvent [151].

2.4.4 Electrolytic method

In electrolytic method the metallic crystals can be grown by selecting the gel medium for controlled growth. In this method a very low d.c electric current of the order of 2-10 mA, is passed through a silica gel charged with suitable acid or electrolytic solution. Copper dendrites [152] and silver dendrites and single crystals [153] have been grown using this electrolytic technique.

2.5 Crystal habit

Crystals with different habits are important both commercially and also in studying their physical properties. Therefore, in gel growth technique, crystals with different habits can be grown by changing different growth parameters, such as, concentration of feed solutions, crystallization temperature and gel structure etc. The temperature of the growth has pronounced effect on habit of crystals.For example, in case of strontium sulphate, all crystals grown at about 35 ºC exhibited {011} and {102} as their habit faces, whereas the crystals grown at about 20 ºC developed {022} habit faces in addition to {011} and {102} faces [153]. McCauley and Gehrhardt [154] observed that during the growth of neodymium carbonate, sodium carbonate incorporated gel enhanced the formation of dendrites and spherulites, while neodymium chloride incorporated gel favored the growth of rhombic plates.

2.6 Advantages and drawbacks of gel growth technique

The gel method of crystal growth has following advantage over the other methods of crystal growth and for this reason it is believed that the gel growth method can prove a significant role in the development of good quality single crystals.

1. Crystallization of the substances having extremely low solubility can be achieved by this method.
2. Since the gel growth proceeds at ambient temperature, the grown crystals would contain relatively less concentration of equilibrium defects.
3. Gels being usually optically transparent, as such the crystal growth can be monitored regularly.
4. Gel is soft and it yields a suitable environment for growing crystals.
5. Crystals of different morphologies and sizes can be obtained by changing the growth parameters.
6. Gel medium considerably prevents convection currents and turbulence.
7. All nuclei are spatially separated.
8. This method has the ability to control the rate of reaction required for crystallization of
a particular material.

9. As this method is extremely simple and inexpensive, good quality of single crystals can be grown even in small laboratories, which do not possess sophisticated instrument.

Besides the above advantages, the gel growth method suffers from the following drawbacks or disadvantages.

1. Growth period is usually very long.
2. The gel growth method has proved much less fruitful in growing large sized crystals, because it is extremely difficult to avoid local super saturations sufficient to initiate spontaneous nucleation.
3. The chance of lattice contamination by impurities from the gel itself is profusely increased.
4. The yield of crystals grown by gel methods is low.

CHAPTER-3

Characterization techniques - A brief review

3.1 Introduction

The crystals are grown to understand their scientific and technological usefulness. After the process of growth, it becomes impossible for us to understand the properties and applications of a material unless their characterization is made. The process of understanding their composition, structure and morphology is called characterization. The characterization is an important process to identify physical and chemical properties of a material and is essential for the proper selection and implementation of substances when used in industrial and scientific applications. Since only one method is not sufficient to characterize a material, therefore, the golden rule of materials characterization is to apply numerous methodologies. The grown crystals in the present work have been characterized using various physico-chemical techniques which include Microscopy Techniques, X-ray diffraction (XRD), Energy Dispersive Analysis (EDAX), Thermal-analysis (TGA/DTA), Carbon Hydrogen and Nitrogen analysis (CHN), Fourier Transform Infrared Spectroscopy (FTIR), Ultraviolet and Visible Spectroscopy (UV-Vis), Photoluminescence (PL) Spectroscopy, Vibrating Sample Magnetometery (VSM) and Electric Impedance Spectroscopy.

3.2. Characterization techniques

3.2.1 Optical microscopy

An optical microscope consisting of an objective lens and an eyepiece is the simplest microscope. The system of objectives and eyepieces usually consist of two or more lenses to correct for lens aberrations. The real image formed by the objective lens is

magnified by the eyepiece. The system of two lenses is maintained at a fixed distance and focusing is achieved by moving the whole assembly, up and down for well resolving of the sample. Since resolution is the smallest separation of two points that are visible as distinct entities and the resolving limit of the light microscope is 0.2 μm. For the optical studies of the grown sample, we used a polarising light microscope available in the solid state research laboratory (Department of Physics), University of Kashmir, Srinagar.

3.2.2 Scanning electron microscopy

A scanning electron microscope (SEM) is a type of a microscope that images a sample by scanning it with a beam of electrons in a raster scan pattern. It is used to find the average crystallite size and the surface morphology of a sample. From the original von Ardenne equipment [155], an improvement of the resolution has been made from 50 nm in 1942 to 0.7 nm, today. It is based on the principle of interaction of electrons generated from X-ray tube with the surface of the sample. The incident electron beam hitting the material surface results the emission of electrons from the specimen in the form of backscattered electrons (BSEs) and secondary electrons (SEs), X-rays, heat and even transmitted electrons. The secondary electrons having low kinetic energy of the order of 50 eV are fed to the detector which converts them into a signal to study of the surface morphology of the materials on the picture tube of a television screen. The test sample is earthed to avoid the accumulation of spatial charge, which can spoil the SEM image. The electron beam and the cathode ray tube scan synchronously so that an image of the surface of the specimen is formed and its photograph is taken. For the materials grown in the present study Hitachi S-3000H electron microscope was used to do their SEM studies. For making the crystalline samples conducting they were coated with gold using a Bal-Tec SCD004 sputter coating. Both the apparatus are available at the University Instrumentation Centre (USIC), University of Kashmir, Srinagar.

3.2.3 Powder X-ray diffraction

X-ray diffraction is the most important methodology used in the characterization of the materials to study their structure, phase and other structural parameters, such as average grain size, crystallinity, strain, and crystal defects. As the physical properties

of solids (e.g electrical, optical, magnetic, ferroelectric, etc.) depend on atomic arrangements of materials, therefore, the determination of the crystal structure is a vital part of the materials characterization. X-rays are used to produce the diffraction pattern because their wavelength λ is typically of the same order of magnitude (1-100 Å) as the spacing d between planes in the crystal. The basic principle for X-ray is that for a fixed wavelength (λ), constructive interference takes place for a fixed set of atomic planes with interplaner distance (d) at an angle of incidence (θ), when conditions satisfy Bragg's law of diffraction $2d\sin\theta = n\lambda$ [156], where n is the order of diffraction.

In powder X-ray diffraction method the sample is ground to a fine powder and each particle of the powder behaves as a tiny crystallite, oriented randomly with respect to the incident beam. A number of particles are expected to be oriented in such a way to satisfy the Bragg's diffraction condition when X-ray beam produced in an X-ray tube is directed on the sample. X-ray diffraction peaks are produced by constructive interference of a monochromatic beam of X-rays scattered at specific angles from each set of lattice planes in a sample. The peak intensities are determined by the atomic arrangements within the lattice planes. Each crystalline solid has unique atomic architecture and consequently has a unique characteristic X-ray powder pattern. These patterns can be used as fingerprints for identification of solid phases. Once the material has been identified, X-ray crystallography may be used to determine its structure, i.e. how the atoms pack together in the crystalline state and the size and the shape of the unit cell, etc. Powder X-ray diffraction analysis of grown crystals in the present work was obtained using a Bruker D8 advance X-ray diffractometer with Cu Kα radiation (λ =1.5406 Å)

3.2.4 Single crystal X-ray diffraction

Single crystal X-ray diffraction is the most authentic crystallographic technique which gives detailed information about the crystalline substances. This technique is most commonly used for precise determination of a unit cell, including cell dimensions and positions of atoms within the lattice. Bond-lengths and angles are directly related to the atomic positions. The size of the crystal required for analysis should be less than $1mm^3$. In single crystal X-ray diffraction, molybdenum is the most common target, with MoK_α radiation = 0.7107 Å. The X-rays produced are collimated and directed

onto the sample. When the geometry of the incident X-rays impinging the sample satisfies the Bragg Equation, constructive interference occurs. A detector records and processes this X-ray signal and converts the signal to a count rate which is then output to a device such as a printer or computer monitor. Since only one crystal is involved in this technique, the patterns obtained are spot patterns and not line patterns as in powder X-ray diffraction. These patterns contain much information about the size and shape of the unit cell or repeat unit of the crystal from the relative positions of the diffracted beams in space. Crystal structures can be solved by analysing the intensities of diffracted X-ray beams. Also, the arrangement of atoms within the unit cell is obtained from the relative intensities of the diffracted beams.

3.2.5 Energy dispersive X-ray analysis

Energy dispersive X-Ray analysis (EDAX) or Energy dispersive X-Ray spectroscopy (EDS) is an analytic technique used to determine the chemical composition of a material. This method is a non-destructive method and gives immediately record of all elements having $Z \geq 11$. When the sample is bombarded by an electron beam, electrons are ejected from the atoms comprising the sample's surface. The resulting electron vacancies are filled by electrons from the higher states, and an X-ray is emitted to balance the energy difference between the two electron's states. EDAX technique detects the X-rays emitted from the sample and the energy of the X-rays is strictly related to the atomic number of the elements excited. Hence the constituents of the specimen can be determined. The intensity of the emitted X-rays will be proportional to the concentration of the elements in the sample. The X-ray energy is characterization of the element from which it is emitted. The EDAX spectrum is a curve between binding energy and intensity of emitted photoelectrons. The peak heights are the measure of the quantity of the concentrated elements incorporated in the specimen. The comparison of the EDAX peaks of two elements in a sample gives an approximate proportion of the elements present. During the present investigation, an energy dispersive spectrometer (OXFORD ISIS-300 system) was used to identify the presence of terbium and oxygen in the grown crystals by determining the atomic as well as weight percentage of terbium and oxygen atoms in the grown crystals.

3.2.6 Carbon Nitrogen and Hydrogen (CHN) analysis

The elemental analysis of Carbon, hydrogen and nitrogen is the most essential so as to prove the elemental composition in an organic sample or a sample containing organic ligands. In its simplest form, simultaneous CHNS analysis requires high temperature combustion (furnace at ca. 1000 ^{o}C) in an oxygen-rich environment. In a typical CHN analysis, the sample under test is weighed in a tin capsule. The required quantity of the material is 2 to 3 mg. The sample is then wrapped in a tin capsule and inserted into a furnace. During the process of combustion, carbon is converted to carbon dioxide; hydrogen to water; nitrogen to nitrogen gas/ oxides of nitrogen and sulphur to sulphur dioxide. The other elements present in the sample get converted into combustion products which are removed by a variety of absorbents and we are left with only carbon dioxide, water, nitrogen and sulphur dioxide. Quantification of the elements requires calibration for each element by using high purity 'micro-analytical standard' compounds such as acetanilide and benzoic acid. In the present study, the grown materials are coordination compounds of terbium and gadolinium with fumarate as a ligand. Therefore, it becomes necessary to carry out CHN analysis of the materials to determine the percentage composition of Carbon and Hydrogen. In the present investigation Carbon and hydrogen contents in the grown crystals were determined by using Vario-EL III CHNS-analyzer.

3.2.7 Thermal analysis

Thermal analysis consists of different techniques in which a physical or chemical change of a material is measured as a function of temperature when the substance is subjected to a controlled increase, or decrease of temperature. These temperature programmed techniques are TGA, DTA or DTG. In the present study, the thermal analysis was carried out by using a Perkin-Elmer thermal analyser in N_2 atmosphere at a heating rate of 10 ^{o}C min^{-1}.

3.2.7.1 Thermal gravimetric analysis

Thermo gravimetric analysis (TGA) is a simple technique in which weight loss or gain due to dehydration or decomposition of a material as a function of temperature during controlled heating is measured [157]. The sample placed in a small pan connected to microbalance is heated isothermally in a controlled manner for a given

time. The atmosphere around the sample may consist of an inert gas, such as nitrogen. The TGA curve plots TGA signal i.e. percent weight loss or gain on the y-axis against the reference material temperature on the x-axis. This weight loss or gain is as a result of the processes involving water desorption, structural water release, structural decomposition, carbonate decomposition, gas evolution, sulfur oxidation, fluoride oxidation, rehydration, and other transformations.

3.2.7.2 Differential thermal analysis

In differential thermal analysis (DTA) the difference in temperature of the sample and a thermally inert reference material are measured as a function of temperature, when both materials are subjected to an identical heat treatment [158]. During the heating or cooling of the sample, it will absorb or liberate energy depending on the transitions that are taking place. The corresponding derivative of the sample temperature from that of the reference material (ΔT) versus the programmed temperature (T) is recorded and explains whether the transition is endothermic or exothermic. Generally phase transition, dehydration, reduction and some decomposition reactions produce endothermic effects, where as crystallization, oxidation and some decomposing reactions produce exothermic effects. The DTA studies in conjunction with TGA provide detailed information regarding the dehydration, decomposition and phase transition of the material during heating.

3.2.8 Fourier transformation infra-red spectroscopy

Fourier transformation infrared spectroscopy (FT-IR) is an analytical technique used to identify organic inorganic materials. This technique measures the absorption of infrared radiation by the sample material versus wavelength. The IR absorption bands identify the functional units, internal structure of molecules and nature of chemical bonds of a compound [159]. In FT-IR technique, the frequency of the incident radiation is varied and the quantity of radiation transmitted or absorbed by the sample is obtained. When the frequency of the incident radiation coincides with the vibrational frequency of some part of the molecule, resonance occurs and absorption of energy takes place. As the molecules return from their excited states to original ground states, the absorption energy is released which results distinct peaks in IR spectrum. Thus FT-IR spectra absorption bands provide a unique fingerprint of the

molecules present in the sample. The FT-IR spectra are usually represented as the plots of intensity versus wave number (in cm^{-1}). To identify the materials being analyzed, the unknown IR absorption spectrum is compared with standard spectra with a spectrum obtained from a known material. Spectrum matches identify the polymer or other constituents in the sample. In the present work, the FT-IR spectra of the grown crystals in the wave number range of 400-4000 cm^{-1} were recorded on a Bruker Vector-22 spectrometer using KBr pellet technique. So, what information can FT-IR provide?

• It can identify unknown materials.

• It can determine the quality or consistency of a sample.

• It can determine the amount of components in a mixture.

3.2.9 Ultraviolet and Visible spectroscopy

Ultraviolet-visible (UV-Vis) spectroscopy is measured by an instrument called UV-Vis spectrophotometer. The basic parts of a spectrophotometer consist of a light source, a holder for the sample, a diffraction grating in a monochromator or a prism to separate the different wavelengths of light, and a detector. The radiation source used for the spectrophotometer is a Tungsten filament (300-2500 nm) or a deuterium arc lamp (190-400 nm) or Xenon arc lamp (160-2000 nm) or more recently, light emitting diodes (LED) [160] for the visible wavelengths. It measures the intensity of light passing through a sample (I), and compares it to the intensity of light before it passes through the sample (Io). The ratio I/Io is called the transmittance, and is usually expressed as a percentage (% T). The absorbance 'A' is based on the transmittance and is given by: $A = -\log [(\% T)/(100 \%)]$. The UV-visible spectrophotometer can also be configured to measure reflectance. In this case, the spectrophotometer measures the intensity of light reflected from a sample (I), and compares it to the intensity of light reflected from a reference material (Io). The ratio *I/I*o is called the reflectance, and is usually expressed as a percentage (% R).

During the present investigation the UV-Vis analysis was carried by Cary 5000 spectrophotometer at SAIF STIC Cochin Kerela.

3.2.10 Photoluminescence spectroscopy

Photoluminescence (PL) is the phenomenon of light emission from a material after it absorbs the photons of an electromagnetic wave. It is the light emission produced by the photo excitation. Following excitation various relaxation processes typically occur in which other photons are re-radiated. The time period from absorption to emission may vary from 10^{-15} s to 10^{-3} s and under certain circumstances delay of emission may even spread to minutes or hours. Photoluminescence (PL) is a non-destructive optical technique used for the characterization of materials which involves the irradiation of the crystal to be characterized with photons of energy greater than the band-gap energy of that material. In case of a crystal scintillator, the incident photons will create electron-hole pairs. When these electrons and holes recombine, this recombination energy will transform partly into non-radiative emission and partly into radiative emission. PL consists of impinging relatively high frequency ($h\nu > E_g$) light onto a material, exciting atomic electrons. Subsequent relaxation may result in the production of photons that are characteristic of the crystal or defect site that emits the light. The variation of photoluminescnce intensity, which depends on the power of the excitation light source, can be used to identify the underling recombination process [161]. For the compounds under study the photo luminescence spectrum was obtained by using Varian Cary-Eclipse spectrophotometer.

3.2.11 Vibrating sample magnetometery

The vibrating sample magnetometer (VSM) is a versatile instrument which makes precise magnetic moment measurements of a sample as a function of temperature, magnetising field and crystallographic orientations.Its sensitivity is extremely high and can be detected from 5×10^{-5} - 5×10^{-6} e.m.u. VSM is also used for recording M-H hysteresis loops and from these loops the parameters such as saturation magnetization, remenant magnetization and coercivity of the sample can be measured directly from hysteresis loops. It is based on the principle of change in flux in a coil when a sample is made to vibrate between the electromagnets. In the vibrating sample magnetometer, the sample vibrates perpendicular to the applied field. The oscillating magnetic field of the vibrating sample induces a voltage in the stationery detection coils. From this voltage, the magnetic properties of the sample are deduced. The idea of a vibrating sample came from Smith's [162] vibrating coil magnetometer. For the present work,

the magnetic moments of the samples were measured by using the Microsense EZ9 vibrating sample magnetometer (Make USA). The facility is availble in the Department of Physics, University of Kashmir.

3.2.12 Electric impedance spectroscopy

The dielectric constant is an essential property of dielectric materials and therefore its determination is very important. Arthur Kennelly was the first to represent impedance with complex numbers [163]. The instrument used for its measurement is called an impedance analyzer or LCR meter. It is based on the principle of a parallel plate capacitor, in which the pellet (sample) is silver coated to act as the capacitor with the sample as the dielectric medium.

It consists of a sample holder which acts as a parallel plate capacitor with the sample as dielectric medium. The measurements are made at low frequencies, typically below 1GHz. The method in which the range of frequency used is from 20 Hz-1GHz has high measurement accuracy.The material is stimulated by an ac source and the actual voltage across it is monitored. The dimensions of the sample, its capacitance and dissipative factor are measured. The measured capacitance is then used to calculate the permittivity of the medium. The dielectric spectroscopy of the compounds grown in the present work was carried out in the frequency range of 20 Hz to 3 MHz and over the temperature range of 15-130 ^{o}C using an electric impedance analyser (Wayne Kerr) and the data was recorded. This facility is also availble in the Department of Physics, University of Kashmir.

The parameters such as dielectric constant ε' and ac conductivity $\sigma_{a.c}$ of the compounds were calculated by using the relations:

$$\varepsilon' = C.t/\varepsilon_o A \text{ and } \sigma_{a.c} = 2\pi f \varepsilon_o \varepsilon' \tan\delta.$$

where, C represents the capacitance (in farads) of the sample, t is the thickness (in meters), A the area (in meter^2) of the sample, $\varepsilon_o = 8.85\times10^{-12}$ Fm^{-1} and f is the frequency (in Hertz) of the applied electric field.

CHAPTER-4

Growth and characterization of terbium, gadolinium and mixed gadolinium-terbium fumarate heptahydrate single crystals.

4.1 Introduction

The methods of growth for obtaining single crystals may be classified according to their phase transition i.e., liquid phase, solid phase and the vapor phase. Though there are so many methods for growth of crystals, no method can be called as an ideal method. Crystal growth in gels [109, 110] is used for growing single crystals of the materials that show poor solubility in water. This technique has been recognized as an alternative to solution-growth method. The gel growth technique has gained considerable importance due to its simplicity and effectiveness in growing single crystals of various compounds. Despite the limitation in the sizes of the gel grown crystals, the main advantage of the gel diffusion technique is that in this method the crystals normaly grow at low temperatures, therefore, there is a minimum concentration of equilibrium defects in the crystals. The gel also prevents the convection currents or turbulences and being chemically inert provides a three dimensional crucible. Moreover, due to the transparency of the gel medium, the growth of crystals can also be monitored regularly in this technique. On the other hand, high temperature techniques are usually expensive and may not be within the reach of every laboratory. A variety of crystals required for the purpose of research and application have been grown in silica gels [164, 165]. Fumarates being insoluble in water and decompose before melting, therefore, for the growth of terbium fumarate, gadolinium fumarate and their mixed fumarate heptahydrate single crystals we have

adopted the single gel diffusion technique. During the single diffusion, one reagent is incorporated in gelling mixture (lower reactant) and another is diffused into the gel (upper reactant), leading to high supersaturation followed by nucleation and the crystal growth. While as in the double diffusion technique, the gel is used to separate the solution containing the reagents by placing the gel in the bent portion of a U-tube and the reagents in its arms.

So far as the crystallization of these coordination compounds is concerned, the high affinity of rare-earth elements for oxygen donor atoms make carboxylates excellent candidates as bridging ligands for preparing stable materials which favours the formation of cluster like solids [166, 167]. The literature survey shows that there are interests in the research of coordination compounds from fumaric acid describing the studies about crystallinity, luminescence, and magnetic properties [65-67, 168]. The thermal decomposition of fumarate with the following metal ions have also been reported in the literature: gadolinium [169], ytterbium [170], transition metals (II) [171], copper [172]. As for as, the rare-earth coordination compounds are concerned, they are the potential candidates which besides showing ferroelectric properties are also thermally stable [173, 174]. Moreover, these types of compounds can be readily characterized by X-ray crystallography methods, which facilitates establishment of structure-property relationships.

The significance of the growth of mixed crystals is that their characteristics are different from that of the crystals of single components grown separately. For example, the variations in the hardness of pure and mixed KBr and KI system are reported in the literature [175]. The physico-chemical characteristics of mixed crystals have brought significant changes in comparison with those of the pure crystals [176]. The structural transitions, variation in thermal stability and modifications in external morphology of mixed crystals are also reported in the literature [138,177-179].

In the present work, fumaric acid (HOOC-CH=CH-COOH) having relatively small central moiety was used as a ligand for the growth of terbium fumarate, gadolinium fumarate and mixed Gd-Tb fumarate heptahydrate single crystals. The growth of solid state compounds of rare-earth fumarates by gel diffusion method and hydrothermal methods are also reported in the literature [180-184]. For the materials characterization of the crystals grown in the present study, we report the results

obtained by X-ray diffraction, FT-IR spectroscopy, elemental analysis (CHN and EDAX), thermo-analytical techniques such as thermogravimetry (TG) and differential thermal analysis (DTA). An attempt has also been made to relate the results on nucleation kinetics with the classical nucleation theory.

4.2 Experimental Procedure

A number of experiments were carried out to grow single crystals of terbium fumarate heptahydrate (TFH), gadolinium fumarate heptahydrate (GFH), and mixed Gd-Tb fumarate heptahydrate (GTFH) crystals in silica gel and agar-agar gel using gel diffusion technique. The chemicals such as terbium nitrate hexahydrate and gadolinium chloride hexahydrate each (99.9 %) were purchased from Chengdu Haoxuan Technology Co.Ltd. China, while as fumaric acid (99.5 %) and sodium meta-silicate (99.5 %) were purchased from Thomas Baker Mumbay, India. For carrying the experimental work for the growth TFH, GFH and GTFH single crystals, the chemicals were used without any further purification. For the growth of TFH and GFH single crystals, terbium nitrate hexahydrate and gadolinium chloride hexahydrate each of molarity (0.1-0.6 M) were used separately as the upper reactants and fumaric acid (0.06-0.08 M) encapsulated in the gel medium was used as the lower reactant. However, for the growth of mixed GTFH crystals an aqueous solution of terbium nitrate hexahydrate (0.1-0.6 M) and gadolinium chloride hexahydrate (0.1-0.6 M) in the volume ratio of 1:1 were used as an upper reactant. The crystals were grown in the crystallizers consisting of glass test tube of length 200 mm and diameter 25 mm. The gel can be prepared by adopting the method of alkali-set gel or acid-set gel. In an alkali-set gel method, a solution of sodium meta silicate of molarity (0.3-0.6 M) was added drop by drop with continuous stirring to an aqueous solution of fumaric acid of molarity (0.06-0.08 M) in the volume ratio of 1:2. The pH of the solution was maintained to the desired range $5.0 \leq pH < 6.0$ by adding 3-4 ml of concentrated nitric acid to about 300 ml of gel solution. A digital pH meter (HANNA instrument; Model pHep) was used for measuring the pH of the gel solution. Gel solution was then transferred to a number of crystallizers up to the three-fourth of their volume. The crystallizers were left for gelation for a few days and the gelation was observed to depend on both the pH of the solution and the environmental temperature. Gel solution with lower pH required more time for gelation than that of the gel solution of

higher pH. Also, it was found that the gel solution of a desired pH required less time for gelation at high temperature and vice-versa. Supernatant solution acting as an upper reactant was then carefully poured over the set gel without damaging the gel/solution interface. A series of experiments were carried out in the temperature range of 15-35 ^{o}C. During the process of nucleation, tripositive rare-earth ions Tb^{3+} and Gd^{3+} ions diffuse through the narrow pores of the gel to react with the fumarate ions $(C_4O_4H_2)^{2-}$ encapsulated in the gel as a lower reactant, giving rise to the formation of TFH and GFH single crystals respectively. But for the mixed fumarate complex, due to the substitutional exchange of the two rare-earth ions (Tb^{3+} and Gd^{3+}), both of the ions coordinate with the fumarate ligand in the ratio of 1:1 for the formation of mixed gadolinium-terbium complex.

The experiments for the growth of pure and mixed rare-earth fumarate crystals were conducted in two types of gels: silica gel and agar-agar gel. The experiments conducted in agar-agar gel did not yield any fruitful results for a very long time. So, most of the work was therefore conducted in silica gel and the following chemical reactions were expected to take place in the silica gel medium for the formation of TFH, GFH and GTFH single crystals.

$$2Tb\,(NO_3)_3 + 3C_4H_4O_4 \rightarrow Tb_2\,(C_4H_2O_4)_3 + 6HNO_3$$

$$2Gd\,Cl_3 + 3C_4H_4O_4 \rightarrow Gd_2\,(C_4H_2O_4)_3 + 6HCl$$

$$Tb\,(NO_3)_3 + Gd\,Cl_3 + 3C_4H_4O_4 \rightarrow Gd\,Tb\,(C_4H_2O_4)_3 + 3HNO_3 + 3HCl$$

The crystallizers were regularly monitored and the crystals were visible just 3-4 days after the upper reactant was added to the set gel. The crystals were harvested after a growth period of 3-4 weeks. The gel was washed away by distilled water and the crystals were left to dry at room temperature. The external morphology of as-grown crystals was studied by using a Hitachi S-3000H Scanning Electron Microscope and a Polarising Optical Microscope (Ortholux-Wetzlar, Germany). The size of these crystals was found to be just equal to $1mm^3$.

4.3 Nucleation rate of gel grown crystals

The nucleation rate may be defined as the number of crystals produced in the entire gel column for a fixed time period. The appearance of a crystal at any place inside the gel column may be associated with the critical nucleation at that place. Hence, the

nucleation rate in a gel system was studied by observing the effect of various growth parameters, such as concentration of upper reactant, gel age (time period from the setting of gel up to the time when the the upper reactant is added), gel density, gel pH and the temperature on the number of crystals that appear in the entire gel column for a specific period of time.

4.3.1 Effect of various growth parameters on nucleation rate of terbium fumarate heptahydrate single crystals

4.3.1.1 Effect of upper reactant concentration

The gel system of pH 5.5 was prepared with sodium meta silicate (0.5 M) and fumaric acid (0.07 M) and kept for gelation in a number of crystallizers. After the gel age of 24 hours, 20 ml of terbium nitrate hexahydrate of different concentrations varying from 0.1-0.6 M was used as an upper reactant and poured over the set gel. The number of crystals in each crystallizer was recorded just after one week of pouring of the upper reactant. It was observed that the number of crystals increases exponentially by increasing the concentration of upper reactant as shown in Fig. 4.1. This type of behaviour has been reported in the literature for crystalization of $KClO_4$ crystals [142]. However, by increasing the upper reactant concentration beyond 0.8 M, a fast precipitation was observed and hence no single crystal growth was observed.

4.3.1.2 Effect of gel age

Gel age may be the time interval between the setting of gel and the time when the upper reactant is added. The setting of gel depends on the gel pH and the temperature. The gel of higher pH and higher temperature takes less time for gelation and vice versa. Gel system of pH 5.5 was prepared with 0.3 M sodium meta silicate and 0.07 M fumaric acid and allowed to set in a number of crystallizers. 20 ml of terbium nitrate hexahydrate (0.5 M) as an upper reactant was carefully poured over the set gel in each crystallizer, kept at different gel ages of 48 hrs, 96 hrs and 192 hrs. It was observed that the crystal count corresponding to the different gel ages decreases linearly with the increase in gel age as shown in Fig. 4.2. Due to increase in gel age, the pore size becomes small and the gel also becomes hard as a result of which the nucleation rate decreases.

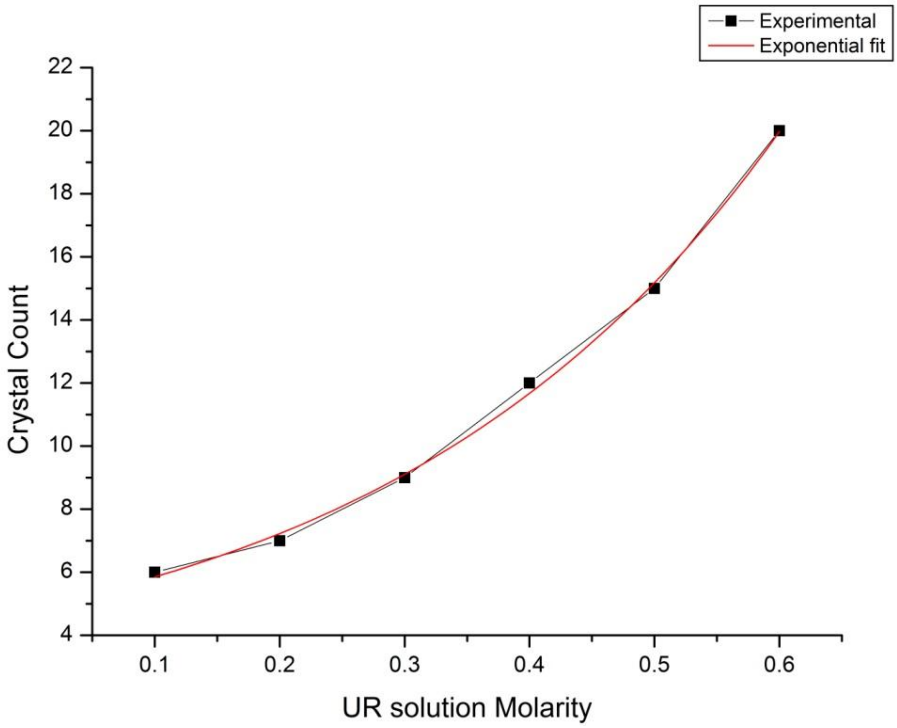

Figure 4.1: Variation of crystal count with upper reactant concentration, keeping other parameters like gel age, gel density and gel pH as constant.

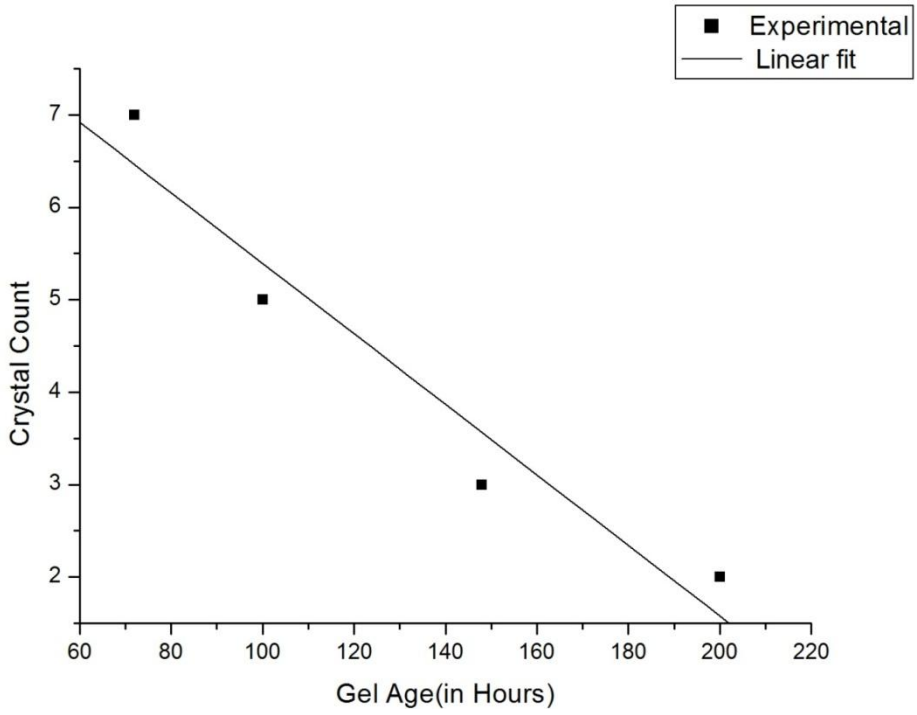

Figure 4.2: Variation of crystal count with the gel age, keeping all other parameters constant.

4.3.1.3 Effect of gel concentration

Gel systems of different gel concentrations were prepared in a number of test tubes keeping all other parameters like gel pH, gel age, temperature and the concentration of upper and lower reactant constant. The crystal count in each test tube was made just ten days after the upper reactant was added. It was observed that the crystal count corresponding to different gel concentrations decreases linearly as shown in Fig. 4.3. Due to increase in gel concentration, the pore size may become small and the gel also becomes hard, therefore the nucleation rate may decrease.

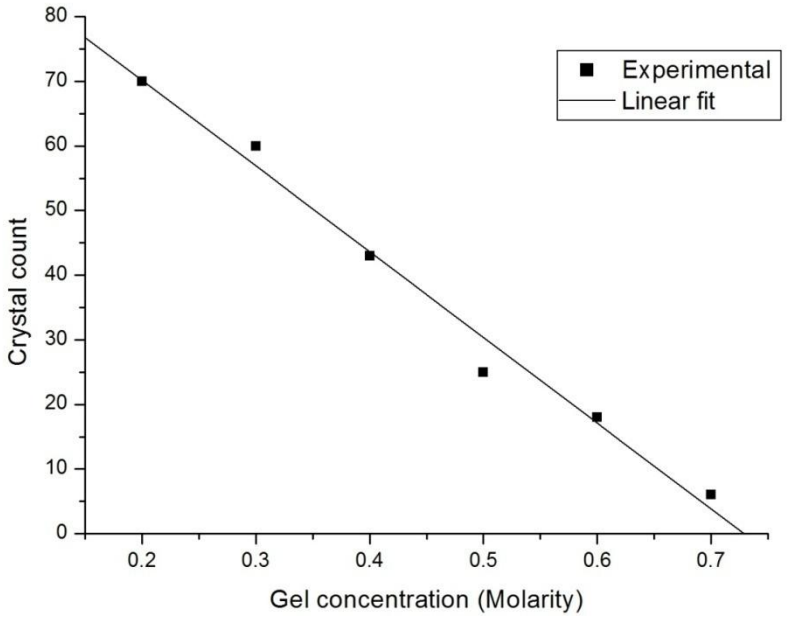

Figure 4.3: Variation of crystal count of with gel concentration at room temperature, keeping other parameters such as gel age, gel pH and upper reactant concentration as constant.

4.3.1.4 Effect of gel pH

For studying the effect on the number of crystals formed inside the gel due to the gel pH, gels of different pH values in the range $5.0 \leq pH < 6.0$ were prepared by keeping all other parameters like gel density, gel age, gel temperature and the concentration of upper and lower reactant constant. The gel pH was adjusted by adding a few drops of conc. HNO_3 to the gel solution. After seven days of growth period, the number of

crystals in the crystallizers maintained at different pH values was counted. It was observed that within a pH range $5.0 \leq pH < 6.0$, the crystal count increased exponentially corresponding to the increase in gel pH as shown in Fig. 4.4. However for the gels of pH less than 5 hardly any crystal was found to nucleate and for the gels of $pH > 6$, a strong precipitation was formed. A photograph as shown in Fig 4.5 depicts that in a desired pH range of $5.0 \leq pH < 6.0$, the nucleation rate increases exponentially with increasing pH.

4.3.1.5 Effect of temperature

The temperature is another important factor for the growth of crystals as well as for gel setting. In the present case, the gel setting was found very weak in winter and the fruitful results of gel setting was found only in summer. A gel system of sodium meta silicate (0.5 M), fumaric acid (0.07 M) and gel pH 5.0 was prepared and after the gel age of 48 hours, 20 ml of terbium nitrate hexahydrate (0.2 M) was carefully poured over the set gel as an upper reactant. The crystallizers were maintained at different temperatures of 15 ^{o}C, 25 ^{o}C, 30 ^{o}C and 35 ^{o}C. As far as the growth of these crystals is concerned, it was observed that at lower temperature of 15 ^{o}C, there were few nucleation sites found in the crystalizer placed on the left and it took longer time to grow the crystals. This may be due to the reason of slow diffusion of the reagents in the gel medium. The number of crystals grown in the crystallizers goes on increasing as the temperature was increased and at a higher temperature of 35 ^{o}C the diffusion rate was observed to be fast, as a result of which there were large number of nucleation sites as depicted in the photograph in Fig. 4.6. After about 7 days of growth period, the number of crystals in each test tube was counted and was observed that the number of crystals increases exponentially with the increase in temperature as shown in Fig. 4.7. Due to the increase in temperature the rate of diffusion of the ions increases, which increases the nucleation rate as per classical nucleation theory [185]. The effect of temperature on the nucleation of tetragonal lysozyme crystals has been reported in the literature [186]. It has also been reported that the free energy of formation of a critical nucleus increases with the increase in temperature [187, 188].

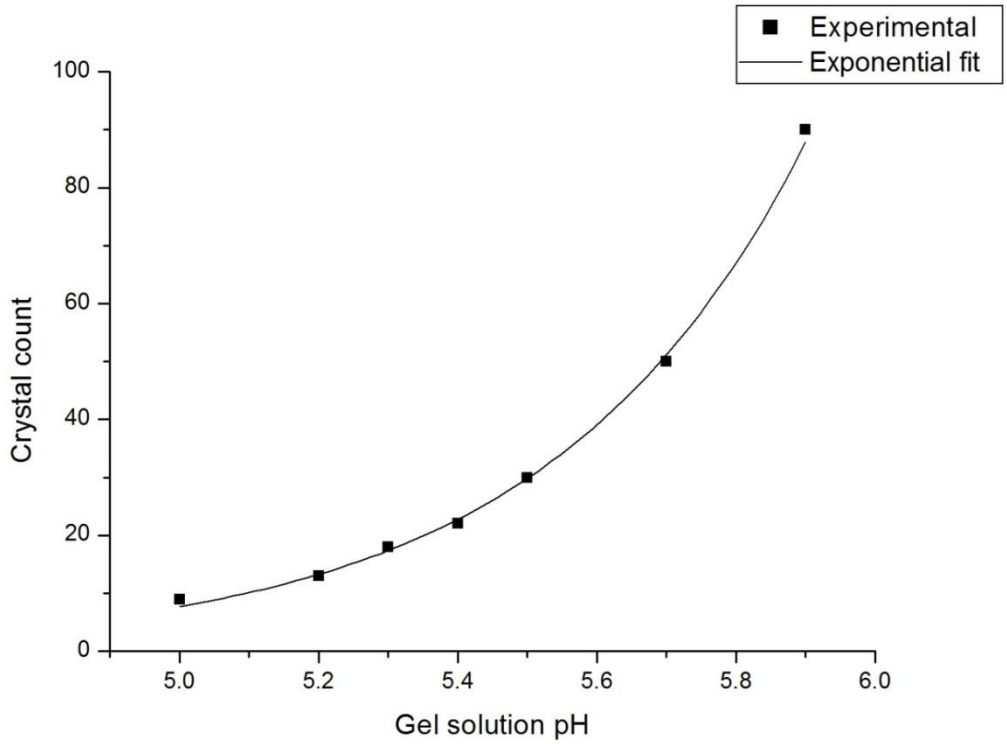

Figure 4.4: Variation of crystal count with gel pH at room temperature, keeping gel age, gel density and upper reactant concentration as constant.

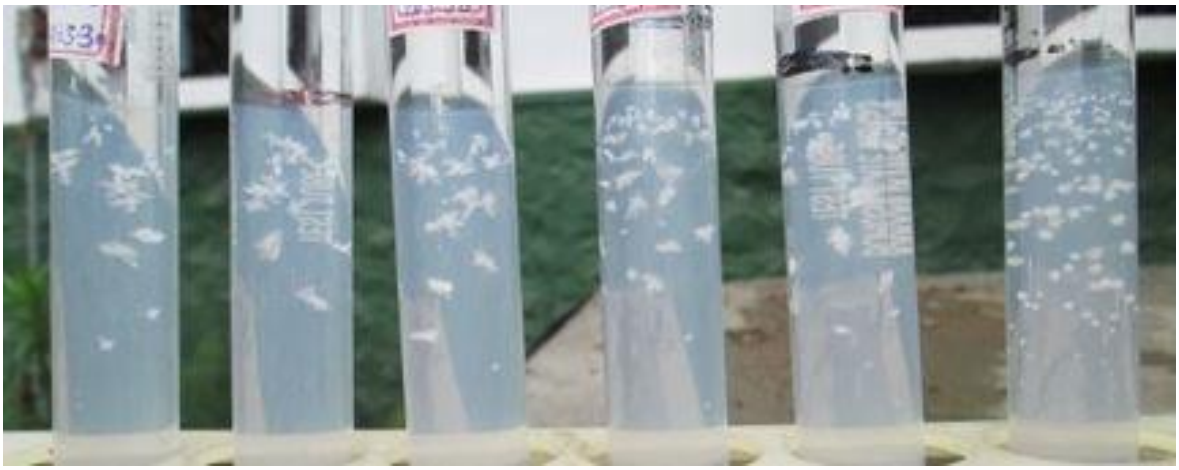

Figure 4.5: Photograph showing increase in nucleation rate with pH in the range $5.0 \leq pH < 6.0$.

Figure 4.6: Photograph showing increase in nucleation rate with an increase in temperature from left to right.

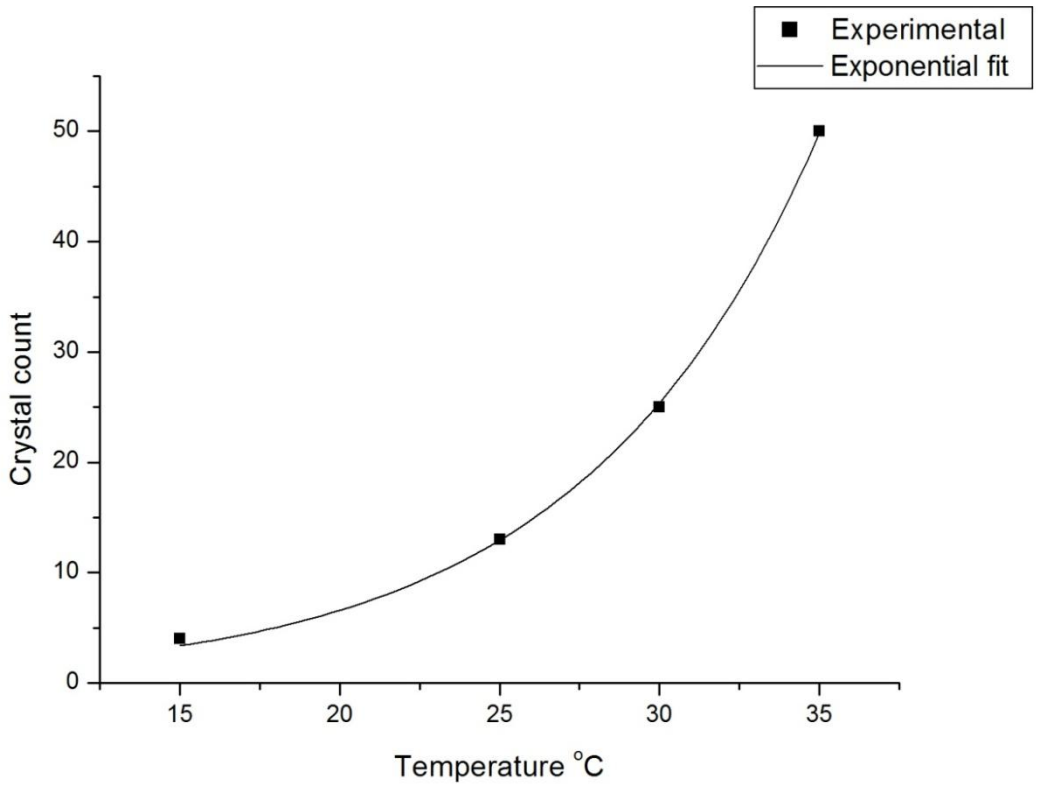

Figure 4.7: Variation of crystal count with temperature at a gel pH of 5.0, keeping the gel density, gel age and upper reactant concentration as constant.

4.3.2 Effect of growth parameters on nucleation rate of gadolinium fumarate heptahydrate (GFH) crystals

A number of experiments were conducted with an aim to grow good quality gadolinium fumarate single crystals suitable for characterization and to observe the effect of various factors on the nucleation rate. The experiments were conducted for different concentrations of upper/lower reactant, gel pH, gel age, gel concentration and for different temperatures. The optimum conditions for the growth of better size and better quality of these crystals are: gel pH 5.0; UR concentration, 0.25 M; LR concentration, 0.07 M; gel ageing, 72 h and gel concentration, 0.4 M. The effect of various growth parameters on the growth of gadolinium fumarate heptahydrate single crystals is summarized in table 4.1.

4.3.3 Effect of growth parameters on nucleation rate of mixed gadolinium-terbium fumarate heptahydrate (GTFH) single crystals

It was again observed that a gel pH in the range $5.0 \leq pH < 6.0$ remained fruitful in yielding mixed single crystals of Gd-Tb fumarate heptahydrate in the upper part of gel column just after 3-4 days of pouring of the upper reactant. For the gel solution of $pH \geq 6.0$, a strong precipitation was observed to form within an hour near the gel/solution interface after pouring of the upper reactant. The experiments were conducted for different concentrations of upper/lower reactant, gel pH, gel age, gel concentration and for different temperatures and the effect of these parameters on the nucleation rate was found exactly the same as that of for the production of pure TFH and GFH single crystals as discussed in section 4.3.1 and 4.3.2. The morphology of the crystals is well faceted and clearly exihibits the symmetry of a monoclinic system.

4.4 Super-saturation as the cause of nucleation

In the pH range $5.0 \leq pH < 6.0$, due to the high electron affinity of oxygen atoms only two H-atoms of the carboxyl group will leave the precipitant ion as $(C_4O_4H_2)^{2-}$, which are anions of fumaric acid and the other two oxygen atoms of fumaric acid are doubly bonded with C-atoms. A decrease in pH results in the addition of more H^+ ions to the system and therefore the concentration of precipitant ions decreases with the decrease in pH [189]. This is due to the common ion effect in which more fumarate ions get neutralized by H^+ ions. Thus, the ionic concentration product

Table 4.1: The effect of different parameters on the nucleation kinetics of gadolinium fumarate heptahydrate single crystals

Experiment	Constant Parameters	Changing Parameters	Results
Variation of UR concentration	LR conc.(0.07 M) Gel age (48h) Gel pH (5.8) Gel conc. (0.4 M)	UR conc. (0.2 M, 0.3 M, 0.4 M,0.5 M)	(i) Nucleation rate increases exponentially with increase in UR conc. (ii) Crystal size of same morphology decreases with increase in UR conc.
Variation of LR concentration	UR conc. (0.25M) Gel age (72 h) Gel pH (5.0) Gel conc. (0.4 M)	LR conc. (0.06 M, 0.07 M, 0.08 M, 0.09 M)	(i) Nucleation rate increases exponentially with increase in LR conc. (ii) Crystal morphology remains same as above.
Variation of gel pH	UR conc. (0.25 M) LR conc. (0.07 M) Gel pH (5.5) Gel conc. (0.4 M)	Gel pH (5.0,5.4, 5.8,6.0)	(i) Nucleation rate increases exponentially with increase in pH for the range $5 \leq$ pH <6. (ii) Single crystal growth conducive for $5 \leq$ pH < 6 (iii) Fast precipitation at pH > 6.
Variation of gel age	UR conc. (0.3 M) LR conc. (0.07 M) Gel pH (5.3) Gel conc. (0.4 M)	Gel ageing (24,48, 72,96 hours)	(i) Nucleation rate decreases linearly with increase in gel age. (ii) Crystals of different Morphologies are formed at higher gel ages.
Variation of gel concentration	UR conc. (0.25M) Gel age (48h) Gel pH (5.5) LR conc. (0.07M)	Gel conc. (0.2M, 0.3 M, 0.4 M,0.5 M)	(i) Nucleation rate decreases linearly with increase in gel conc. (ii) Well faceted crystals are formed at gel conc. of 0.4 M.
Variation of temperature	UR conc. (0.25M) Gel age (48h) Gel pH (5.0) LR conc. (0.07M) Gel conc. (0.4M)	Temperature 15 ^{o}C 25 ^{o}C 30 ^{o}C 35 ^{o}C	(i) Nucleation rate increases exponentially with increase in temperature. (ii) Size of crystals decreases with increase in temperature.

Abbreviations used: Upper reactant (gadolinium chloride) UR; Lower reactant (fumaric acid) LR.

$[Tb^{3+}]$ $[(C_4O_4H_2)^2]$ or $[Gd^{3+}]$ $[(C_4O_4H_2)^{2-}]$ decreases and becomes just equal to the solubility product K_{sp}. As such, the value of local supersaturation at different sites inside the gel changes and thus the initial nuclei get sufficient time to grow both in lateral and longitudinal direction for the formation of single crystals. But, at very low pH less than 5.0, the ionic product becomes much less than the solubility product K_{sp} and the solution becomes under-saturated. At this very low pH, the crystals do not grow at all. However, at higher pH, the ionic concentration product is greater than the solubility product K_{sp}, therefore, a strong precipitation occurs near the gel- solution interface [190]. The experimental results as described in section 4.3.1 reveal that the number of crystals grown in the entire gel column for a fixed period of time increases exponentially with the increase in concentration of upper reactant, gel pH and temperature as shown in Fig. 4.1, Fig. 4.4 and Fig. 4.7 respectively. Whereas, the crystal count decreases linearly with the increase in gel age and gel concentration as shown in Fig. 4.2 and Fig. 4.3 respectively. This type of behaviour has been reported for crystal growth of some other rare-earth compound [191]. Such types of trends in crystal count corresponding to various growth parameters were also observed by Arora et al [192]. The linear variations of these trends are consequences of variation of gel structure which may include pore size, cross linkage of cell boundaries etc. Due to increase in gel age and gel concentration, the pore size becomes small and the gel also becomes hard, as a result of which the nucleation rate decreases [109]. Due to this the supersaturation and hence nucleation probability decreases as many nuclei find themselves in cells of too small size to support growth to visible crystal sizes. The exponential growth of crystals may be discussed in the light of classical nucleation theory [140]. As discussed in section 2.3.1 of chapter-2, the = n. (2.13) gives the nucleation rate i.e, the number of nuclei formed per unit time per unit volume can be expressed as, $\mathbf{J = J_0 exp}\left[\frac{-16\pi\sigma^3\,\Omega^2}{3k^3T^3(lnS)^2)}\right]$, where J_o is a pre-exponential numerical factor.

The above equation shows that the nucleation rate depends on three main variables; temperature T, degree of supersaturation S, and interfacial tension σ. The interfacial tension σ has negligible effect on the probability of nucleation, if the growth occurs in the same medium and at constant temperature the probability of nucleation is mainly determined by the concentration of reactants and the gel structure

which can be affected by gel pH, gel concentration and gel age etc. Thus, by increasing the molarity of upper reactant and keeping the other parameters constant, probability of Tb^{3+} ions to react with fumarate ions in the gel increases. This increases the supersaturation and leads to an increase in the probability of nucleus formation as per classical nucleation theory. Thus, it is expected that the number of crystals will increase with the increase in probability of nucleation, hence the number of crystals in the gel column increases exponentially as shown in Fig. 4.1. The increase in supersaturation leading to an increased number of lysozyme crystals has also been reported by Judge et al. [186]. Further at constant temperature, by increasing the value of pH within a range $5.0 \leq pH < 6.0$, the ion concentration product $[Tb^{3+}]$ $[(C_4O_4H_2)^{2-}]$ or $[Gd^{3+}]$ $[(C_4O_4H_2)^{2-}]$ increases and may lead to increase in the crystal count as shown in Fig. 4.4. From the classical nucleation theory, the nucleation rate increases exponentially up to a certain temperature called the critical temperature. Beyond the cricitical temperature the nucleation rate falls because of the degree of superaturation S, for which critical nucleation decreases as a function of temperatute ($\ln S \propto 1/T$). As a result of which the nucleation rate goes through a maximum only up to the critical temperature. However, in the present investigation the variation of number of crystals with temperature has been obtained much below the critical temperature after which the nucleation rate starts decreasing. The difficulty in obtaining the complete nucleation rate curve for gel systems is due to instability of the gel itself at high temperatures. Fig. 4.7 shows the variation of crystal count corresponding to the different temperature of crystallizers. The dependence of nucleation rate on the crystallization temperature has been reported to be in accordance with the classical nucleation theory [193].

4.5 Characterization

4.5.1 General morphology

As far as the morphology of crystals grown in the present study is concerned, the experimental results for a gel solution of gel pH in the range $5.0 \leq pH < 6.0$ yielded the single crystals in the upper part of gel column just after 3-4 days of pouring of the upper reactant at a normal room temperature environment. Fig. 4.8 (a) and (b) shows an optical micrograph and SEM micrograph of a typical single crystal of terbium

fumarate heptahydrate (TFH), whereas, Fig. 4.8 (c) shows a SEM micrograph of a small region of (100) face at a magnification of 8500X. The magnified image of the crystal face shows that the growth of (100) face takes place by two-dimensional spreading and piling up of layers. Such type of growth normally takes palce when the supersaturation is high. Fig. 4.8 (d) shows a schematic diagram depicting the general morphology of a typical TFH single crystal. This diagram has been obtained by using the Krystal Shaper software (http://www.jcrystal.com/products/krystalshaper). The morphology of the crystal is well faceted and clearly exihibits the symmetry of a monoclinic system. Fig. 4.9 (a) shows SEM micrograph of a typical single crystal of gadolinium fumarate heptahydrate (GFH) and Fig. 4.9 (b) shows its schematic diagram depicting the general morphology. Fig. 4.10 and Fig. 4.11 show the SEM micrograph and optical micrograph of mixed gadolinium-terbium fumarate heptahydrate (GTFH) single crystals respectively.

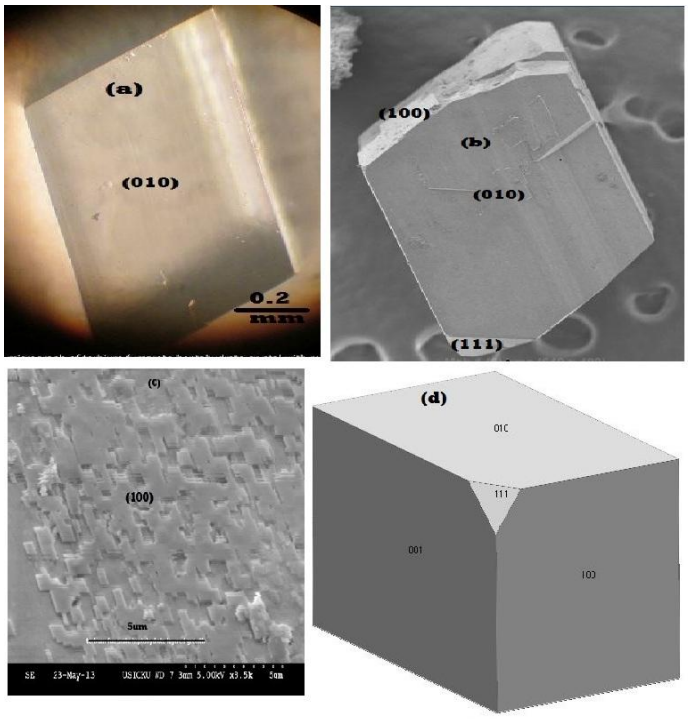

Figure 4.8: (a) Optical micrograph (b) SEM micrograph at a magnification 65X. (c) SEM micrograph of (100) face at a magnification 8500X illustrating the two dimensional layered growth and (d) Schematic diagram illustrating the general morphology, of a typical terbium fumarate heptahydrate single crystal.

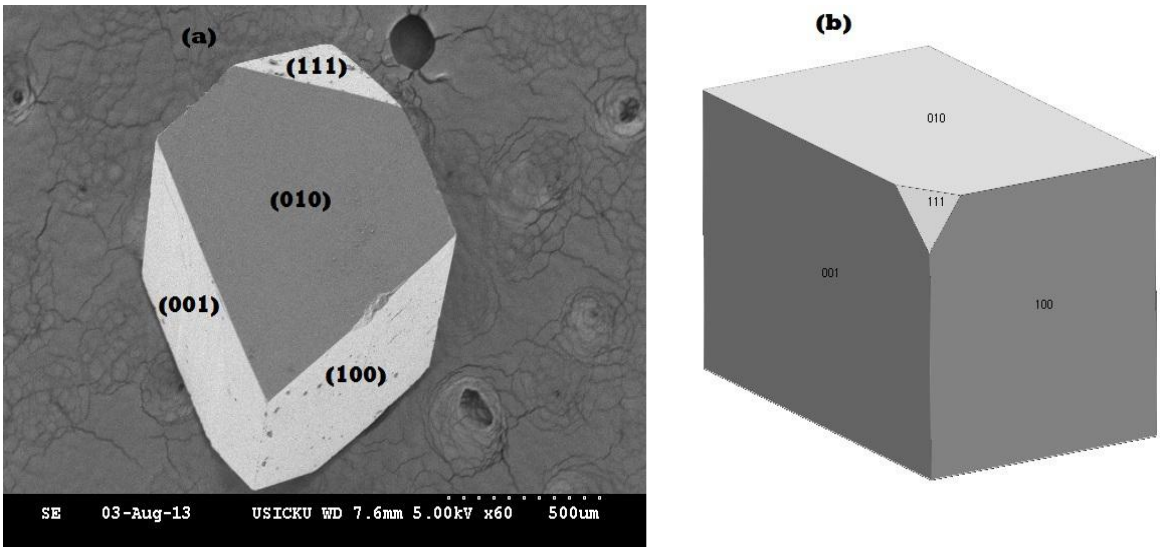

Figure 4.9: (a) SEM micrograph at a magnification 60X and (b) Schematic diagram depicting the general morphology, of a typical GFH single crystal.

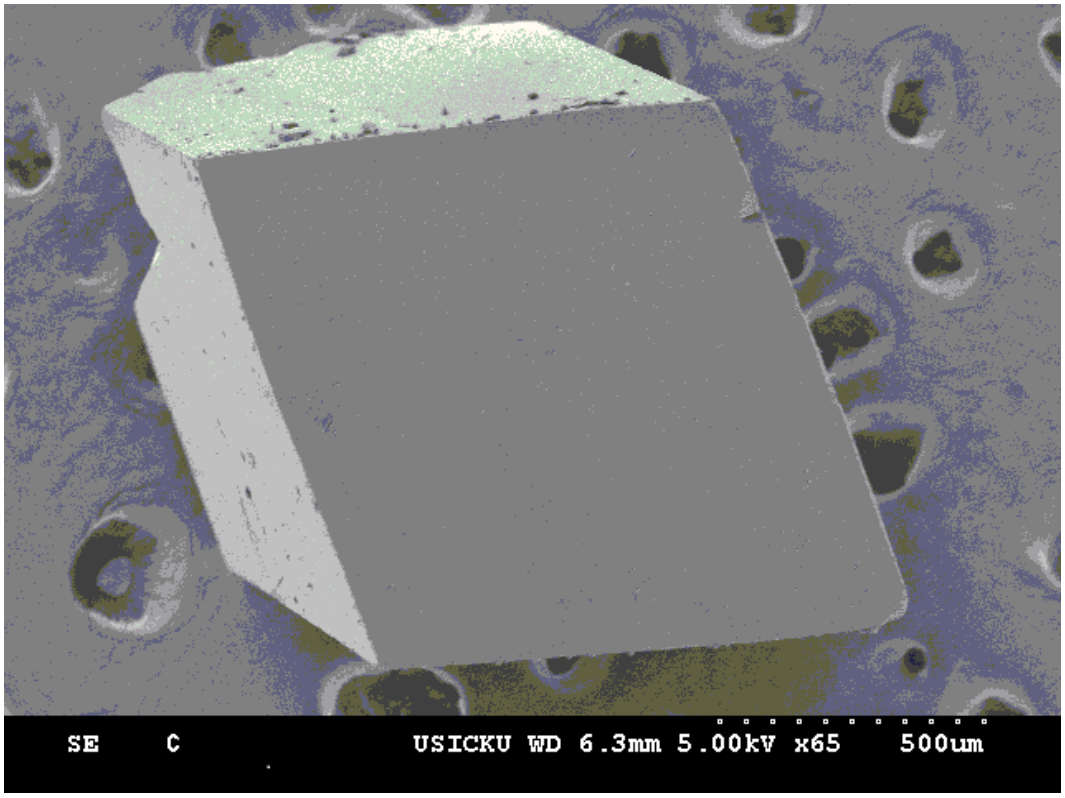

Figure 4.10: SEM micrograph of mixed GTFH single crystal at a magnification 65X.

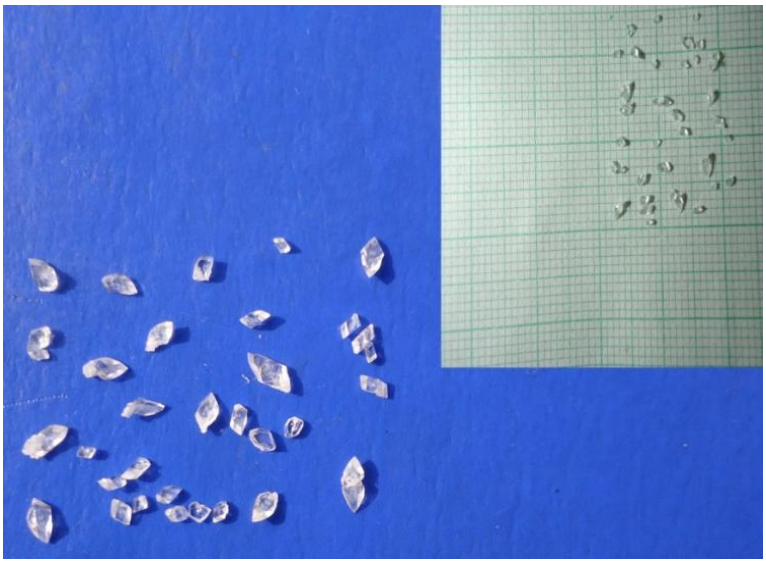

Figure 4.11: Optical micrograph of some typical single crystals of mixed GdTb fumarate.

4.5.2 Powder X-ray diffraction results

As far as the powder X-ray diffraction of any material is concerned, the occurrence of highly resolved peaks at specific Bragg angles indicates that such a material is a crystalline solid. Each peak represents a certain lattice plane and can therefore be characterized by a Miller index. The powder XRD patterns of the compounds grown in the present work are given below. Powder X-ray diffraction (PXRD) data was collected using a Bruker D8 advance X-ray diffractometer with monochromated Cu-Kα radiation (λ=1.5406 Å).

4.5.2.1 Powder XRD of terbium fumarate heptahydrate crystals

Fig.4.12 shows the powder XRD pattern of terbium fumarate heptahydrate. Well defined peaks in the pattern suggest the crystallinity of the grown compound. To identify the phase of terbium fumarate heptahydrate (TFH) complex, a phase matching search was carried out using the Crystallography Open Database [COD ID #7006886] [194]. The powder pattern of samarium fumarate was simulated using a program, Reflex, incorporated in the Accelrys Materials Studio software. Reflex uses a novel indexing algorithm X-Cell [195], along with three well known and popular indexing algorithm, TREOR90, DICVOL91, and ITO. The Reflex simulates X-ray, neutron, and electron powder diffraction patterns based on models of crystalline materials. The simulated powder pattern of samarium fumarate was generated from its

Crystallographic Information File (cif) obtained from the Crystallography Open Database website. The simulated powder pattern of samarium fumarate heptahydrate and the experimental powder pattern of TFH compound is shown in inset of Fig. 4.12 (a, b). The powder XRD pattern of the compound matches well with the simulated powder XRD pattern of samarium fumarate heptahydrate. As such, it is suggested that TFH compound grown in the present work is isomorphous with samarium fumarate heptahydrate [66], belonging to space group $P2_1/n$. This space group belongs to a centro-symmetric class of crystals.

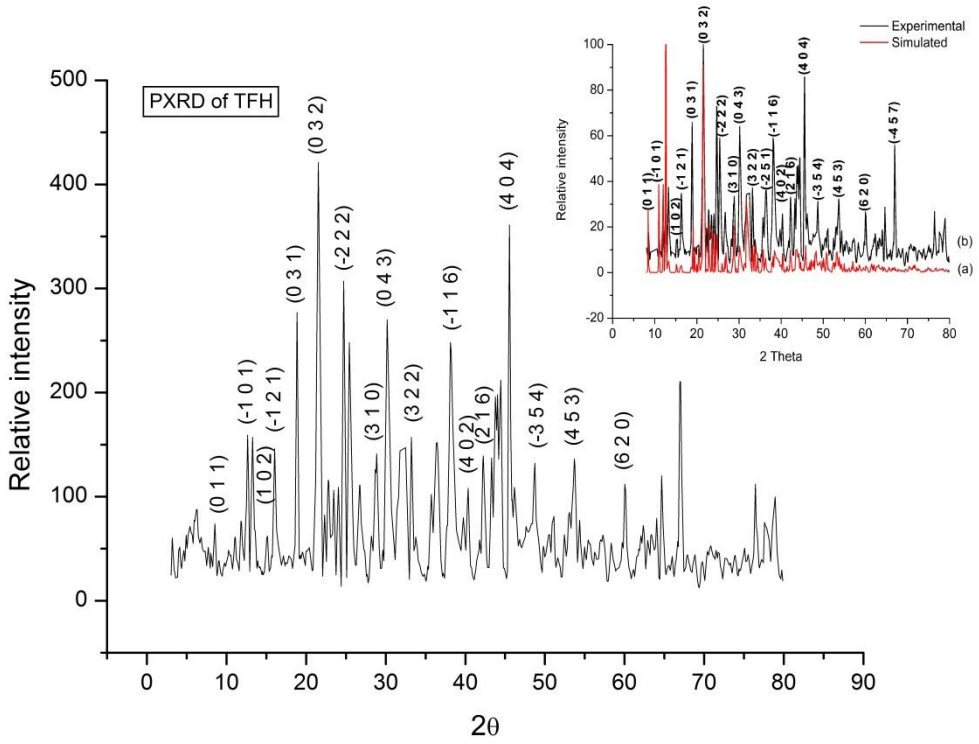

Figure 4.12: PXRD of terbium fumarate heptahydrate with inset graph showing: (a) Simulated powder pattern of samarium fumarate heptahydrate (b) powder pattern of terbium fumarate heptahydrate.

4.5.2.2. Powder XRD of gadolinium fumarate heptahydrate crystals

The powder XRD pattern of gadolinium fumarate heptahydrate crystals is shown in Fig. 4.13. The powder X-ray data was indexed using CRYSFIRE program [196]. The as-grown GFH crystals belong to monoclinic system withspace group $P2_1/n$. The cell parameters obtained are: a= 9.225 Å, b= 14.501 Å, c= 14.645 Å, $\alpha = 90^o$; $\beta = 91.26^o$ and $\gamma = 90^o$.

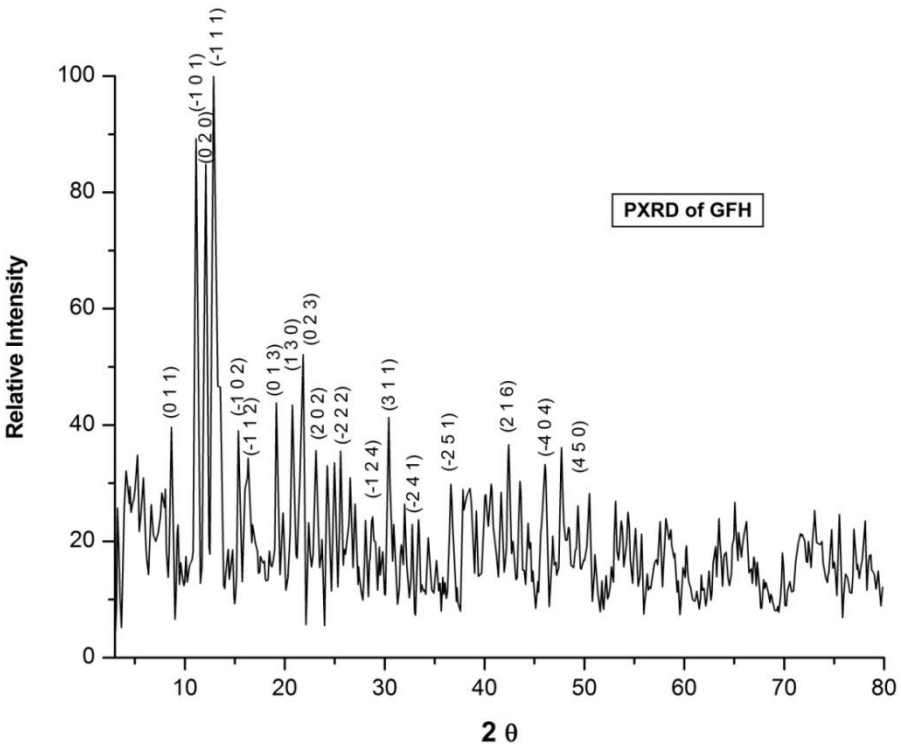

Figure 4.13: PXRD pattern of gadolinium fumarate heptahydrate single crystals.

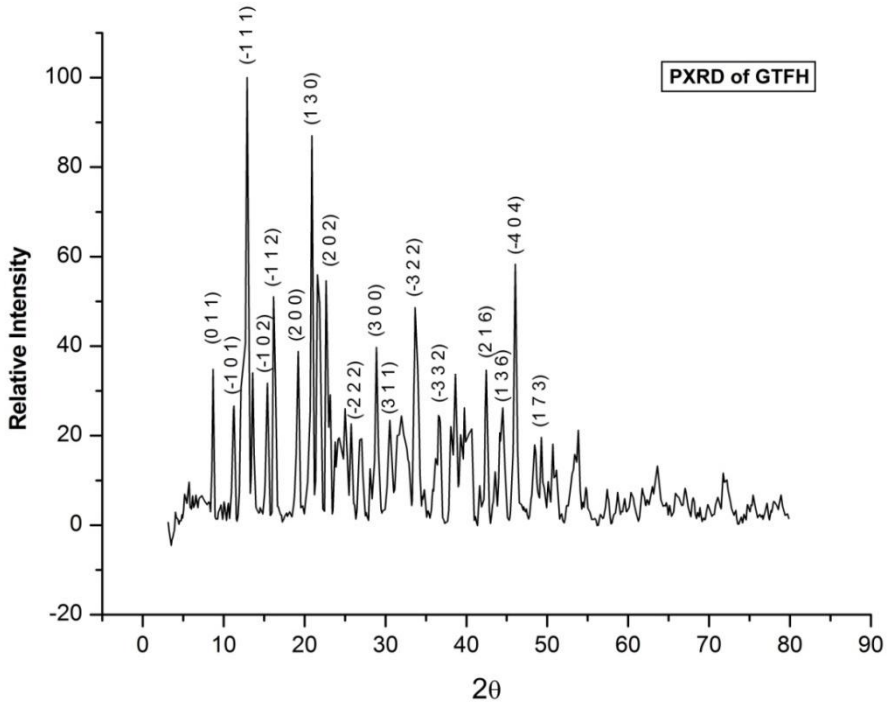

Figure 4.14: PXRD pattern of mixed gadolinium-terbium fumarate single crystals.

4.5.2.3. Powder XRD of gadolinium-terbium fumarate heptahydrate crystals

Fig.4.14 shows the powder XRD pattern of mixed gadolinium-terbium fumarate heptahydrate (GTFH) crystals. Its powder data was also indexed using CRYSFIRE program in the same way as mentioned before. The mixed GTFH crystals were also found to belong to monoclinic system with the space group $P2_1/n$. The cell parameters were found to be: a= 9.2705 Å, b= 14.3701 Å, c= 14.3602 Å, $\alpha = 90^o$; $\beta = 91.41^o$ and $\gamma = 90^o$.

4.5.3 Comparative study of X-ray diffraction results

From the powdered X-ray data of the title compounds, various planes of reflections were indexed by using Crysfire programme [196]. The observed d-values for different 2θ with hkl indices of the corresponding planes for GFH and mixed GTFH crystals were matched with the simulated powder pattern of terbium fumarate heptahydrate (TFH) crystals and their comparative results are tabulated in Table 4.2. The close agreement between the d-values of single and mixed rare-earth fumarate crystals support our assumption that the fumarate crystals containing two rare-earth elements of comparable ionic radii (Tb= 1.095Å; Gd= 1.107 Å) can be formed by substitutional exchange of ions and are isostructural with single rare-earth fumarate crystals. The substitutional exchange of ions of two rare-earths of comparable ionic radii and the iso-structurality of mixed compound with single component crystals is also reported in the literature [197]. Moreover, from the powdered X-ray data of GFH and GTFH crystals, their lattice parameters were evaluated. These lattice parameters were found very close to the lattice parameters of TFH crystals as obtained from its single crystal X-ray diffraction analysis which will be discussed in section 4.5.4. Therefore, the isostructural nature of as-grown crystals can also be confirmed by their comparative study of lattice parameters as tabulated in Table 4.3. As such, it is suggested that both pure and mixed rare-earth fumarate crystals grown in the present work are isomorphous to each other.

Table 4.2: Comparative results of observed d-values, 2θ values and miller indices of XRD results of pure and mixed rare-earth fumarate heptahydrate crystals.

Terbiumfumarate heptahydrate			**Gadoliniumfumarate heptahydrate**			**Mixed fumarate heptahydrate**		
2θ(deg)	d- values	(h k l)	2θ(deg)	d- values	(h k l)	2θ(deg)	d- values	h k l
8.544	10.387	0 1 1	8.577	10.303	0 1 1	8.698	10.156	0 1 1
11.045	8.035	-1 0 1	11.076	7.882	-1 0 1	11.242	7.875	-1 0 1
12.045	7.328	0 2 0	12.075	7.321	0 2 0	12.161	7.185	0 2 0
12.878	6.933	1 1 1	12.875	6.925	-1 1 1	12.895	6.906	-1 1 1
15.358	5.743	1 0 2	15.363	5.796	-1 0 2	15.386	5.744	-1 0 2
16.358	5.415	-1 2 1	16.344	5.382	-1 1 2	16.399	5.333	-1 1 2
19.192	4.637	0 3 1	19.218	4.611	0 1 3	19.210	4.634	2 0 0
20.838	4.274	2 1 1	20.743	4.281	1 3 0	20.863	4.255	1 3 0
21.839	4.071	0 3 2	21.863	4.049	0 2 3	21.867	4.067	1 3 1
23.172	3.852	-2 2 1	23.195	3.864	2 0 2	23.122	3.850	2 0 2
25.652	3.523	-2 2 2	25.597	3.463	-2 2 2	25.674	3.453	-2 2 2
28.986	3.079	3 1 0	28.780	3.099	-1 2 4	28.878	3.198	3 0 0
30.486	2.936	0 4 3	30.505	2.928	3 1 1	30.505	2.941	3 1 1
32.133	2.778	-1 1 5	32.770	2.734	-2 4 1	32.670	2.745	1 5 0
33.466	2.674	3 2 2	33.391	2.668	-2 4 2	33.627	2.660	-3 2 2
36.125	2.231	-2 5 1	36.104	2.222	-2 5 1	36.121	2.231	-2 5 1
42.159	2.111	2 1 6	42.131	2.119	2 1 6	42.142	2.125	2 1 6
46.094	1.967	4 0 4	46.102	1.971	-4 0 4	46.102	1.969	-4 0 4
49.407	1.844	2 2 7	49.401	1.841	4 5 0	49.301	1.845	1 7 3

Table 4.3: Comparative study of lattice parameters of terbium fumarate, gadolinium fumarate and mixed gadolinium-terbium fumarate heptahydrate crystals.

Chemical formula	$Tb_2(C_4H_2O_4).7H_2O$ (From SXRD analysis)	$Gd_2(C_4H_2O_4).7H_2O$ (calculated)	$GdTb(C_4H_2O_4).7H_2O$ (calculated)
Space group	$P2_1/n$	$P2_1/n$	$P2_1/n$
Lattice type	Monoclinic	Monoclinic	Monoclinic
a, Å	9.4495	9.225	9.2705
b, Å	14.6561	14.501	14.3701
c, Å	14.7272	14.645	14.3602
α, deg	90	90	90
β, deg	91.318	91.26	91.41
γ, deg	90	90	90
V, $Å^3$	2039.1	2076.3	1913

4.5.4 Single Crystal X-ray diffraction of terbium fumarate heptahydrate

4.5.4.1 Introduction

Single crystal X-ray diffraction is a versatile analysis and its importance has increased by the improvement of the experimental devices, which resulted in the progress of crystal structure solution and refinement methodologies [198]. The size of the crystal used should be 0.1-0.2 mm in the three direction of space. From single crystal X-ray data it is possible to solve and refine the crystal structure of any new material. For the determination of crystal structure of a TFH crystal, its single crystal XRD analysis was carried out by using Bruker Kappa Apex ii single crystal X-ray diffractometer. The structure was solved by direct methods and refined by full-matrix least squares cycles in SHEL XL-97 [199].

4.5.4.2 Structural analysis

Fig. 4.15 shows the asymmetric unit of terbium fumarate heptahydrate in which the unique Tb-ion is 8-fold coordinated by four fumarate groups and two water molecules to accomplish a very distorted tri-capped trigonal prism around the Tb-ion. Two of the

fumarate ligands are coordinated in monodentate and the other two in bidentate mode. Thus out of the eight coordinated oxygen atoms, two originate from water molecules and six from fumarate ligands. But, in the asymmetric cell structure the fourth fumarate group with monodentate mode is not seen. The coordination of oxygen atoms with each Tb^{3+} ion can be seen from the ORTEP diagram as shown in Fig. 4.16, where Tb cation is coordinated to eight oxygen atoms. Unit cell of terbium fumarate crystal contains four Tb atoms (Z=4) is shown in Fig. 4.17 and its selected bond lengths (Å) are given in table 4.4. The molecular structure has 2-fold symmetry so that asymmetric unit comprises of one Tb cation, 1.5 fumarate anion and two water molecules. Tb-O distances are from 2.332Å- 2.595Å, with an intradimer Tb….Tb distance of 4.165Å.

Table 4.4: Selected bond lengths of terbium fumarate single crystals.

Selected Bond lengths (Å)		Selected Bond lengths (Å)	
Tb(1)-O(1)	2.439	C(10)-H(101)	0.9250
Tb(1)-O(2)w	2.423	C(11)-C(12)	1.470
Tb(1)-O(3)	2.451	C(11)-H(111)	0.9350
Tb(1)-O(4)	2.376	C(12)-O(13)	1.277
Tb(1)-O(5)	2.595	C(12)-O(14)	1.257
Tb(1)-O(6)	2.435	O(15)-C(16)	1.261
Tb(1)-O(7)	2.416	C(16)-O(17)	1.267
Tb(1)-O(8)w	2.332	Tb(1)-C(8)	2.929

As expected, the frame work of the compound is microporous and has small 1D void channels as shown in packing diagram shown in Fig. 4.18, which gives a view of 3-D porous frame work. The small channels are partially occupied by both the lattice and coordinated water molecules. In this diagram colour code for Tb is blue; C, green; O, red and H, white. It can be seen that each fumarate ligand acts as a bridging ligand connecting two Tb atoms into two dimensional chiral structure. The layers are linked together through a complicated H-bonding scheme involving the water ligands, hydroxyle O-atoms and carboxylate O-atoms as shown in packing diagram.

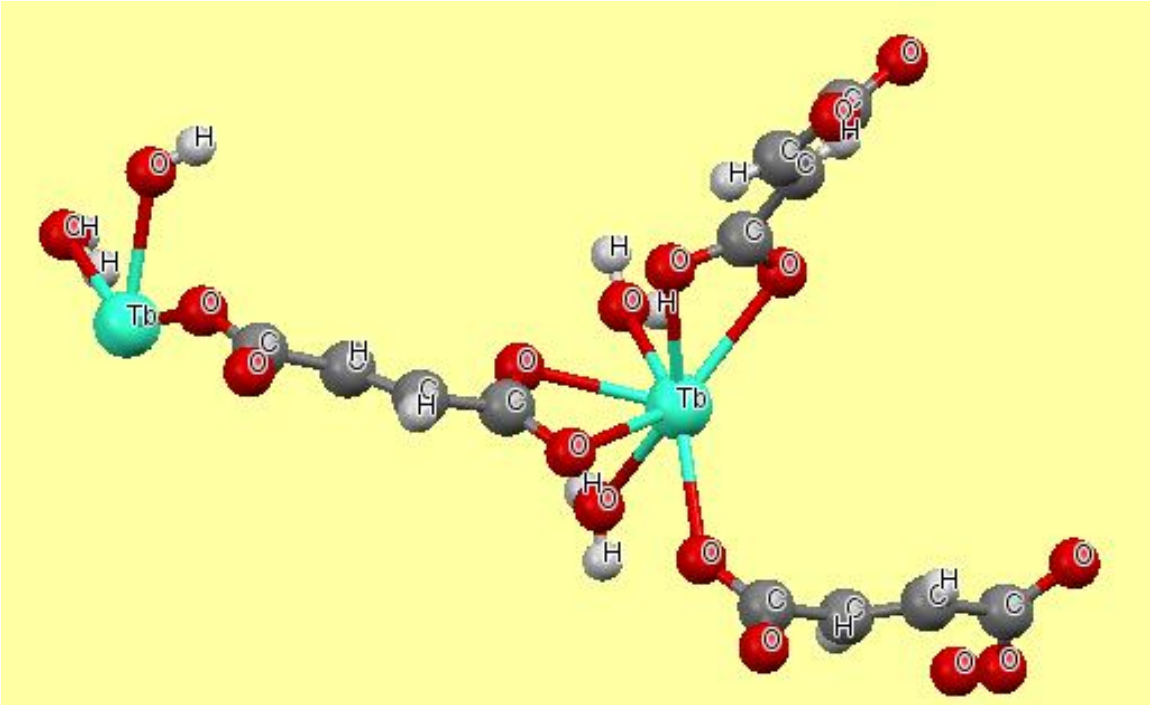

Figure 4.15: Assymmetric unit of terbium fumarate heptahydrate.

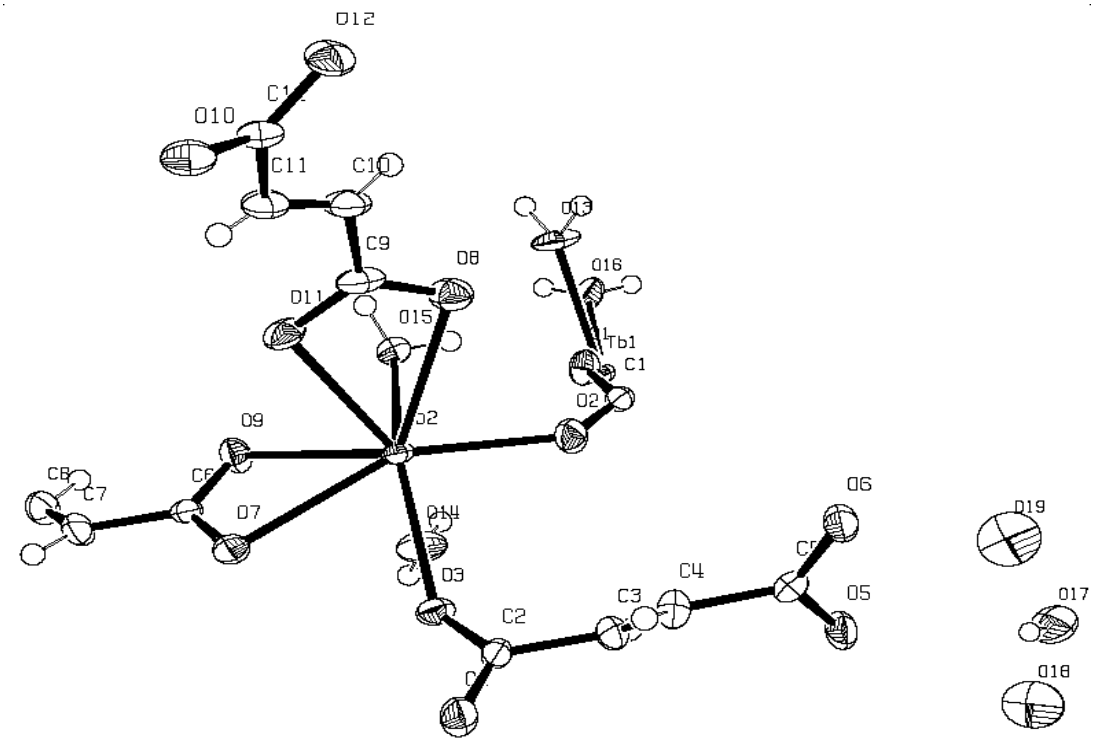

Figure 4.16: ORTEP diagram showing lattice and co-ordinated water molecules in TFH crystals.

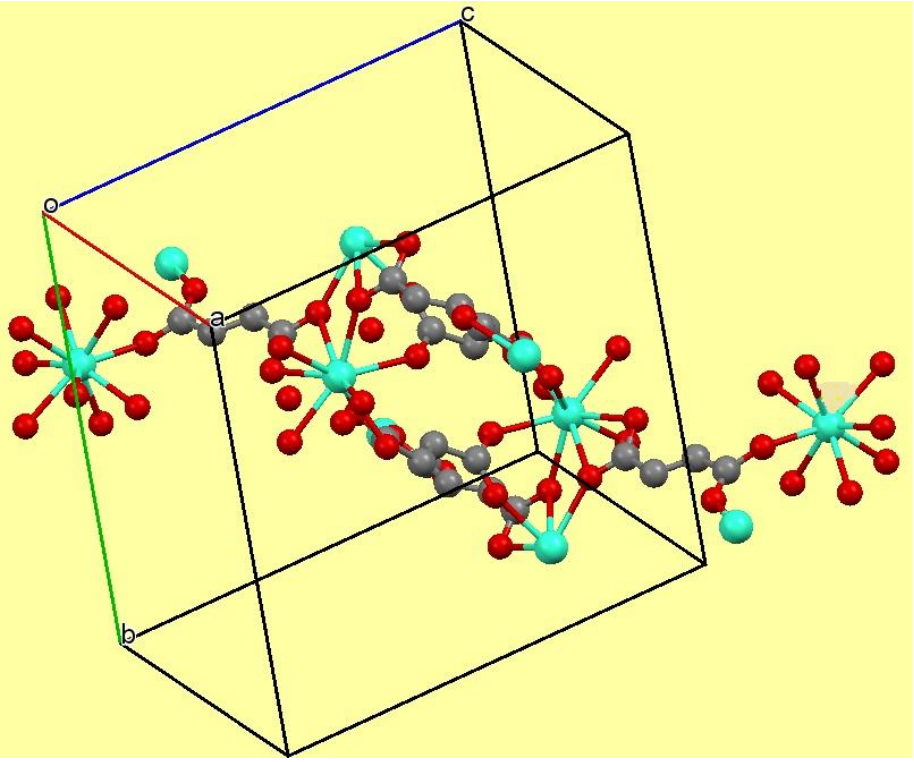

Figure 4.17: Unit cell of terbium fumarate crystal.

4.5.4.3 Co-ordinating behaviour of fumarate ligand

The carboxylate group of fumaric acid exhibits different co-ordinating behaviour. In certain cases, its both oxygen atoms are bonded to the same Tb^{3+} ion forming a loop while as in other cases it acts as a bridge wherein one oxygen atom is bonded with one Tb^{3+} ion and the other oxygen atom with other Tb^{3+} ion as shown in Fig. 4.19. Fumarate ligand shows three types of bridging coordination modes with Tb^{3+} ion. Two of them (L1 and L2) consist of mixed bidentate bridging and chelating modes, while the third type (L3) shows bis-chelating mode.

4.5.4.4 Crystal structure refinement

Crystal structure data for terbium fumarate heptahydrate and its isomorphous compound samarium fumarate heptahydrate crystals is given in Table 4.5. It is observed that the compound under investigation, being isomorphous with samarium fumarate heptahydrate [66], consists of seven water molecules. The presence of these water molecules has been confirmed by the strong absorption band at 3395.28 cm^{-1} in

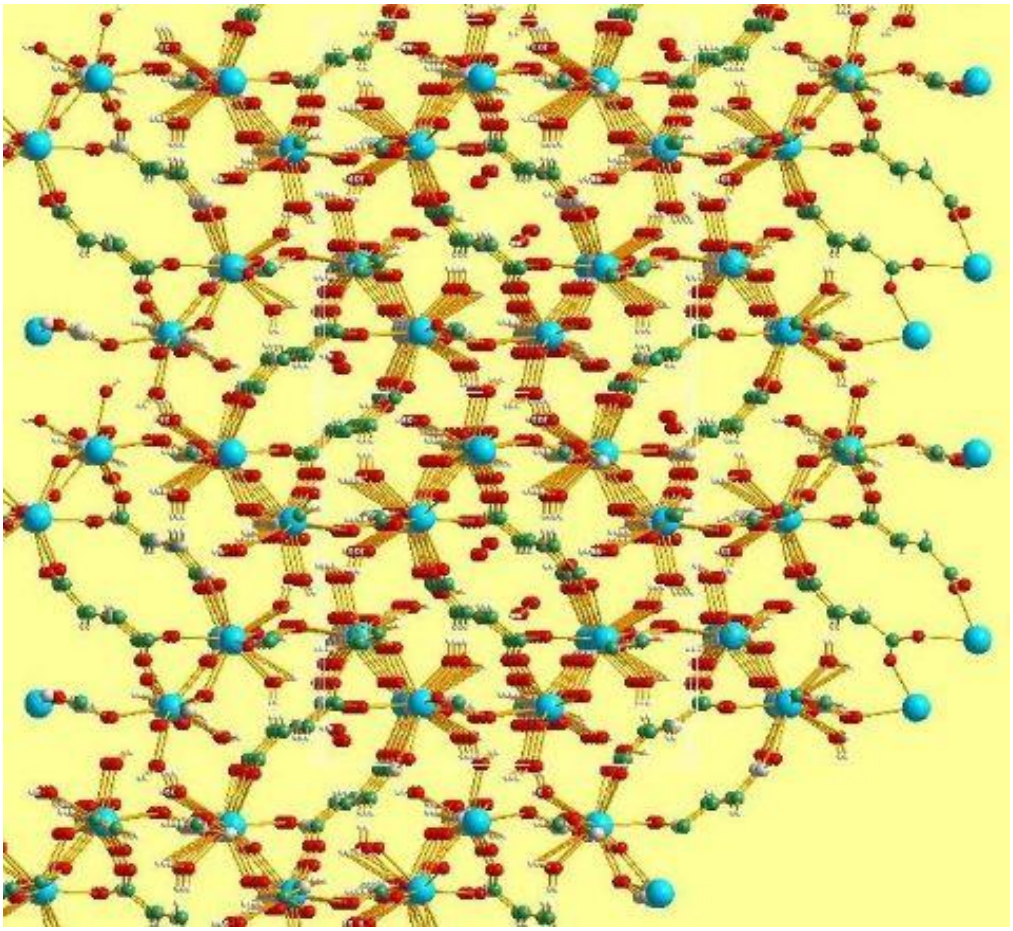

Figure 4.18: Packing diagram of terbium fumarate heptahydrate crystal.

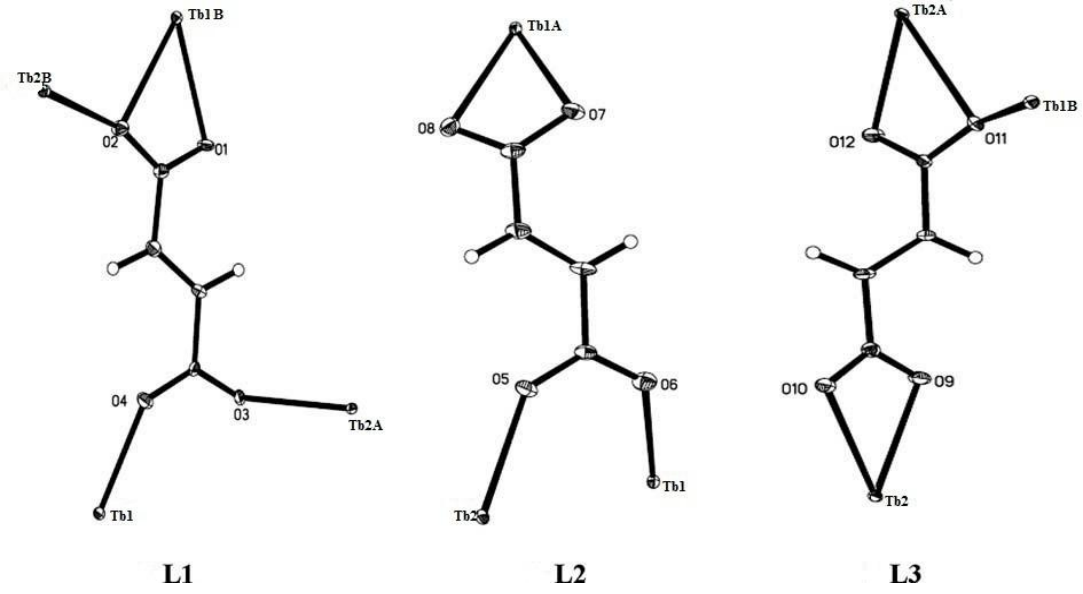

Figure 4.19: Three distinct bonding modes of fumarate ligand in terbium fumarate compound.

Table 4.5: Crystal structure and refinement data for terbium fumarate heptahydrate and its isomorphous compound samarium fumarate heptahydrate single crystals.

	Present compound	Samarium fumarate
Empirical formula	C_{12} H_6 O_{19} Tb_2	$C_{12}H_6O_{19}Sm_2$
Formula weight	772.01	768.98
Crystal size, mm^3	0.60 x 0.50 x 0.30	0.28 x 0.21 x 0.11
T, K	296(2)	293(2)
Space group	$P2_1/n$	$P2_1/n$
Crystal system	Monoclinic	Monoclinic
λ, Å	0.71073	0.710 73
a, Å	9.4495(7)	9.5178(2)
b, Å	14.6561(13)	14.6999(3)
c, Å	14.7272(12)	14.8740(3)
α, deg	90	90
β, deg	91.318(3)	91.2425(3)
γ, deg	90	90
V, $Å^3$	2039.1(3)	2080.54(7)
Z	4	4
d, g/cm^3	2.515	2.363
F(000)	1440	1472
Absorption co. μ(mm^{-1})	6.976	5.685
Reflns. Collected	15134	36935
Unique reflns.	4847	6765

fourier transform infrared spectra of the sample as discussed in section 4.5.7. From the crystal structure refinement data, the space group of the title compound has been found as $P2_1/n$. The ORTEP diagram as shown in Fig. 4.16 shows the presence of both coordinated and lattice water molecules in the title compound which has also been reported elsewhere [200]. It is clear from this figure that each Tb^{3+} ion is coordinated to eight oxygen atoms; out of which six oxygen atoms originate from fumarate ligands and the two from coordinating water molecules (O_{14} and O_{15}). The three non-bonded water molecules (O_{17}, O_{18} and O_{19}) are also shown in the ORTEP

diagram. This is in total conformity with the empirical formula of the compound $[Tb_2(fumarate)_3(H_2O)_4].3H_2O$ for which each Tb^{3+} ion is bonded with 1.5 fumarate ions and two oxygen atoms of water. The compound has same terbium-fumarate ratio of 2:3 as per reported samarium fumarate complex [66].

4.5.5 Elemental analysis

4.5.5.1 EDAX analysis

EDAX analysis is a technique which is widely used to analyze the chemical components in a material under SEM. In this method, the X-rays produced as a result of the electron beam interactions with the sample are detected to analyse it. The X-ray data is processed to obtain the percentage of each measured element present in the sample. In order to confirm the presence of heavy elements, like terbium, gadolinium, carbon and oxygen in the grown samples, all the crystals were characterized by EDAX. In the present work an energy dispersive spectrometer (OXFORD ISIS-300 system) was used to identify the presence of these elements. Fig. 4.20, Fig. 4.21 and Fig. 4.22 show the EDAX spectra of TFH, GFH and GTFH crystals. Table 4.6 shows the comparative atomic and mass percentage of the elements like oxygen, carbon, gadolinium and terbium as obtained from EDAX of the three compounds. So it confirms that the mixed GTFH crystal consists of Gd and Tb in the ratio of 1:1.

Table 4.6: Comparative quantitative EDAX data of TFH, GFH and GTFH crystals.

	Terbium fumarate			Gadolinium fumarate			Mixed Gd-Tb fumarate		
Element	Energy (keV)	Mass % age	Atom % age	Energy (keV)	Mass % age	Atom % age	Energy (keV)	Mass % age	Atom % age
Carbon	0.277	34.86	50.35	0.277	29.66	43.68	0.277	19.98	37.75
Oxygen	0.525	42.95	47.22	0.525	48.75	53.89	0.525	40.57	56.52
Terbium	1.24	22.19	2.43	-	-	-	1.24	20.09	2.84
Gadolini-um	-	-	-	6.053	21.59	2.43	1.185	19.36	2.87
Total		100	100		100	100		100	100

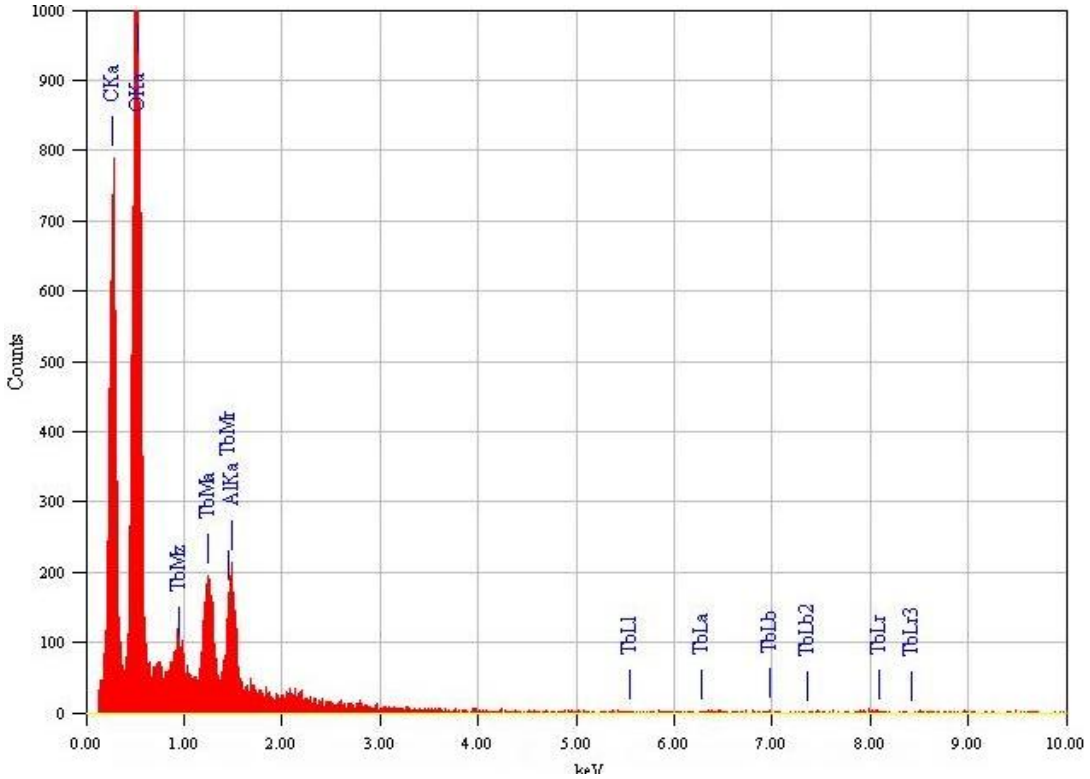

Figure 4.20: EDAX spectrum of terbium fumarate crystals.

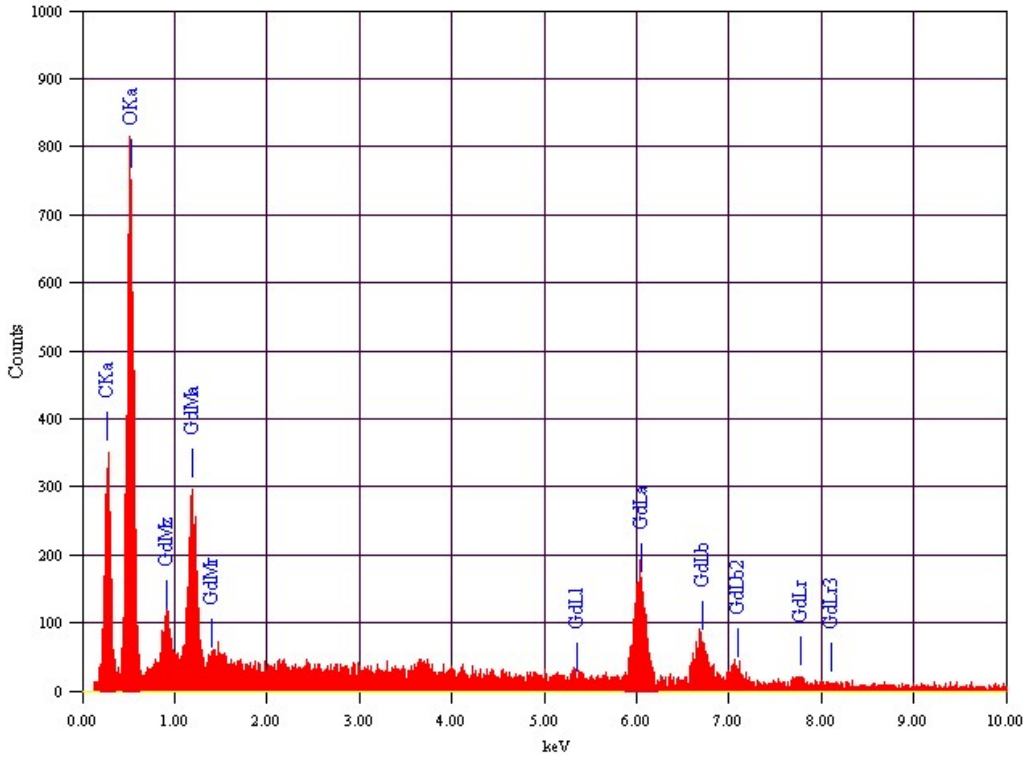

Figure 4.21: EDAX pattern of gadolinium fumarate crystals.

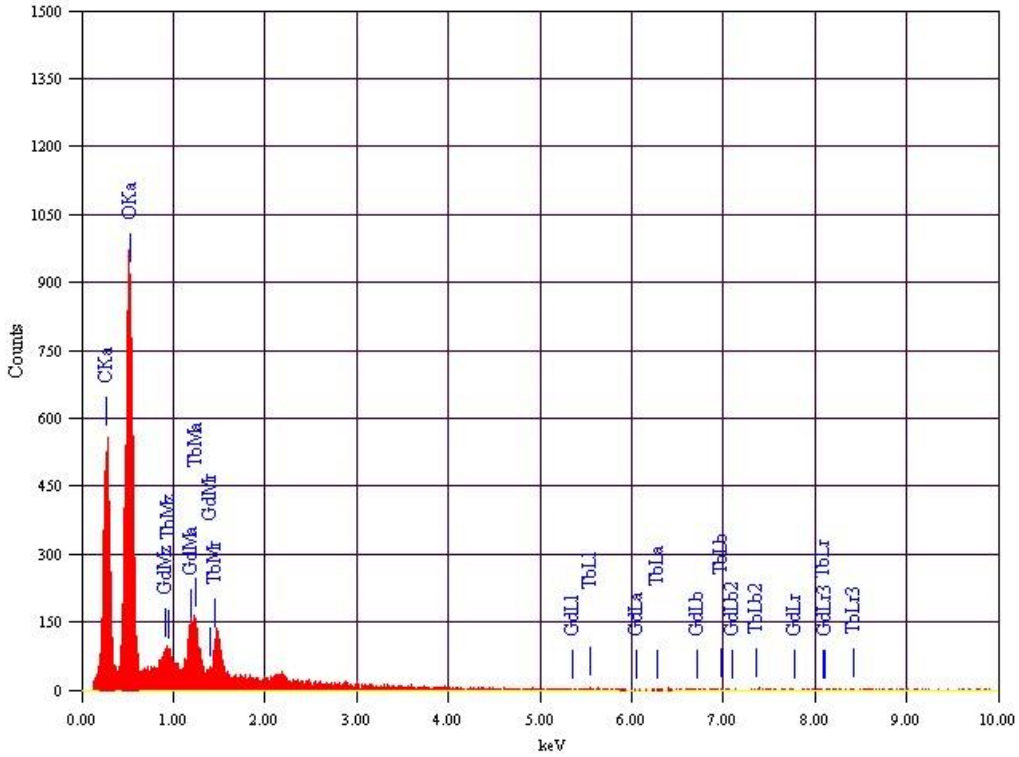

Figure 4.22: EDAX spectrum of mixed Gd-Tb fumarate crystals.

4.5.5.2 CHN analysis

From the CHN analysis of three different compounds as shown in table 4.7, their chemical formula was suggested to be $Tb_2(C_4O_4H_2)_3.7H_2O$; $Gd_2(C_4O_4H_2)_3.7H_2O$ and $GdTb(C_4O_4H_2)_3.7H_2O$ respectively. The presence of seven water molecules in each compound has been supported by their respective thermal analysis as discussed in section 4.5.6. The carbon and hydrogen contents in the grown crystals were determined by using Vario-EL III CHNS-analyzer.

Table 4.7: CHN analysis of TFH, GFH and GTFH crystals.

	Terbium fumarate		Gadolinium fumarate		Mixed Gd-Tb fumarate	
Element	% Mass Calculated	% Mass Experimental	% Mass Calculated	% Mass Experimetal	% Mass Calculated	% Mass Experimental
Carbon	18.33	18.56	18.28	18.06	18.37	18.45
Hydrogen	2.56	2.41	2.55	2.11	2.57	2.02
Nitrogen	0	0	0	0	0	0

4.5.6 Thermal analysis

Thermo gravimetric analysis (TGA) and differential thermal analysis (DTA) are very important characterization techniques which throw light on the thermal stability of the substances. These are utilized for the characterization of decomposition behaviour of the materials.

Simultaneous TGA/DTA curves of TFH, GFH and GTFH single crystals are shown in Fig. 4.23, Fig. 4.24 and Fig. 4.25 respectively. For each compound, the thermal analysis was carried out on a powdered sample by using a Perkin-Elmer thermal analyser in N_2 atmosphere at a heating rate of 10 ^oC/min. The single component rare-earth fumarates i.e TFH and GFH compounds displayed mainly two steps of thermal decomposition for the formation of their oxides in the temperature range of 30–715 ^oC. But the mixed GTFH compound displayed three steps of thermal decomposition for the formation of its oxide in the temperature range of 24- 840 ^oC. Thus, in the temperature range of 80–150 ^oC, TFH compound loses all the seven water molecules corresponding to an endothermic DTA peak at 132.63 ^oC with a weight loss of 16.40 % (calculated weight loss : 16.04 %) and GFH compound also loses all the seven water molecules corresponding to an endothermic DTA peak at 133.63 ^oC with a weight loss of 16.40 % (calculated weight loss : 16.33 %). After the dehydration, both the compounds remain nearly intact until 410 °C, beyond which they decompose. In the second thermal decomposition step of these compounds in the temperature range 410-650 ^oC corresponding to an exothermic DTA peak at 481.5 ^oC, the TFH crystals with experimental weight loss of 37.33 % (calculated loss= 37.42 %) attributes to the liberation of three intra water molecules, six molecules of carbon monoxide and six carbon particles. And in the temperature range of 420-650 ^oC corresponding to an exothermic DTA peak at 484.59 ^oC, the GFH crystals with experimental weight loss of 37.33 % (calculated loss= 38.10 %) also attribute to the liberation of three intra water molecules, six molecules of carbon monoxide and six carbon particles.The liberation of intra water molecules, carbon and carbon monoxide from the anhydrous metal organic compound is also reported in the literature [201]. Therefore, in the temperature range of 38–650 ^oC for TFH crystals, the experimentally observed weight loss of 53.73 % is much closer to the calculated weight loss of 53.46 % and for GFH crystals the experimentally observed weight loss of 53.73 % is much closer to the calculated weight loss of 54.43 %. Likewise, formation of oxides of

some other fumarate compounds is reported in the literature [66, 180]. Thus from TGA/DTA graph of the two compounds, only two chemical reactions have been proposed to take place for each during their thermal decomposition as under:

$$(1)\ Tb_2(C_4O_4H_2)_3.7H_2O \xrightarrow[38-150\ ℃]{-7H_2O} Tb_2(C_4O_4H_2)_3.$$

$$Tb_2(C_4O_4H_2)_3 \xrightarrow[150-650\ ℃]{-(6CO+3H_2O+6C)} Tb_2O_3\ (\text{Terbium oxide})$$

$$(2)\ Gd_2(C_4O_4H_2)_3.7H_2O \xrightarrow[38-150\ ℃]{-7H_2O} Gd_2(C_4O_4H_2)_3.$$

$$Gd_2(C_4O_4H_2)_3 \xrightarrow[150-650\ ℃]{-(6CO+3H_2O+6C)} Gd_2O_3\ (\text{Gadolinium oxide}).$$

In order to confirm the oxide formation of these compounds during their second step of thermal decomposition, the powder X-ray diffraction pattern was obtained for the final product of one of the isomorphous compound terbium fumarate heptahydrate and is discussed in section 6.3.1 of chapter-6.

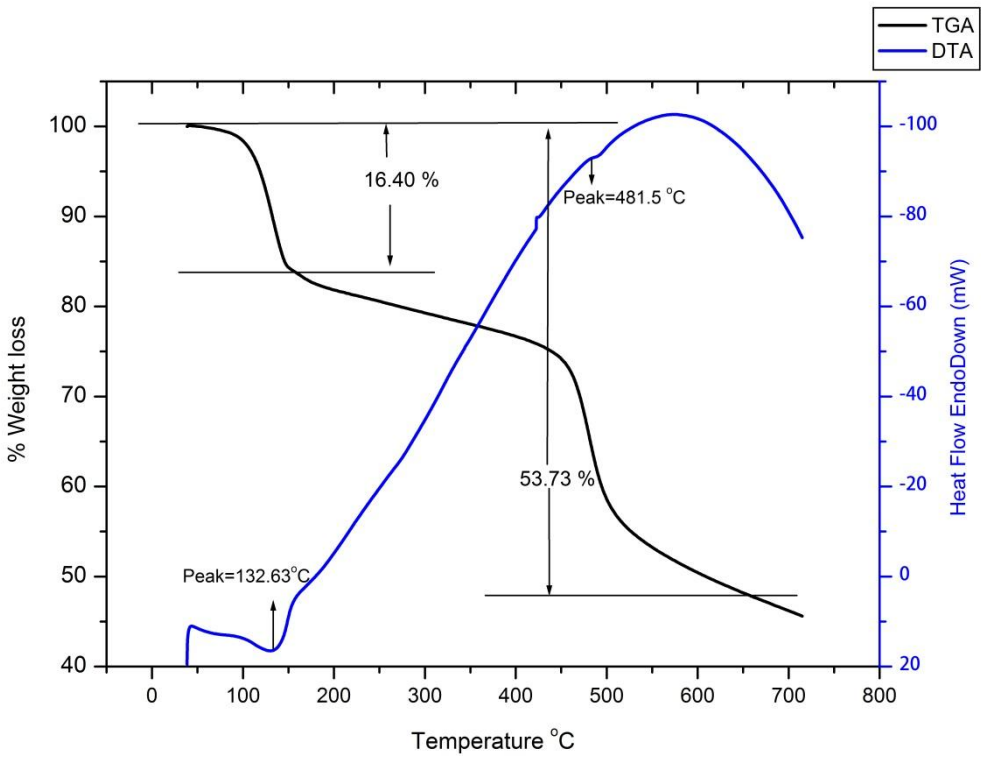

Figure 4.23 TGA/DTA curves of terbium fumarate heptahydrate crystals.

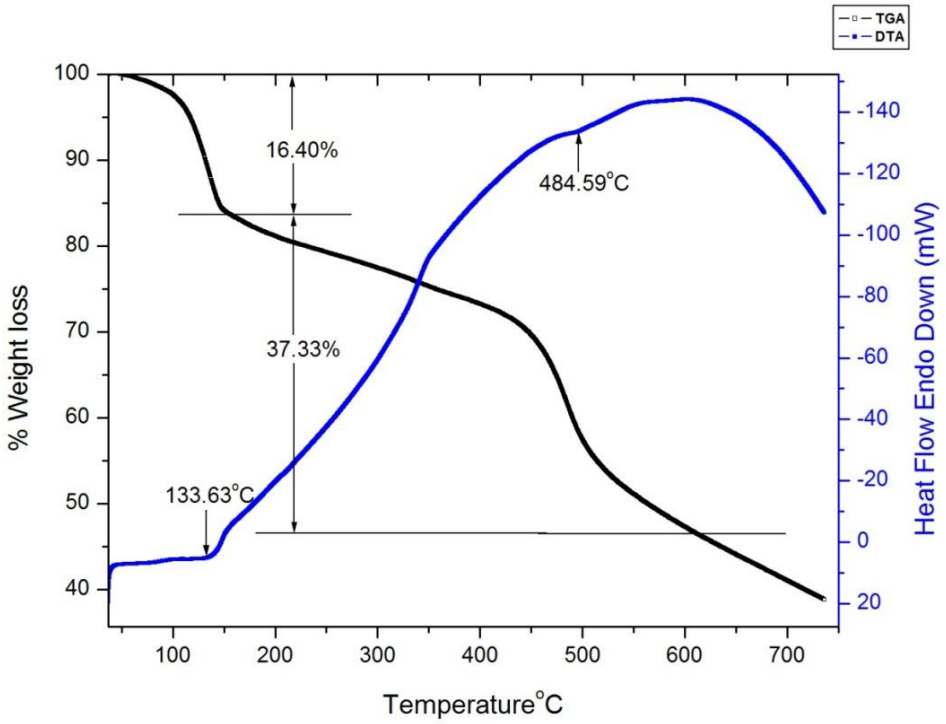

Figure 4.24 TGA/DTA curves of gadolinium fumarate heptahydrate crystals.

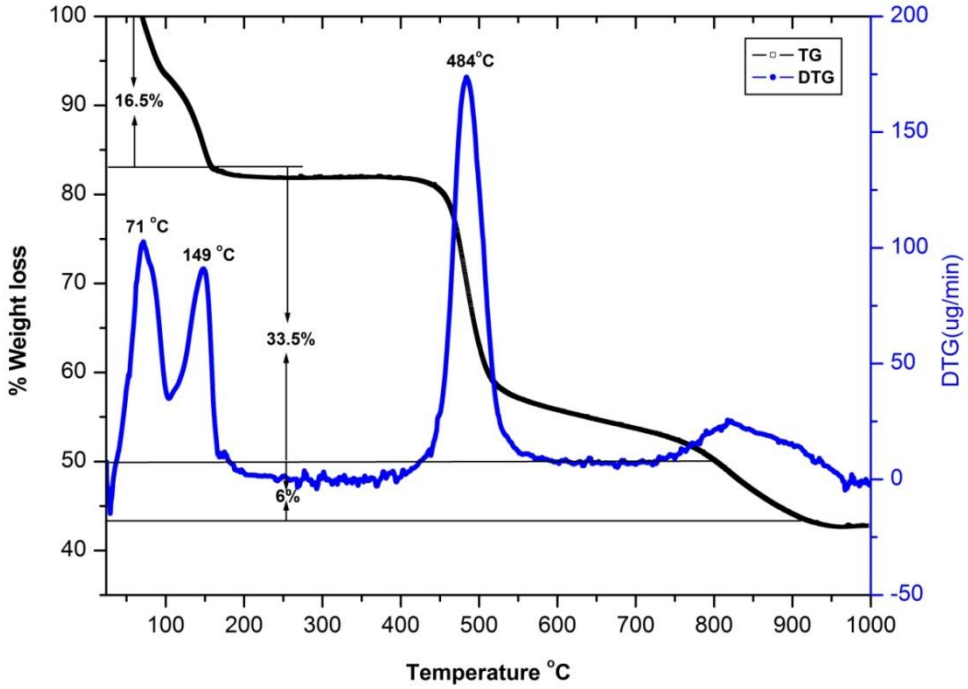

Figure 4.25 TGA/DTA curves of mixed GTFH crystals.

Unlike pure fumarate crystals, the mixed fumarate crystals display three steps of thermal decomposition in the temperature range of 24–1000 ^{o}C as shown in Fig. 4.25 The compound loses all the seven water molecules in the temperature range of 85–150 ^{o}C. The DTG peaks at 85 ^{o}C and 149 ^{o}C may correspond to the liberation of three lattice and four coordinated water molecules respectively from the title compound. Thus, in the temperature range 85–150 ^{o}C for GTFH crystals the experimental weight loss= 16.5 % (calculated weight loss: 16.18 %). After the dehydration, the anhydrous GTFH compound remains nearly intact until 450°C, beyond which it decomposes in two decomposition steps corresponding to DTG peaks at 484 ^{o}C and 840 ^{o}C respectively. This decomposition temperature of the mixed dehydrated compound is more than that of the pure fumarate compound reported earlier, thereby suggesting that the mixed fumarate compound is more thermally stable than the pure fumarate compounds. In the temperature range of 450- 820 ^{o}C, corresponding to the DTG peak at 484 ^{o}C, the experimental weight loss of 33.5 % (calculated weight loss=32.11 %) attributes to the liberation of three intra water molecules, four molecules of carbon monoxide, and seven carbon particles for the formation of an unstable intermediate, dioxy carbonate. The formation of dioxy carbonate of mixed rare-earth oxalates is reported in the literature [197]. The intermediate dioxy carbonate formed by per oxo linkage is stable only for a very narrow range of temperature (~ 20 ^{o}C) and is then reduced to $GdTbO_3$. Thus, corresponding to the DTG peak at 840 ^{o}C in the temperature range of 820- 1000 ^{o}C, the reduction of this intermediate compound into the oxide form occurs with the release of one carbon dioxide molecule with the experimental weight loss= 6 % (calculated weight loss=5.65 %). From TGA/DTG graph, the total observed weight loss of 56 % (calculated weight loss=54 %) indicates that the final product may be $GdTbO_3$. Likewise, the formation of oxides of mixed rare-earth oxalate single crystals is reported in the literature [197]. The thermal studies on GTFH crystals are in good agreement with the proposed chemical formula and hydration number of these crystals. Thus, in the temperature range of 24–1000 ^{o}C, the mechanism of thermal decomposition of GTFH crystals in different chemical equations resulting the final product as the oxide of mixed rare-earth fumarate may be described as follows:

$$[GdTb\ (C_4O_4H_2)_3(H_2O)_4].3H_2O \xrightarrow[85℃-150℃]{-7H_2O} GdTb\ (C_4O_4H_2)_3.$$

$$GdTb\ (C_4O_4H_2)_3 \xrightarrow[450℃-820℃]{-(4CO+3H_2O+7C)} GdTbO_2CO_3.$$

$$GdTbO_2CO_3 \xrightarrow[840℃-1000℃]{-CO2} GdTbO_3$$

4.5.7 FTIR spectroscopy of terbium fumarate, gadolinium fumarate and mixed gadolinium-terbium fumarate crystals

FTIR spectrum of the grown compounds in the wavenumber range of 400 - 4000 cm^{-1} was recorded on a Bruker Vector-22 spectrometer using KBr pellet technique. Fig. 4.26, Fig. 4.27 and Fig. 4.28 show respectively the FTIR spectrum of TFH, GFH and GTFH single crystals recorded at a resolution of 4 cm^{-1} in the wave number range of 400-4000 cm^{-1}. These figures give the absorption peaks/bands assigned to the different functional groups associated with the fumarate ion in three isomorphous compounds. Table 4.8 gives the comparative study of the absorption peaks of three isomorphous compounds showing the presence of water molecules due to the OH stretching mode of vibration. Virtually the absence of bands in the range 1700-2900 cm^{-1} suggests the replacement of acidic hydrogen of COOH group by metal cations. A band centered arround 1540.84 cm^{-1} is due to asymmetric stretching of coordinated carboxylate group $\nu_{as}(COO^-)$. Another absorption band arround 1399.92 cm^{-1} is attributed to the symmetric stretching of the carboxylate group $\nu_s(COO^-)$ [159]. The difference between the asymmetric $\nu_{as}(COO^-)$ and symmetric $\nu_s(COO^-)$ absorption frequencies indicates the bridging mode of the carboxylate group [202]. The value of $\Delta\nu$ is 140.92 cm^{-1}, 136.4 cm^{-1} and 137.97 cm^{-1} respectively for TFH, GFH and GTFH single crystals. It is generally believed that $\Delta\nu$ is below 200 cm^{-1} for the bidentate carboxylate moiety, but above 200 cm^{-1} for the monodentate carboxylate moiety. As such, in the present study, the carboxylate moiety acts as bidentate for both the pure and mixed fumarate compounds grown in the present study. The strong and sharp band at 1214.20 cm^{-1}may be attributed to in plane bending and 983.91 cm^{-1} may be attributed to symmetric C-C stretching vibrations. The sharp peaks observed arround

804.72 cm^{-1} and at 585.75 cm^{-1} corresponds to the combined effect of in plane bending motion δ (O-C-O) and the presence of metal oxygen bond [203].

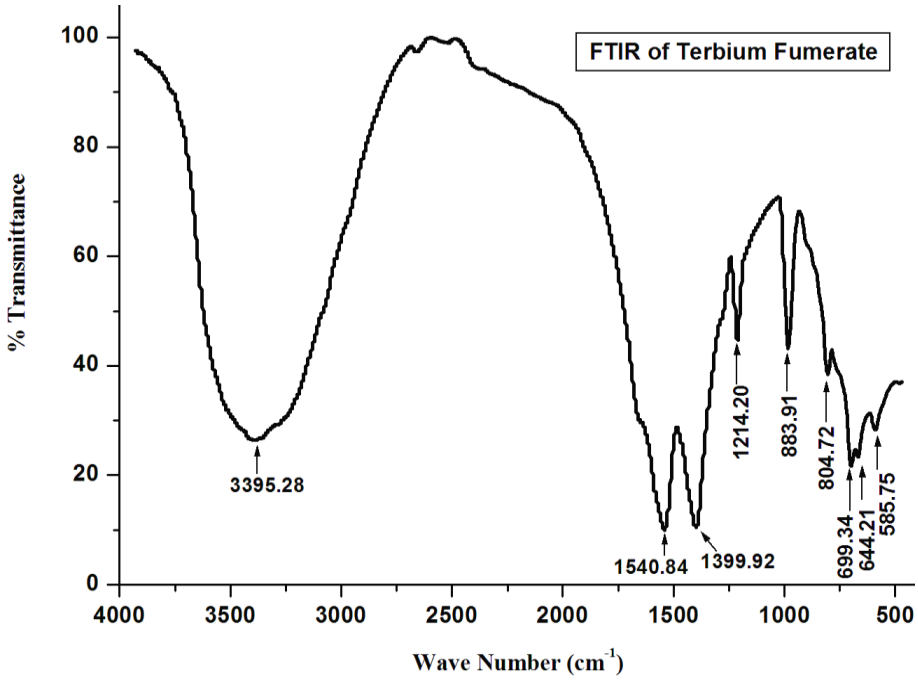

Figure 4.26: FTIR spectrum of terbium fumarate heptahydrate single crystals.

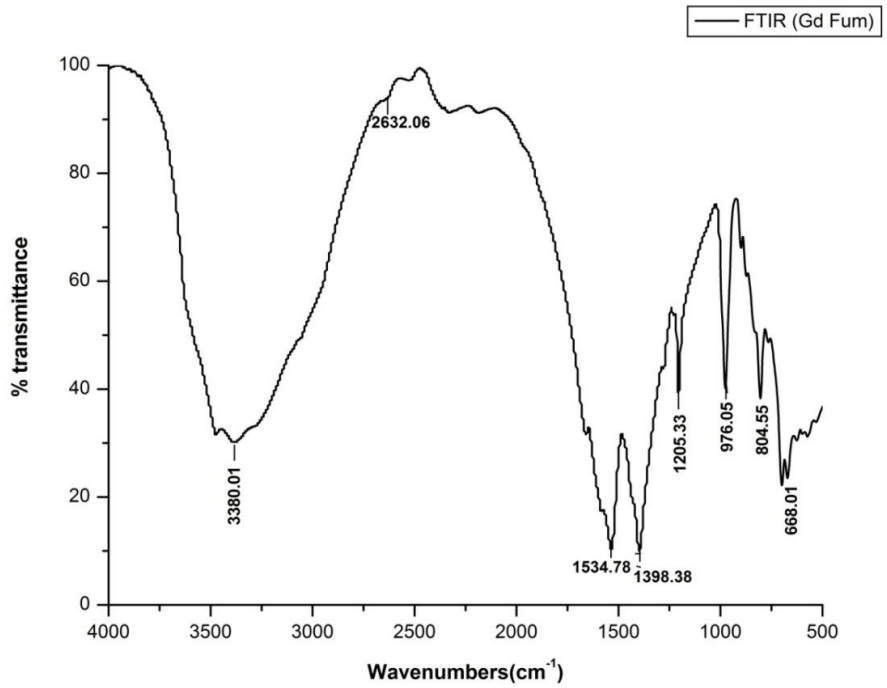

Figure 4.27: FTIR spectrum of gadolinium fumarate heptahydrate single crystals.

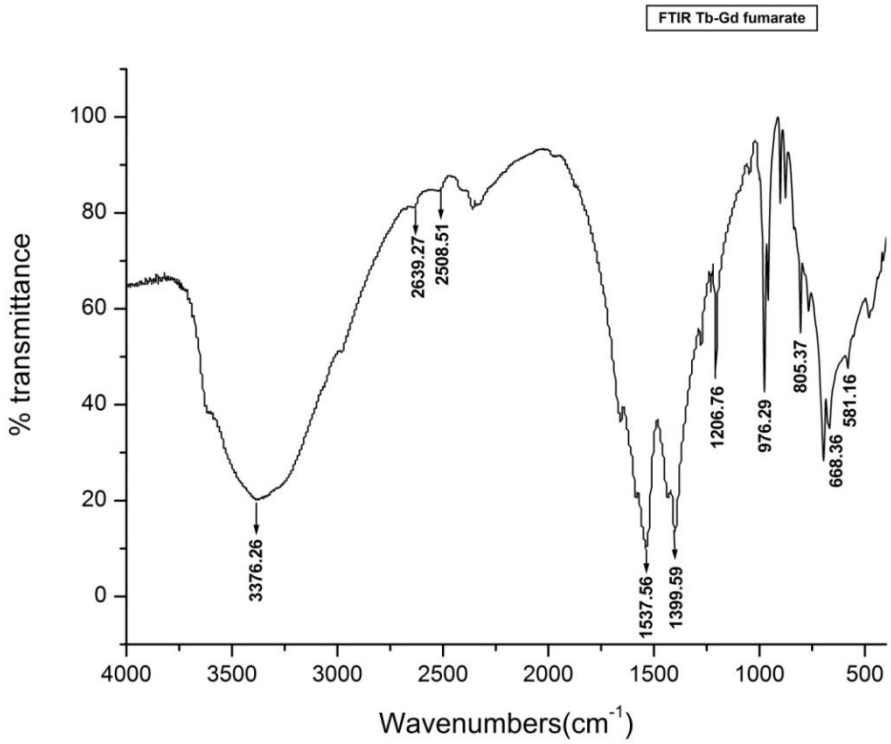

Figure 4.28: FTIR spectrum of gadolinium-terbium fumarate heptahydrate single crystals.

Table 4.8: Comparative FTIR data of pure and mixed fumarate compounds.

(TFH) IR Peaks/ bands (cm−1)	(GFH) IR Peaks/ bands (cm−1)	(GTFH) IR Peaks/ bands (cm−1)	Assignments of peaks/bands
3395.28	3380.01	3376.26	ν_s (OH)+ν_{as} (OH) of water and carboxylic acid
2649.06	2648	2639.27	C-H stretch
1540.84	1534.78	1537.56	$\nu_{as}(COO^-)$
1399.92	1398.38	1399.59	ν_s (COO^-)
1214.20	1205.33	1206.76	C-O –H stretching vibration
983.91	976.05	976.29	C – C symmetric stretching vibrations
804.72	804.55	805.37	δ (O-C-O)
-	668.01	668.36	M-O bond
585.75	-	581.16	M-O bond

Conclusions

1. The single gel diffusion technique has been successfully used for the growth of terbium fumarate, gadolinium fumarate and mixed Gd-Tb fumarate heptahydrate single crystals. The different growth parameters in the transparent gel medium were observed to affect the nucleation rate of these crystals. The optimized parameters for the good crop of these crystals are: gel pH= 5.0- 6.0; gel concentration = 0.5 M; gel age= 72 hours; concentration of lower reactant= 0.06- 0.07 M; concentration of upper reactant= 0.2- 0.3 M and temperature= 30– 40 ^{o}C.

2. The nucleation rate of these crystals in silica gel was found to be in conformity with the classical nucleation theory.

3. EDAX analysis confirmed the presence of heavier elements in the grown compounds and from their CHN analysis, a general formula could be established for these compound as Tb_2 $(C_4O_4H_2)_3.7H_2O$; Gd_2 $(C_4O_4H_2)_3.7H_2O$ and GdTb $(C_4O_4H_2)_3.7H_2O$.

4. The crystallinity of the materials was evidenced by XRD analysis. The phase matching search of the compounds showed that they are isomorphous to samarium fumarate heptahydrate and hence isomorphous to each other.

5. The single crystal X-ray diffraction study of terbium fumarate crystal confirms the earlier phase matching of its powder pattern with the simulated powder pattern of samarium fumarate, thus confirming the isomorphous nature of the two compounds. Moreover, from single crystal XRD refinement, the cell parameters and the water of hydration of the compound were also confirmed. The single crystal XRD also shows the porosity of the compound.

6. Well matching of observed ‘d’ values for different 2θ and hkl indices of the corresponding planes of terbium fumarate, gadolinium fumarate and mixed fumarate crystals show that they are isomorphous to each other. The calculated cell parameters of GFH and GTFH crystals were found nearly same as that of the cell parameters of terbium fumarate single crystals as obtained from its single crystal X-ray diffraction. As such, it substantiates our view point that the crystals grown in the present work are isomorphous to each other.

7. Thermo gravimetric analyses of the compounds substantiated their proposed formula as obtained from their elemental analysis. The pure fumarate compounds show two steps of thermal decomposition till the formation of their oxides, while as

the mixed fumarate complex showed three steps of thermal decomposition for the formation of its oxide.

8. Presence of all the functional groups associated with a fumarate ligand was confirmed by the FT-IR spectrum. FTIR comparative study indicates that the fumarate ligand in both pure and mixed rare-earth fumarate crystals act as bidentate ligand as well as monodentate.

9. Scanning electron microscopic results suggested that the external morphology of both pure and mixed rare-earth fumarate crystals is monoclinic.

CHAPTER-5

Dielectric and conducting behaviour of terbium, gadolinium and mixed gadolinium-terbium fumarate heptahydrate single crystals.

5.1 Introduction

Metal-organic compounds are highly being considered as an alternative to inorganics for many reasons. They are cheaper and their structure can be easily modified through chemistry, thus making them highly versatile. The single crystal growth of metal-organic compounds with unusual dielectric, ferroelectric and second order non-linear optical (NLO) properties is currently considered as one of the vital issues. In the class of metal-organic coordination compounds the rare-earth coordination compounds are potential candidates which besides showing dielectric and ferroelectric properties are also thermally stable [204] and also have the ability to incorporate both photoluminescent centers and magnetic properties [205]. Study of dielectric characteristics indicates the response of the material to an electric field. Different polarizations may result into the variation in dielectric constant ε' and dielectric loss (tanδ) of a material. Study of variations in dielectric constant ε' with respect to the temperature is very useful in the study of phase transition taking place in the materials. Bhat et al [206, 207] have reported dielectric studies of some rare-earth coordination compounds. Torres et al [78] have observed two phase transitions in the cadmium tartrate crystals, one due to structural changes and the other due to loss of water molecules. Since, the title compounds belong to the centro-symmetric space group $P2_1/n$, therefore, their dielectric anomaly due to the structural changes is ruled out at the very outset. The dielectric anomaly found in the compounds under report

has been attributed to their dehydration. Dielectric properties of some inorganic fumarate compounds have also been reported in the literature [208, 209]. During the last few years, a number of efforts were made by the researchers to find out new solids with high ionic conductivity for industrial applications, such as solid state batteries, fuel cells, sensors, etc [91]. As reported in the literature, the proton conduction of these solids may play a role in a number of processes. The direct application of solid-state proton conduction occurs in the situations where there is a requirement to transmit hydrogen across some intervening barrier. This occurs in fuel-cell technology as already mentioned in general introduction chapter-1. The properties which are relevant to the function in fuel cells is reported in the literature [94]. The proton is the only ion which may be expected to form and be mobile in molecular organic solids, and hence may play an important role in intra molecular biological processes. Correspondingly, a number of specific biological processes appear to depend on proton transfers [95-97] for example, photosynthesis, where a primary process involves proton liberation and migration across a membrane, certain enzymatic processes etc. In order to understand the dielectric characteristics and the temperature and frequency dependence of ac conductivity of gel grown pure and mixed rare-earth fumarate crystals, measurements of the concerned parameters were taken and the results obtained thereof are presented in this chapter.

5.2 Dielectric polarization and its frequency dependence

In a dielectric medium which is also called an insulator, the polarization can be produced by an external electric field. Therefore, the concept of polarization becomes important in modifying the electric field both inside and outside the material. The different types of polarization processes depend on the structure of molecules in a material. For example, H_2O molecule has a permanent dipole moment even in the absence of an electric field and at the same time CO_2 molecule posseses no permanent dipole moment. It is because that unlike CO_2 molecule, in H_2O molecule the two OH bonds do not lie along the same straight line. Although a dipolar substance has permanent moments, yet the net polarization vanishes in the absence of external electric field due to the random orientation of moments. But, due to the external electric field applied to a substance, the molecular dipoles tend to align with the field and results a net polarizability, which is called dipolar polarizability.

$$\text{Thus, } \mu = \alpha_o E \qquad (5.1)$$

where, μ is dipole moment (C-m^2) and α_o is the dipolar polarizability (F-m^2).

For the molecules with ionic bonds, the external electric field tends to stretch the length of these bonds by displacing the +Ve and –Ve ions towards the opposite poles of the applied field. Due to the change of this dipole length, a net dipole moment is produced in the unit cell, which was zero before the application of electric field. This polarization produced as a result of relative displacements of oppositely charged ions is called ionic polarizability.

$$\text{Thus, } \mu = \alpha_i E \qquad (5.2)$$

where μ is dipole moment (C-m^2) and α_i is the ionic polarizability (F-m^2).

Electronic polarisability occurs in case of neutral atoms due to the relative displacement of its orbital electrons. In the absence of electric field the centre of –Ve charges (cloud of electrons) coincide with the centre of nucleus, thus resulting the formation of neutral atom. But due to the external electric field, the electron cloud gets distorted in a direction opposite to the field. Thus each atom attains a charge dipole which affects the applied field both inside and outside the material.

$$\text{Thus, } \mu = \alpha_e E \qquad (5.3)$$

Therefore the total polarizability is given by

$$\alpha = \alpha_o + \alpha_i + \alpha_e \qquad (5.4)$$

In case of covalent crystals (Ge or Si) which are non-ionic and non-dipolar, the polarizability is entirely electronic in nature and in dipolar substances all the three contributions are present. But in general when the dielectric materials are not single crystals and are either amorphous or polycrystalline, then they include space charge polarizability as well.

$$\text{Thus, } \alpha = \alpha_o + \alpha_i + \alpha_e + \alpha_d \qquad (5.5)$$

where, α_d is space charge polarizability.

The frequency dependence of several contributions to the polarizability over a wide range extending from the static all the way up to the UV- regions [210], is shown in Fig. 5.1. It can be seen that in the microwave region from $\omega = 0$ to $\omega = \omega_d$, the polarizability is essentially constant and in the neighbourhood of ω_d, it decreases by a substantial amount due to the dipolar contribution ω_d. When the frequency exceeds ω_d i.e $\omega > \omega_d$, the field now oscillates so rapidly that the dipoles do not follow but remain essentially stationary. Thus, the polarizability remains constant in the frequency range

from $\omega_{d\ to}\ \omega_i$ and then drops down at the IR region. For the frequency range $\omega > \omega_i$, the ions with their heavy masses do not follow the very rapidly oscillating field and consequently the ionic polarizability vanishes. Thus, in the frequency range above the IR only the electronic polarizability remains effective because of the fact that electrons being very light follow the fast changes of the applied field at high frequency. This range includes both the visible and UV regions. At still higher frequencies i.e $\omega > \omega_e$, the electronic contributions also vanishes as the electrons now are also not able to follow the fast changes of oscillations.

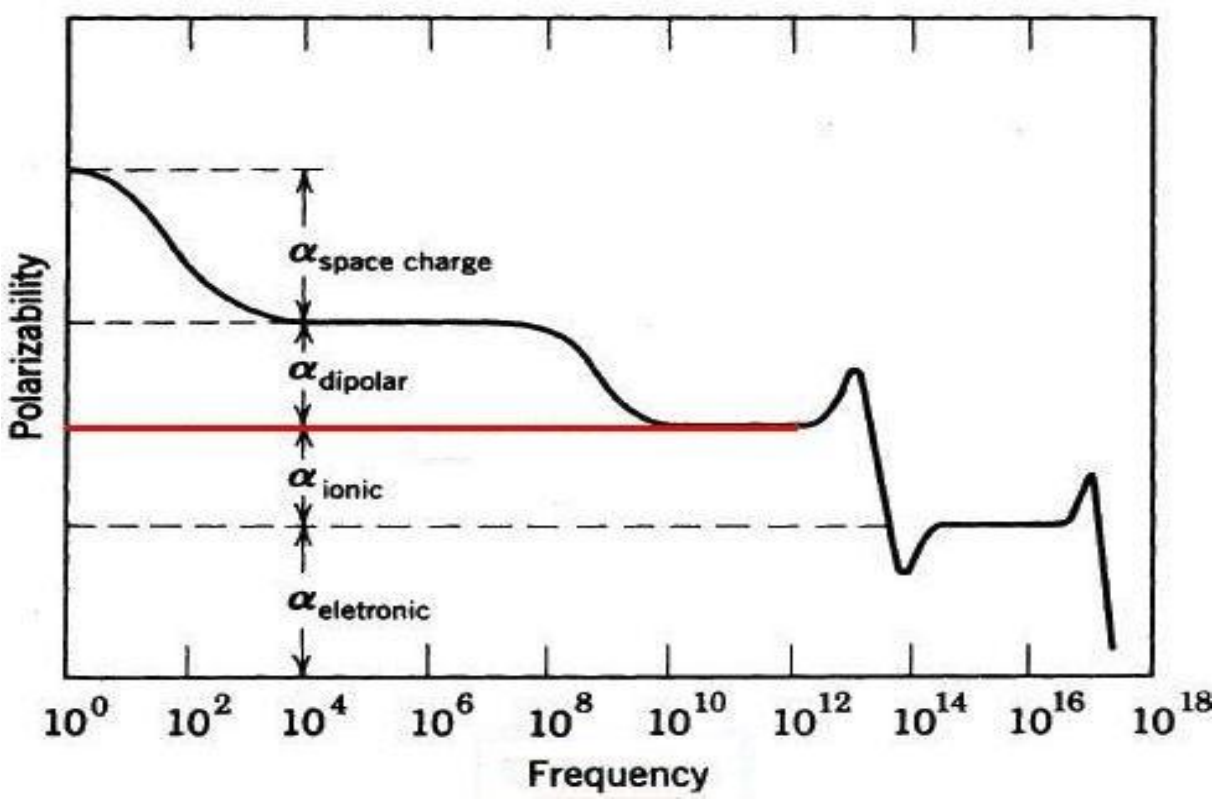

Figure 5.1: Variation of total polarizability with frequency

M. A. Omar, Elementary Solid State Physics Pearson education, Inc. ; 381 & 410-412, (2007).

5.3 Dielectric dispersion: An overview

On the microscopic level we can say that the response of a polar molecule to the externally applied electric field is dependent on the viscosity of the material. The lattice vibrations/ intermolecular forces are responsible for the account of viscous effects. The ability of the molecule to respond to the field is expressed in terms of a

relaxation time τ, where the angular relaxation frequency $\omega = \frac{1}{\tau}$. Above a certain frequency of the field $\omega_{o,}$ the polar molecule can not follow the applied field and hence will not contribute to the permittivity of the medium.

Out of different theories of dielectrics, the first model given by Debye [211] relates to noninteracting polar molecules, for which the susceptibility function is given by

$$\chi(\omega) \propto \frac{1}{1 + i\left(\frac{\omega}{\omega_p}\right)} \qquad (5.6)$$

where, χ is the complex susceptibility, ω the angular frequency and ω_p is the frequency at which maximum loss occurs. This maximum loss occurs when ω_τ corresponds to the critical frequency ω_p and the location of this peak gives the magnitude of the relaxation time τ [212]. The Debye theory occurs in the materials of low concentration dipoles dispersed in a non- polar host polymer matrix and are not bound to the polymer chains. Since Debye response is meant for liquids and gases, therefore Cole-Cole model [213] modified the Debye equations by introducing a parameter α. The Cole-Cole susceptibility function can be therefore written as

$$\chi(\omega) \propto \frac{1}{1 + i\left(\frac{\omega}{\omega_p}\right)^{1-\alpha}} \qquad (5.7)$$

where, α is an impirical constant lies between 0-1.

Davidson and Cole [214] later modified this expression to fit the experimental data, which is given by

$$\chi(\omega) \propto \frac{1}{1 + i\left(\frac{\omega}{\omega_p}\right)^{\beta}} \qquad (5.8)$$

where, β is a parameter lying in the range of 0-1.

However, the best result can be obtained by using a generalized form of these two equations given by Havrilak and Negami [215],

$$\chi(\omega) \propto \frac{1}{\left[1 + i\left(\frac{\omega}{\omega_p}\right)^{1-\alpha}\right]^{\beta}} \qquad (5.9)$$

The Havrilak and Negami equation of two parameter function could be used for getting best results for fitting of experimental data. However, a two parameter equation for the susceptibility function χ(ω), claimed to be a universal relaxation law was proposed by Jonscher by introducing the concept of power law frequency response of dielectric relaxations suitable for fitting experimental data for a wide

range of dielectric materials [216]. According to this law, the complete capacitance and the corresponding susceptibility can be expressed as

$$\chi(\omega) \propto C(\omega) = B(i\omega)^{n-1} = B\left[\sin\frac{n\pi}{2} - i\cos\frac{n\pi}{2}\right]\omega^{n} \qquad (5.10)$$

where, C is the complex capacitance, B is the proportionality constant and the exponent n whose value lies between 0 and 1 defines the frequency dependence. Moreover, for this power law relation, the real and imaginary components maintain a constant frequency-independent ratio, i.e.,

$$\frac{C''(\omega)}{C'(\omega)+C_{\infty}} = \frac{\chi''(\omega)}{\chi'(\omega)} = \cot\left(\frac{n\pi}{2}\right) \qquad (5.11)$$

Based on the concept of universal law, the experimentally observed behavior for various dielectric dispersions can be explained with dipolar, quasi-dc, and diffusive mechanisms. For the bound dipolar case, the fractional power law behavior is given by

$$\chi(\omega) \propto \chi(0)\left(\frac{i\omega}{\omega_p}\right)^{n-1} \; : \; \omega >> \omega_p \quad (5.12)$$

$$\chi(0) - \chi(\omega) \propto \chi(0)\left(\frac{i\omega}{\omega_p}\right)^{m} \; : \omega << \omega_p \qquad (5.13)$$

where ω_p is the peak frequency and $\chi(\omega)$ is the susceptibility at very low frequency. We can write the alternative equations for bound dipolar case by using Eq.5.11 as:

$$\chi''(\omega) = \cot\left(\frac{n\pi}{2}\right)\chi'(\omega) \propto \omega^{n-1} : \omega >> \omega_p \qquad (5.14)$$

$$\chi''(\omega) = \tan\left(\frac{m\pi}{2}\right)[\chi(0) - \chi'(\omega)] \propto \omega^{m} : \omega << \omega_p \qquad (5.15)$$

where χ' and χ'' are the real and imaginary parts of the susceptibility, respectively. According to Jonscher, this susceptibility function can be expressed as

$$\chi''(\omega) \propto \frac{1}{\left(\frac{\omega}{\omega_p}\right)^{-m} + \left(\frac{\omega}{\omega_p}\right)^{1-n}} \qquad (5.16)$$

The quasi-dc dispersion has been observed experimentally at frequencies below 1 Hz in which some of the charges are weakly bound and partially free to move. For frequencies less than characteristics rate ω_c, the quasi-dc dispersion is represented by

$$\chi(\omega) \propto \chi(0)\left(\frac{i\omega}{\omega_c}\right)^{-p}$$

$$= \chi(0)\left(\frac{\omega}{\omega_c}\right)^{-p} \times \left[\cos\left(\frac{p\pi}{2}\right) - \sin\left(\frac{p\pi}{2}\right)\right] \qquad (5.17)$$

and for frequencies greater than the characteristics rate

$$\chi(\omega) \propto \chi(0) \left(\frac{i\omega}{\omega_c} \right)^{n-1}$$

$$= \chi(0) \left(\frac{\omega}{\omega_c} \right)^{n-1} \times [\ \sin(\frac{n\pi}{2}) - i\cos(\frac{n\pi}{2})] \qquad (5.18)$$

The equivalent presentation for this behaviour can be written as

$$\chi''(\omega) = \cot(\frac{n\pi}{2})\, \chi'(\omega) \ \propto \omega^{n-1} : \omega >> \omega_c \quad (5.19)$$

$$\chi''(\omega) = \tan(\frac{p\pi}{2})\, \chi'(\omega) \ \propto \omega^{n-1} : \omega << \omega_c \quad (5.20)$$

The exponent 'n' in dipolar response which defines the degree to which the displacements of a dipole to those of its environment form a cluster and the exponent m is a measure of the extent to which one cluster can affect the others and can be taken as the efficiency of dipolar displacement between clusters. Therefore, when m approaches unity, it shows the situation in which the disturbance is spread almost homogeneously over the system as equilibrium is approached. In quasi-dc process, p is a measure of the efficiency of the charge transport between the clusters. Any deviation of p from unity defines the degree of inefficiency of the charge transport in the system and is a measure of the degree of long-range homogeneity. In the quasi-dc process, the real and imaginary parts of the susceptibility increase steadily with decreasing frequency, with a small exponent value of p at frequency $< \omega_c$, followed by a flat loss behaviour above **ω.** The dielectric behaviour discussed so far involves dielectric loss due to the polarization mechanism. But many of the dielectric materials exhibit loss with the conduction of charge carriers that add to the total loss. This conduction loss is given by

$$\epsilon'' = \frac{\sigma}{\omega} \qquad (5.21)$$

where, ϵ'' is the dielectric loss factor and σ is the electrical conductivity of the material. In QDC process no loss peak is observed and the real and imaginary parts of susceptibility increases rapidly towards low frequencies without any sign of saturation and follows a parallel trend in a log-log representation and obey a power law of the type:

$$\chi \propto \omega^{n-1} ; 0 < n < 1 \qquad (5.22)$$

where, χ is the electric susceptibility of the material which is related to real dielectric constant as: $\chi = \epsilon' - 1$

The universal fractional power law is obeyed by variety of solid materials, including low loss dielectrics, dipolar materials, hopping electronic systems, ionic conductors, semiconductors, p-n junctions, interfacial phenomena and mechanical relaxation [217]. It should be noted that dipolar system will exhibit loss peaks, whereas carrier dominated systems exhibit QDC responses. In the present study pure and mixed rare-earth coordination compounds have been grown, all of which show QDC behaviour as discussed in the proceeding sections of this chapter.

5.4 Experimental Procedure

Single crystals of terbium fumarate heptahydrate (TFH), gadolinium fumarate heptahydrate (GFH) and mixed GdTb fumarate heptahydrate (GTFH) were grown by single diffusion gel technique [109, 110] at a temperature range of 15-40^{o} C using sodium meta silicate gel as a medium of growth. These crystals grown by gel diffusion technique were small in size to be used directly for dielectric analysis, therefore, their dielectric studies were carried out on powdered samples in the form of compressed pellets. For the preparation of pellets, the crystals were ground to a fine powder by adding 2-3 drops of acetone and the powder was then pressed into circular pellets of diameter 13 mm and thickness 1.0- 1.5 mm under a pressure of 200 kg/cm^2 using a hand operated hydraulic press. Silver paint was used as a conducting paste and was applied on both sides of the pellets to make them capacitors with the material as dielectric medium. The dielectric spectroscopy of these compounds was carried out in the frequency range of 20 Hz to 3 MHz and over the temperature range of 15- 130 ^{o}C using an impedance analyser (Wayne Kerr) and the data was recorded. A microprocessor based furnace fitted with a temperature controller along with a temperature sensor and a specially designed sample holder was used to heat the sample at a heating rate of 2 ^{o}C/min. The instrument directly provided the values of capacitance C and dielectric loss tan (δ). Other parameters such as dielectric constant ε' and ac conductivity $\sigma_{a.c}$ of the compounds were computed by using the relations:

$$\varepsilon' = C.t/\varepsilon_o A \text{ and } \sigma_{a.c} = 2\pi f \varepsilon_o \varepsilon' \tan\delta.$$

where, C represents the capacitance (in farads), t the thickness (in meters), A the area (in meter^2) of the sample, $\varepsilon_o = 8.85\times10^{-12}$ Fm^{-1}, f is the frequency (in Hertz) of the applied electric field and the conductivity $\sigma_{a.c}$ is measured in ohm^{-1} m^{-1}.

5.5 Dielectric characteristics

The variation of dielectric constant ε', dielectric loss (tanδ) and ac conductivity σ_{ac} with temperature and frequency of terbium fumarate heptahydrate (TFH) , gadolinium fumarate heptahydrate (GFH) and mixed gadolinium terbium fumarate heptahydrate (GTFH) was carried out in the temperature range (15- 150 ^{o}C) under the application of applied ac field in the frequency range (20Hz- 3MHz). The results obtained thereof are described as follows:

5.5.1 Dependence of dielectric constant and dielectric loss on temperature

The variation of real part of dielectric constant ε' of TFH, GFH and GTFH crystals corresponding to different temperatures at different frequencies in the range (1 kHz to 3 MHz) of the applied ac field is shown in Fig.5.2, Fig.5.3 and Fig.5.4 respectively. As can be observed from these figures, the dielectric constant remains temperature independent up to 60 ^{o}C or 70 ^{o}C as the case may be and then it increases almost exponentially with the temperature and attains a peak around a temperature of 85 ^{o}C in case of TFH crystals and 95 ^{o}C in case of GFH and GTFH crystals. The dielectric constant then decreases on further increasing the temperature. The dielectric anomaly of the three compounds found at a temperature of 85 ^{o}C or 95 ^{o}C may suggest a phase transition of the materials. To account for this behaviour, we have two possibilities: (1) due to dehydration of water molecules associated with the title compounds and/or (2) due to the structural changes of the compound. Torres et al [78], have observed two phase transitions in the cadmium tartrate crystals; one due to structural changes and the other due to loss of water molecules. Though each of the compounds belong to the Centro symmetric space group $P2_1/n$, therefore, the dielectric anomaly in these compounds due to the structural changes is ruled out at the very outset. This dielectric anomaly can be attributed to the dehydration of the compounds, which is also in good agreement with their thermo gravimetric analysis. The fact that the water molecules in the crystal boundary bring the anomalous dielectric peak may be discussed as follows:

As a matter of fact, water is a typical polarized molecule. When the temperature is lower than 60 or 70 ^{o}C, water molecules are confined at the crystal surface of the compounds by slight interaction, which would prevent the reorientation of a molecular dipole. However, with the increase in temperature, the interaction would be

broken down step by step and the water molecules could re-orientate freely. This leads to an increase of dielectric constant beyond 60 or 70 ^{o}C and reached a maximum at about 85 ^{o}C for TFH crystals and 95 ^{o}C for GFH and GTFH crystals. The orientational polarization occurs only in the materials composed of molecules with an asymmetrical structure in which the centroid of the negative charge (mainly electrons) and that of the positive charge (mainly nuclei) are not coincident. These molecules will, therefore, possess permanent dipole moments in the absence of external fields. In water molecules the bonding structure is asymmetrical, so the centroid of the negative charge is not coincident with that of the positive charge, thus resulting in a net permanent dipole moment. Beyond the transition temperatures, T_o= 85 ^{o}C or 95 ^{o}C the decrease in dielectric constant of the materials may be due to the decrease in orientational polarization by gradual loss of water molecules and by the randomness of the permanent dipole moments. The terbium fumarate complex being isomorphous with samarium fumarate heptahydrate [66] contains three lattice water molecules and four coordinated water molecules. The presence of these seven water molecules in TFH crystals has been shown by an ORTEP diagram after solving its crystal structure reported in section 4.5.4 of chapter- 4, and reported elsewhere [200]. As discussed in previous chapters that the mixed rare-earth compound is isomorphous to the single component rare-earth compound, therefore, all the three compounds may contain three lattice water molecules and four coordinated water molecules. From the thermal analysis of all the three compounds, it is found that the three lattice water molecules escape in the temperature range 80-130 ^{o}C, as such the dielectric constant of the materials goes on decreasing beyond the transition temperature of 85 ^{o}C or 95 ^{o}C . In the temperature range 124.5-150 ^{o}C corresponding to endothermic DTA/DTG peaks at 132.63 ^{o}C and 149 ^{o}C for pure and mixed fumarate crystals, the remaining four coordinated water molecules also escape from each compound. Hence, corresponding to the complete dehydration, the dielectric constant of the compounds decreases much and attains a small constant value. In order to confirm that the dielectric anomaly of the materials is due to the presence of water molecules, another experiment was carried out in which the pellets of different samples were heated for their dehydration to a temperature of 150 ^{o}C for about 2 hours. The dielectric constant of the preheated pellets was recorded corresponding to the different temperatures at a frequency of 1 kHz. It was found that the anomalous dielectric peak disappeared completely for both

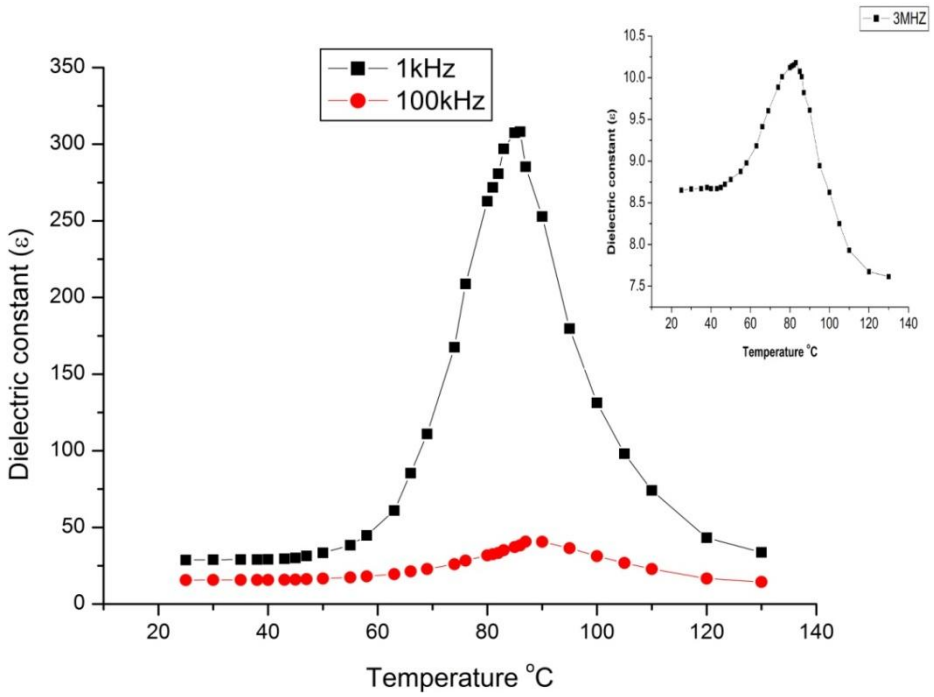

Figure 5.2: Variation of dielectric constant (ε') with temperature of terbium fumarate heptahydrate compound at the frequencies 1 kHz, 100 kHz and 3 MHz.

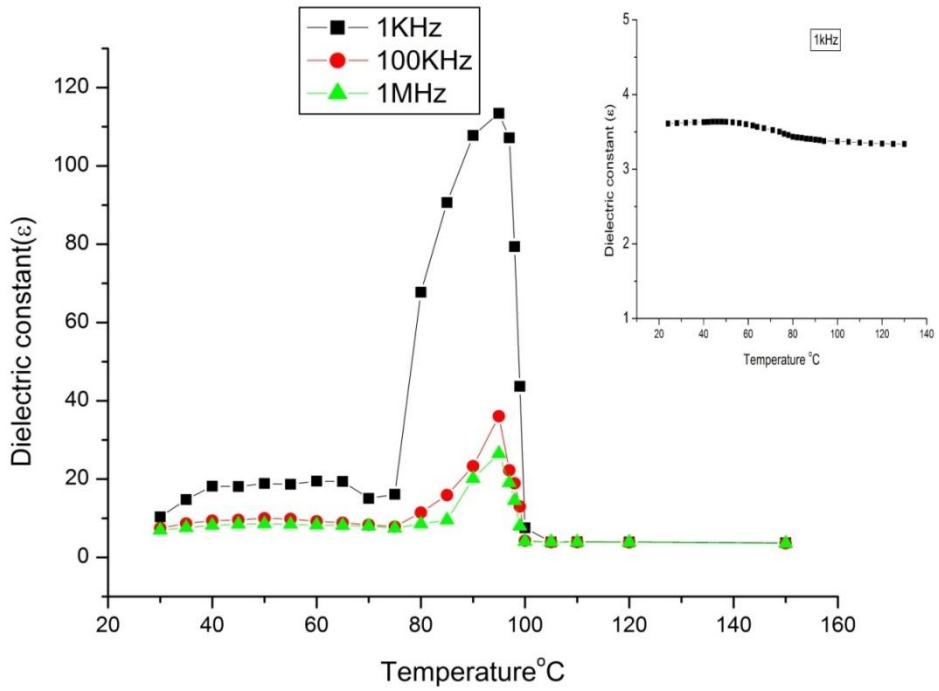

Figure 5.3: Variation of dielectric constant with temperature of gadolinium fumarate heptahydrate crystals at different frequencies before dehydration and the inset of the graph showing variation of dielectric constant with temperature of the dehydrated compound at a frequency of 1kHz.

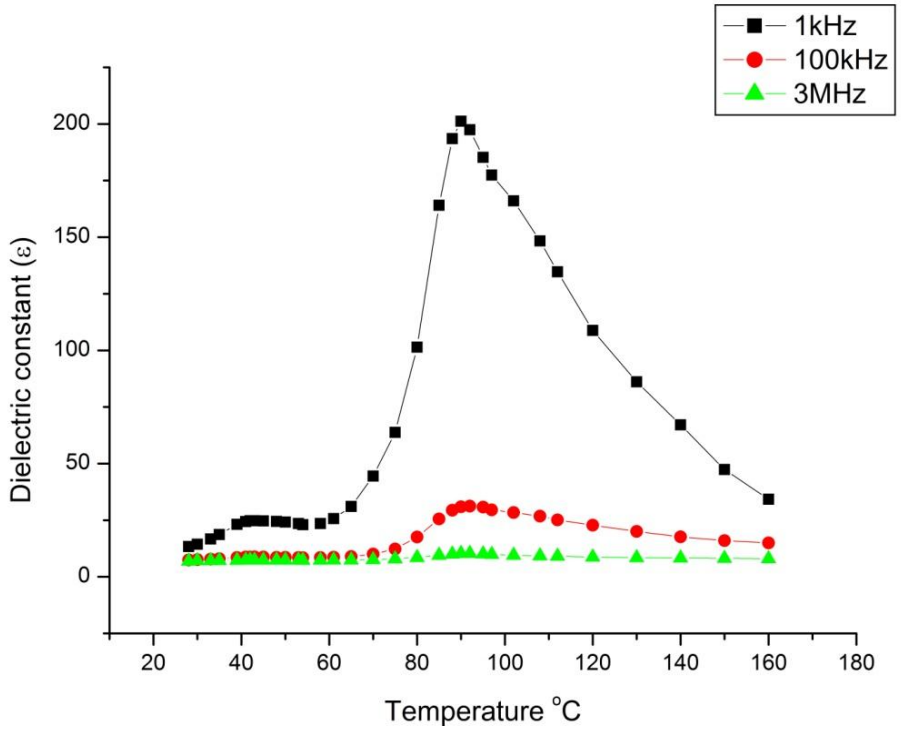

Figure 5.4: Variation of dielectric constant (ε') with temperature of mixed gadolinium-terbium fumarate heptahydrate compound at the frequencies 1kHz,100 kHz and 3MHz.

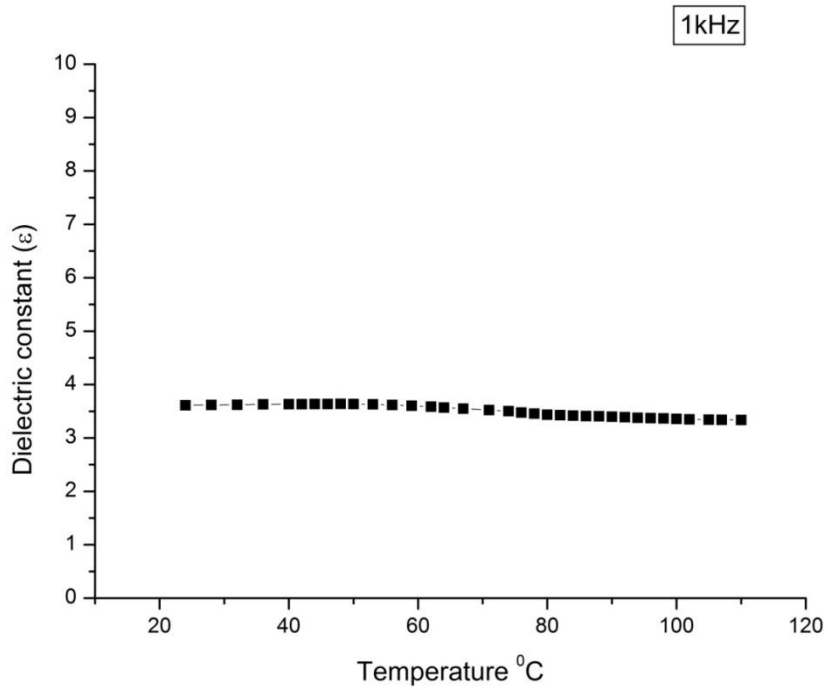

Figure 5.5: Graph between dielectric constant (ε') and temperature of dehydrated compound : terbium fumarate at 1kHz.

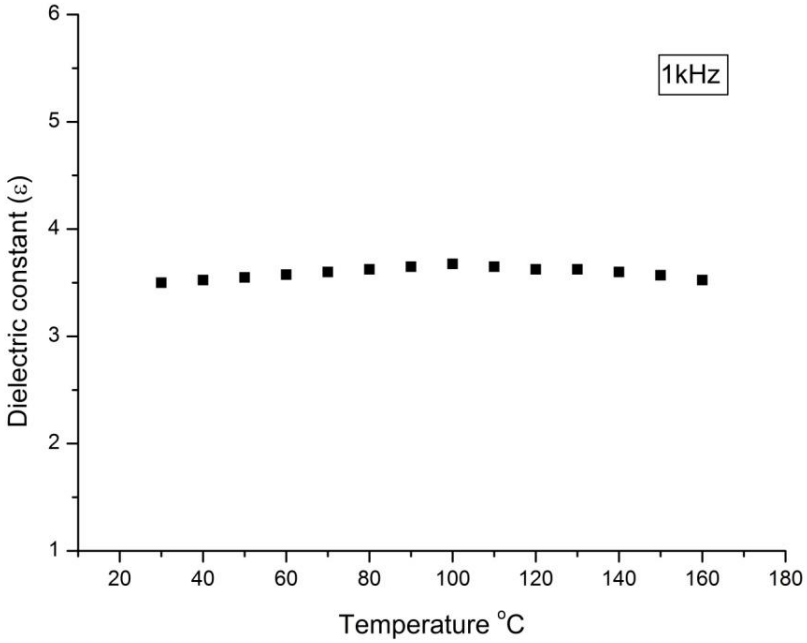

Figure 5.6: Graph between dielectric constant (ε') and temperature of dehydrated compound of mixed gadolinium-terbium fumarate at 1kHz.

pure and mixed fumarate crystals as shown in inset Fig. 5.3, Fig. 5.5 and Fig.5.6 respectively for gadolinium fumarate, terbium fumarate and mixed gadolinium-terbium fumarate compounds. As such, it is suggested that the dielectric anomaly of all these crystals is mostly due to the presence of lattice and coordinated water molecules. Thus the water molecules absorbed to the crystal boundary of a compound could impose great impact on the dielectric property and may contribute to the anomalous dielectric peak as also reported in the literature [218-220].

The dependence of dielectric loss (tanδ) also exhibits a similar type of variation with frequency at different temperatures for pure and mixed rare-earth fumarate crystals, showing again a peak around at 85 ^{o}C for pure terbium fumarate heptahydrate and at 95 ^{o}C for mixed gadolinium terbium fumarate heptahydrate as shown respectively in Fig.5.7 and Fig.5.8. It is obvious that the reorientation of a molecule involves the energy required to overcome the resistance of the surrounding molecules, so the orientation process is strongly temperature dependent. For terbium fumarate heptahydrate the increase in dielectric constant in the temperature range

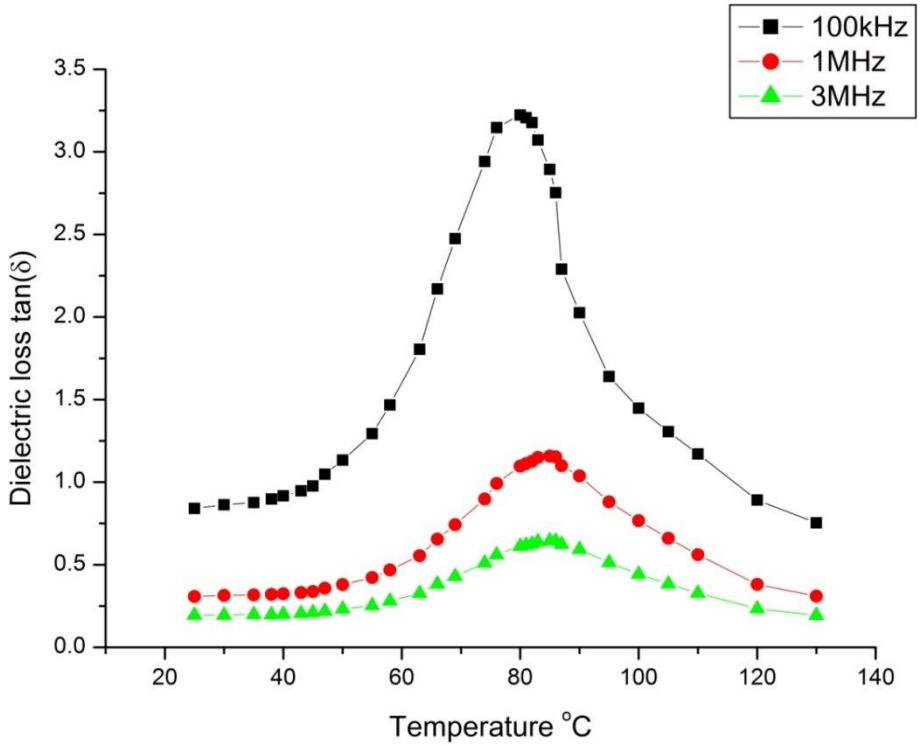

Figure 5.7: Variation of dielectric loss (tanδ) with temperature of pure rare-earth (TFH) crystals at frequencies 100 kHz, 1MHz and 3MHz.

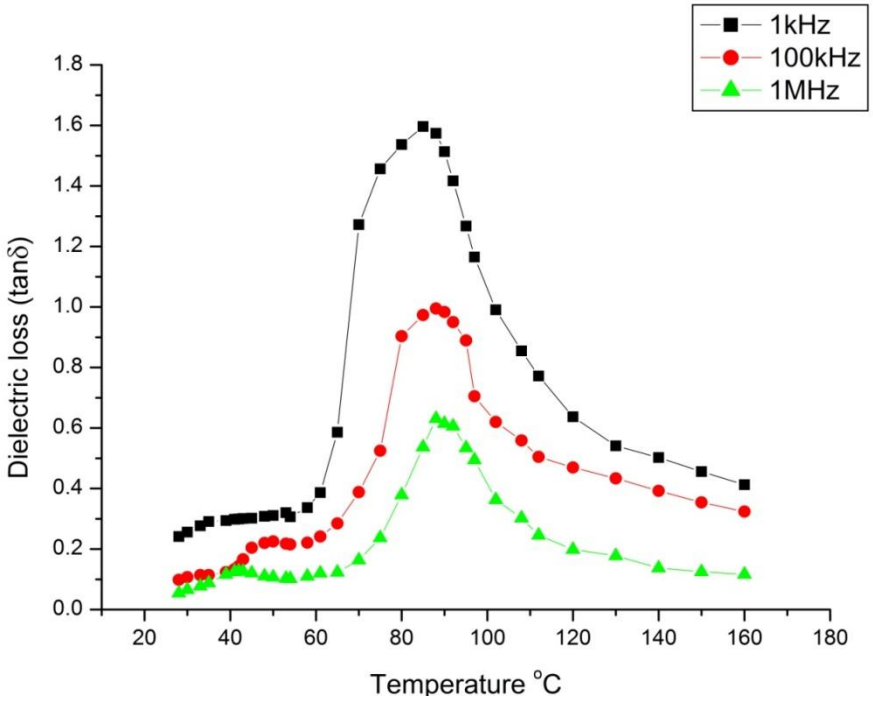

Figure 5.8: Variation of dielectric loss (tanδ) with temperature of mixed rare-earth fumarate (GTFH) crystals at frequencies 1kHz, 100kHz and 1MHz.

$60 < T < 85\ ^{o}C$, more energy is dissipated for reorienting the permanent dipoles in the direction of the applied field, as such the dissipation loss also increases within the temperature range $60 < T < 85\ ^{o}C$ as depicted in Fig.5.7. And for mixed Gd-Tb fumarate heptahydrates, the dissipation loss increases in the temperature range $70 < T < 95\ ^{o}C$, which is close to that of terbium fumarate heptahydrate. It is therefore clear from the graph that the dielectric loss peak is almost frequency independent and is a consequence of polar dielectrics, where apart from dipole losses, losses due to electrical conduction also occur [221].

5.5.2. Dependence of dielectric constant and dielectric loss on frequency

The variation of dielectric constant ε' and dielectric loss (tanδ) as a function of frequency at different temperatures for TFH, GFH and GTFH crystals respectively shown in Fig.5.9, Fig.5.10 and Fig.5.11 show a normal behaviour of the dielectric materials. It is observed that the dielectric constant and dielectric loss both decrease with increase in frequency. The decrease of dielectric constant with increase of frequency, a normal dielectric behaviour can be explained on the basis of polarisation mechanism. There are four primary mechanisms of polarisation in materials: i.e. electronic, ionic or atomic, dipolar or orientational and space charge or interfacial polarisation. At low frequencies, all the mechanisms of polarisation contribute to the dielectric constant. Since the dielectric studies were carried out on pellet samples, we expect the space charge polarisation to be dominant. The high rise of dielectric constant at lower frequencies may be attributed to space charge polarisation due to grain boundary effects. With the increase in frequency, the contributions from different polarisations start decreasing. This exhibits that at very high frequencies the mechanical system cannot follow the fast changes of the electric field, implying that all types of polarization mechanisms vanish except electronic polarization. At high frequency, the electronic polarization remains effective because of the fact that electrons being very light follow the fast changes of the high frequency applied field. This range includes both the visible and UV regions. At still higher frequencies (above the electronic frequency $\omega_{e)}$ i.e. $\omega > \omega_e$, the electronic contributions also vanishes as the electrons now are also not able to follow the fast changes of oscillations. Thus, the response of the materials to extremely high frequencies of the external field is missing. The dependence of dielectric loss (tanδ) also exhibits a

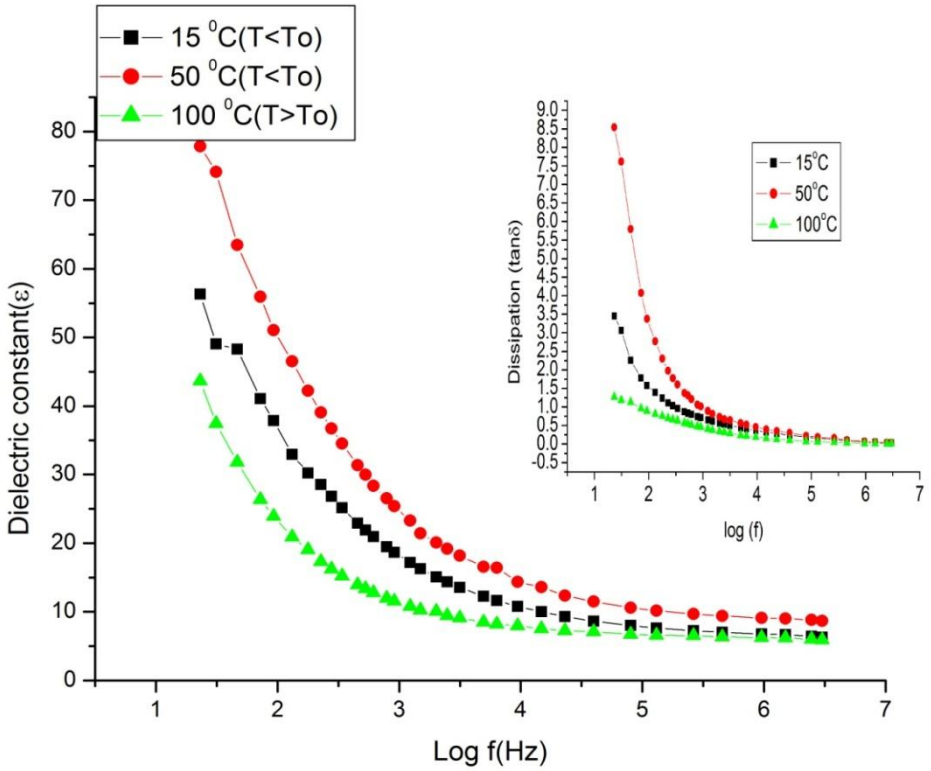

Figure 5.9: Variation of dielectric constant (ε') with frequency of pure TFH crystals with the inset graph between dielectric loss and frequency at temperatures 15 °C, 50 °C and 100 °C.

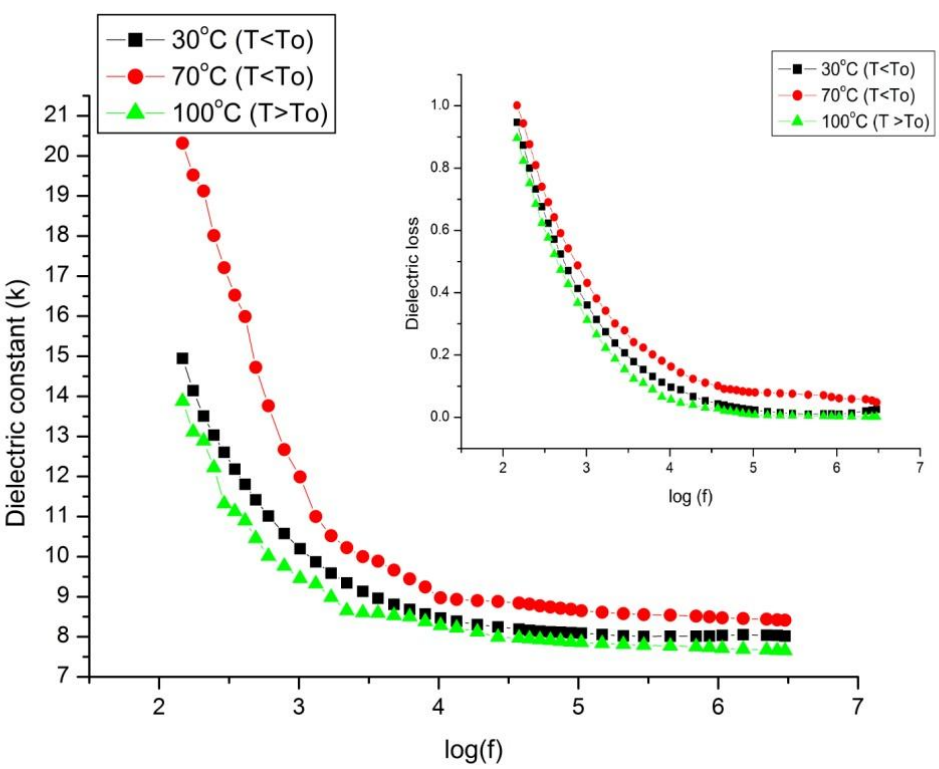

Figure 5.10: Variation of dielectric constant (ε') with frequency of pure GFH crystals with the inset graph between dielectric loss and frequency at temperatures 30 °C, 70 °C and 100 °C.

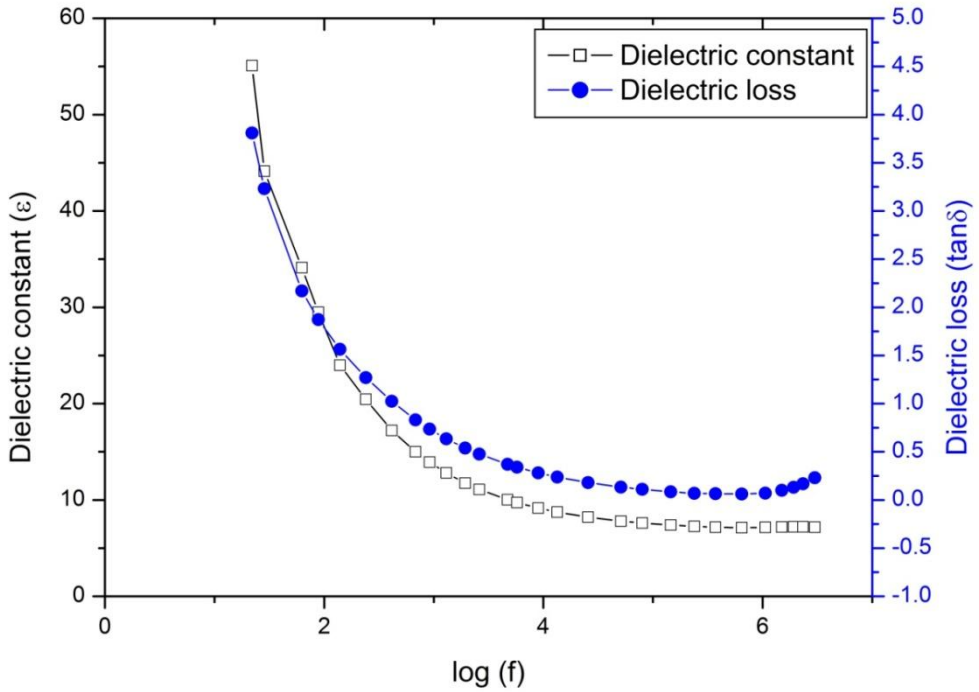

Figure 5.11: Variation of dielectric constant (ε') and dielectric loss with frequency of mixed GTFH crystals at a temperature 30 ^{o}C.

similar type of variation with frequency at different temperatures as shown in inset figures of pure and mixed rare-earth fumarate crystals. With increasing frequency, the dipoles cannot follow the rate of changes, so, they react to such fields more weakly. It is observed that the losses are smaller at higher frequencies. In other words the dielectric loss is almost frequency independent beyond the frequency of 100 kHz. The low value of dielectric loss indicates that the grown crystals are reasonably of good quality. From these figures, the absences of any loss peak in the dielectric dispersion of the materials suggest their behaviour to be that of low frequency dispersion (LFD) or the quasi-dc process [222]. The real and imaginary parts of the susceptibility increase rapidly towards low frequency without any sign of saturation and follow a parallel trend in a log-log representation and obey a power law of the type: $\chi \propto \log \omega^{-(1-n)}$, where $0 < n < 1$, where χ is the electric susceptibility of the material which is related to real dielectric constant as, $\boldsymbol{\chi = \acute{\varepsilon} - 1}$.

In case of materials under study, i.e for pure TFH crystals, n = 0.7 and for mixed GTFH crystals n= 0.34, which are obtained from the slope of $\log \boldsymbol{\chi}$ verses

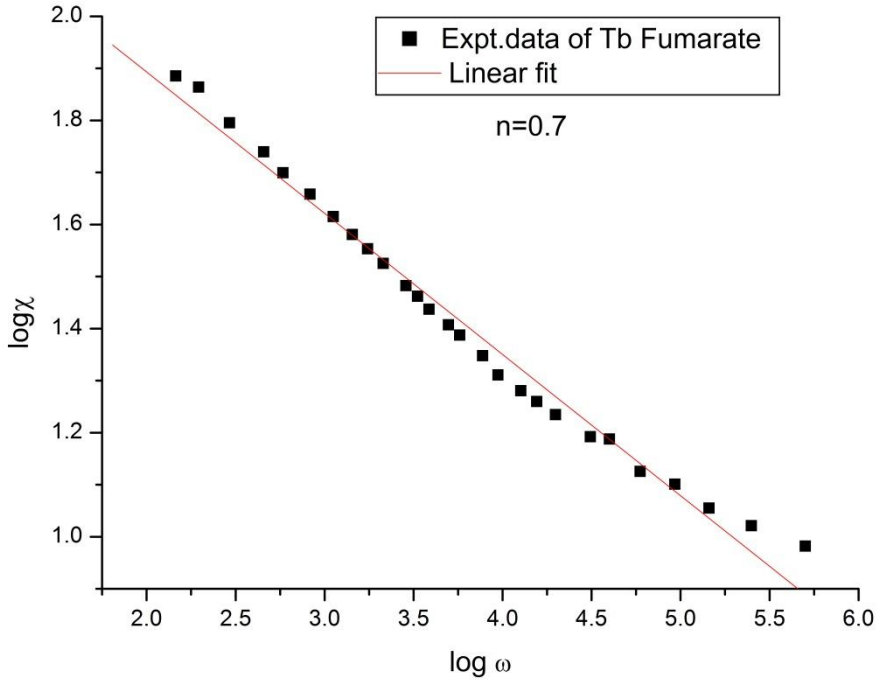

Figure 5.12: Variation of susceptibility with frequency of terbium fumarate heptahydrate crystals.

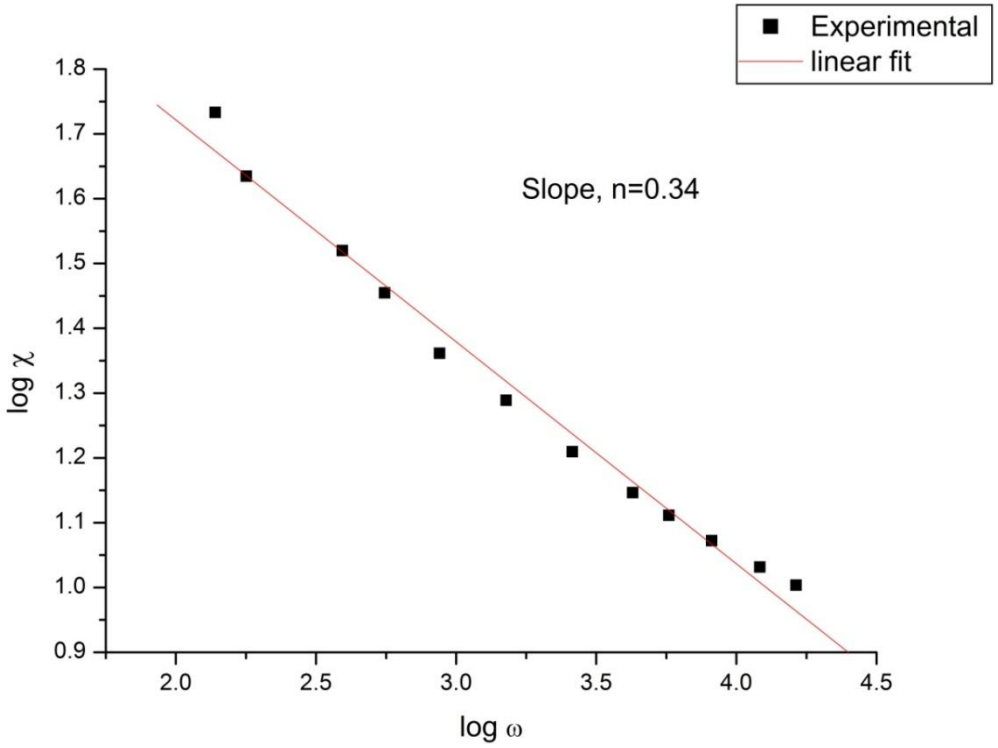

Figure 5.13: Variation of susceptibility with frequency of mixed GTFH crystals.

log ω as shown in Fig.5.12 and Fig.5.13 respectively. And as for as, the literature is concerned, the value of 'n' has been estimated to lie between 0.5-1.0 [223]. As reported earlier in this chapter that the universal fractional power law is obeyed by the variety of solid materials, including low loss dielectrics, dipolar materials, hopping electronic systems, ionic conductors, semiconductors, p-n junctions, interfacial phenomena and mechanical relaxation [217].

5.6. Conduction behaviour

5.6.1. Temperature dependent ac conductivity

Fig. 5.14, Fig. 5.15 and Fig. 5.16 show the variation of ac conductivity with temperature at different frequency of terbium fumarate, gadolinium fumarate and mixed gadolinium-terbium fumarate heptahydrates respectively. The ac conductivity σ_{ac} shows a strong dependence on both the temperature and frequency of the applied ac field for both pure and mixed rare-earth fumarate compounds. The rise of conductivity upon increasing the frequency and temperature is a common response for polymeric and semiconductor samples [224]. It is due to the tremendous increase of the mobility of charge carriers in the complex. An increase in the values of ac electrical conductivity is driven by mobility of free charges (i.e. polarons and free ions) as the temperature is increased. Such a type of behaviour is almost same as reported for some other rare-earth co-ordination compounds by Bhat et al [206, 207]. In the temperature range $30 < T < 70$ ^{o}C, the a.c conductivity of both pure and mixed crystals is almost temperature independent. Above 70 ^{o}C, the ac conductivity increases and approaches a maximum value at about 85 ^{o}C and 95 ^{o}C for TFH crystals and mixed GTFH crystals respectively and then decreases beyond this temperature. The increase in conductivity in the temperature range $70 < T < 85$ ^{o}C for TFH crystals or $70 < T < 95$ ^{o}C for mixed GTFH crystals may be due to an increase in the concentration of mobile charge carriers due to the dissociation of water molecules present in the material into H^{+} and OH^{-} ions. This type of conduction known as protonic conduction is also reported in the literature [225]. When the temperature is increased beyond the transition temperature, the concentration of dissociated ions of water molecules decreases due to the dehydration of lattice and coordinated water

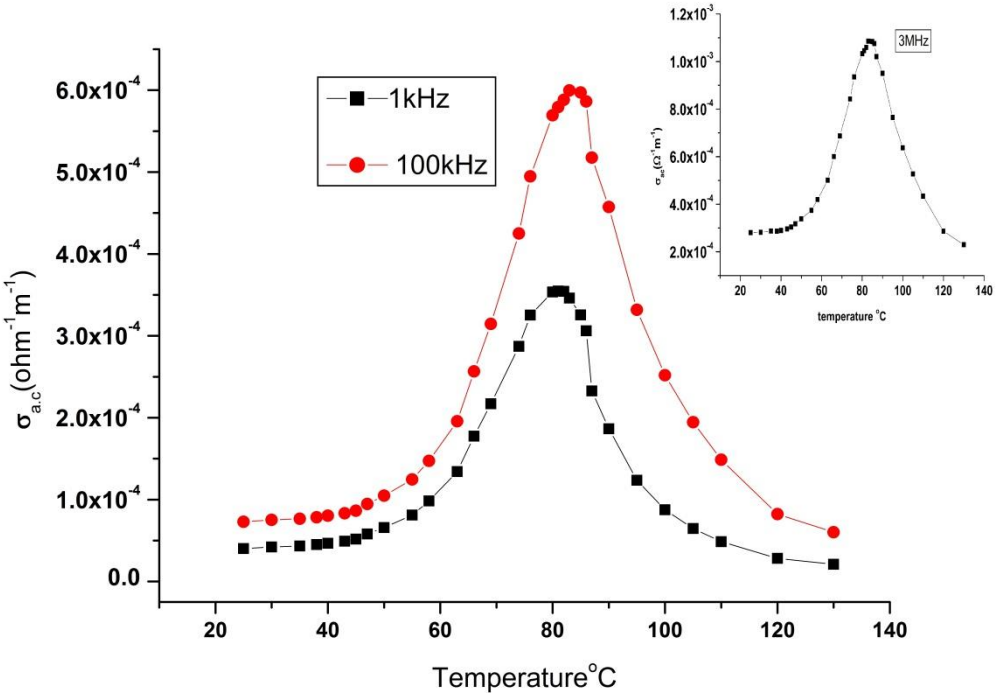

Figure 5.14: Variation of a.c conductivity with temperature of TFH crystals at frequencies 10 kHz and 100 kHz with the inset graph at 3MHz.

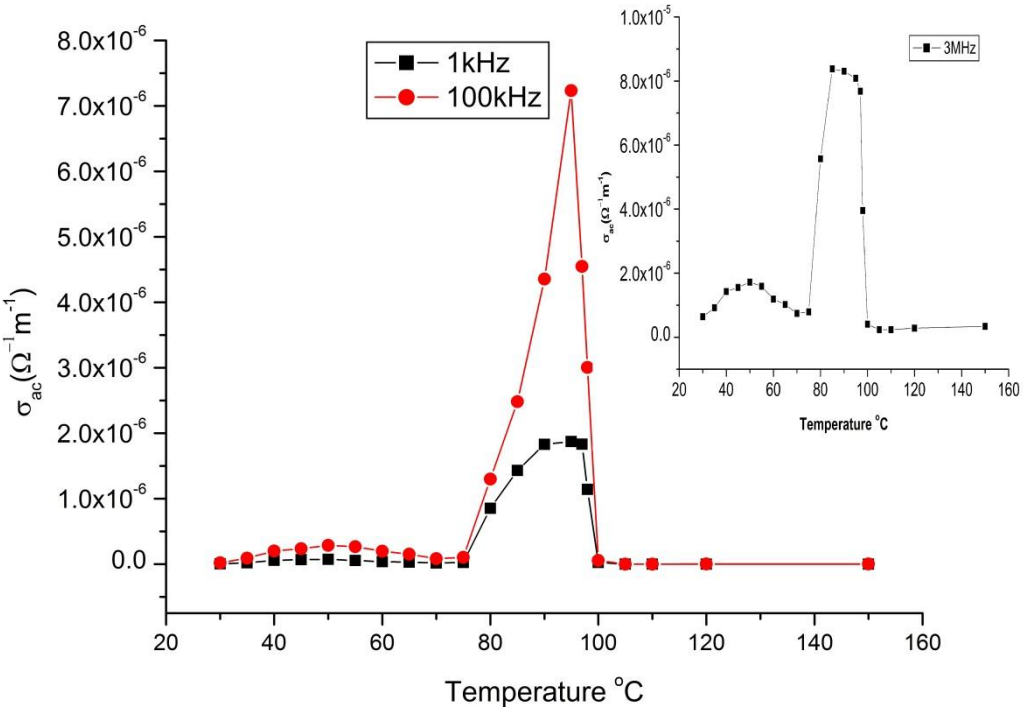

Figure 5.15: Variation of ac conductivity of GFH crystals as a function of temperature at frequencies 1 kHz, 100 kHz and 3 MHz.

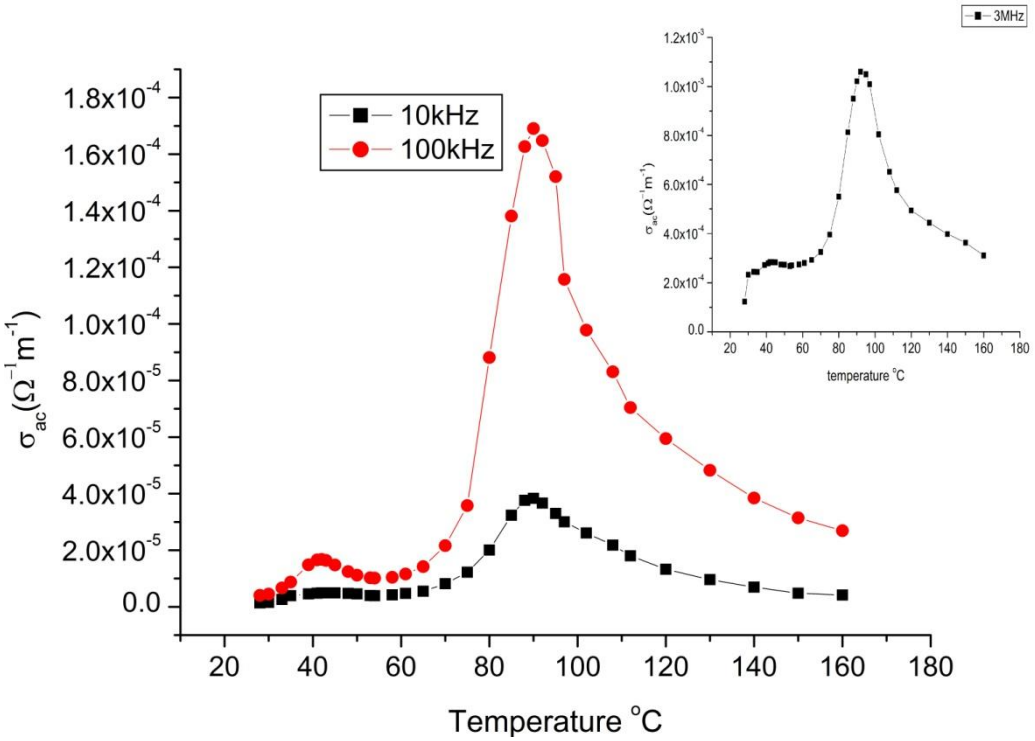

Figure 5.16: Variation of a.c conductivity with temperature of GTFH crystals at frequencies 10 kHz and 100 kHz with the inset graph at 3 MHz.

molecules in the temperature range 80-150 ^{o}C as reported in the thermal analysis of the compounds. Except gadolinium fumarate, the ac conductivity shown by TFH and mixed GTFH crystals vary from 10 $^{-4}$ to 10 $^{-3}$ ohm $^{-1}$ m $^{-1}$ which is just more than that of the reported values for other coordination compounds [225, 226]. The ac conductivity shown by gadolinium fumarate crystals is however ~10 $^{-6}$ ohm $^{-1}$ m $^{-1}$.

The activation energy E_a which is defined as the minimum energy to overcome the potential barrier in the composite system was calculated before the transition temperature by using the Arrhenius equation $\sigma = \sigma o \exp (E_a/kT)$. Fig. 5.17 and 5.18 show a plot of ln σ_{ac} versus 1000/T at 10 kHz just before the transition temperature and the slopes of these graphs give the activation energy of the ions before the transition which is equal to 0.56 eV for TFH crystals and o.86eV for mixed GTFH crystals. The same order of activation energy has also been reported in the imidazolium salts of dicarboxylic acids, where the electrical conductivity has been explained as due to proton transfer through hydrogen bonds [227]. The other hydrogen bonded systems in which a.c conductivity takes place due to proton transfer is also reported [228]. In order to confirm that the conductivity of the material is due

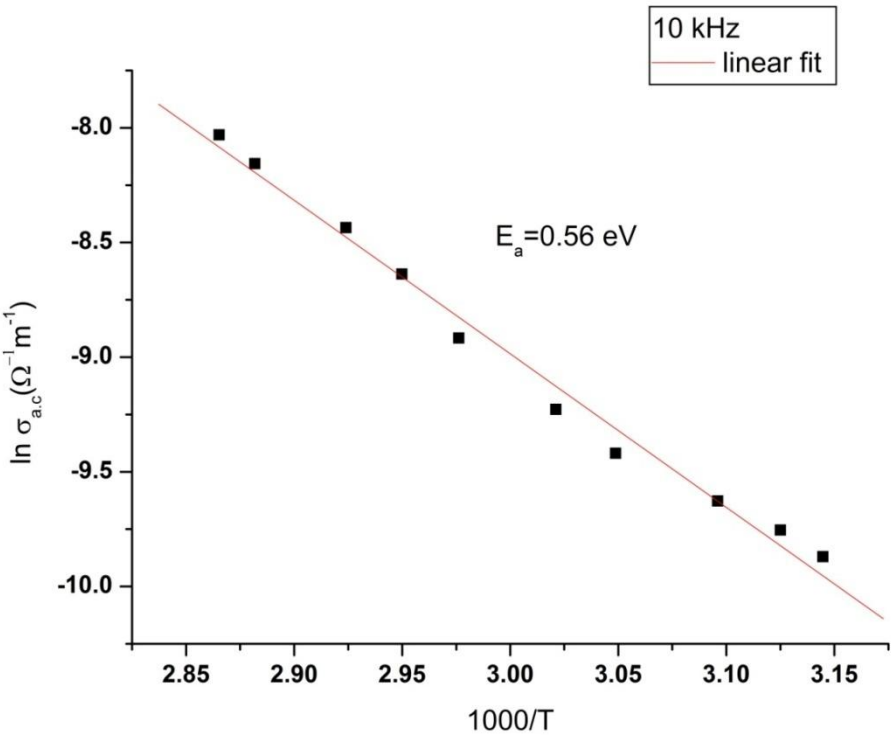

Figure 5.17: Graph between conductivity (σ_{ac}) and 1000/T of TFH crystals at 1 kHz.

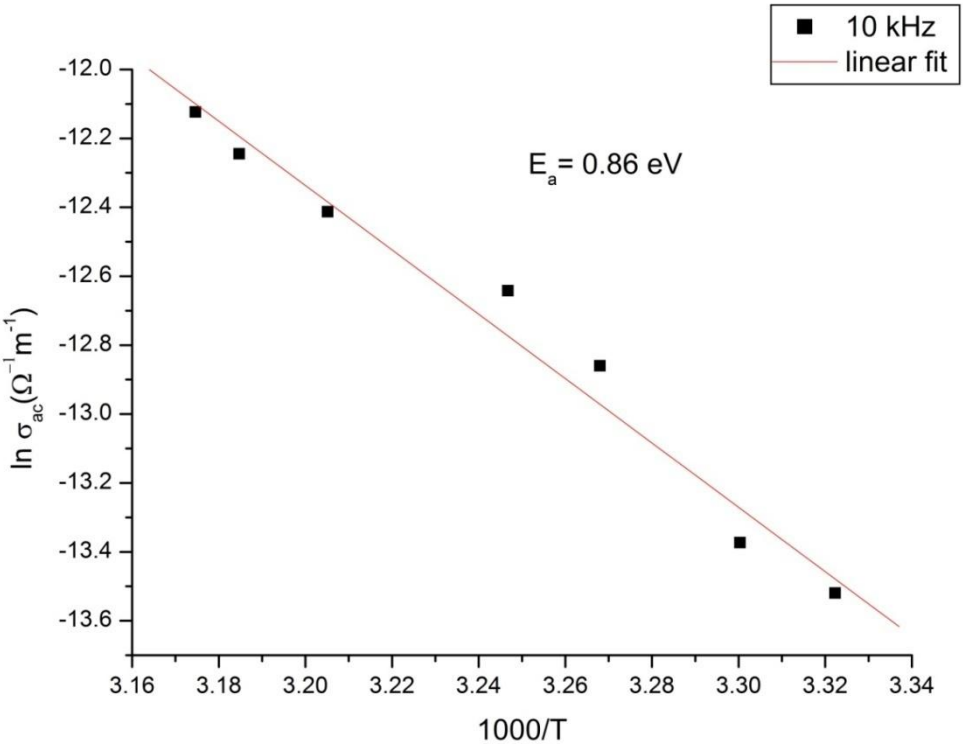

Figure 5.18: Graph between conductivity (σ_{ac}) and 1000/T of GTHF crystals at 1 kHz.

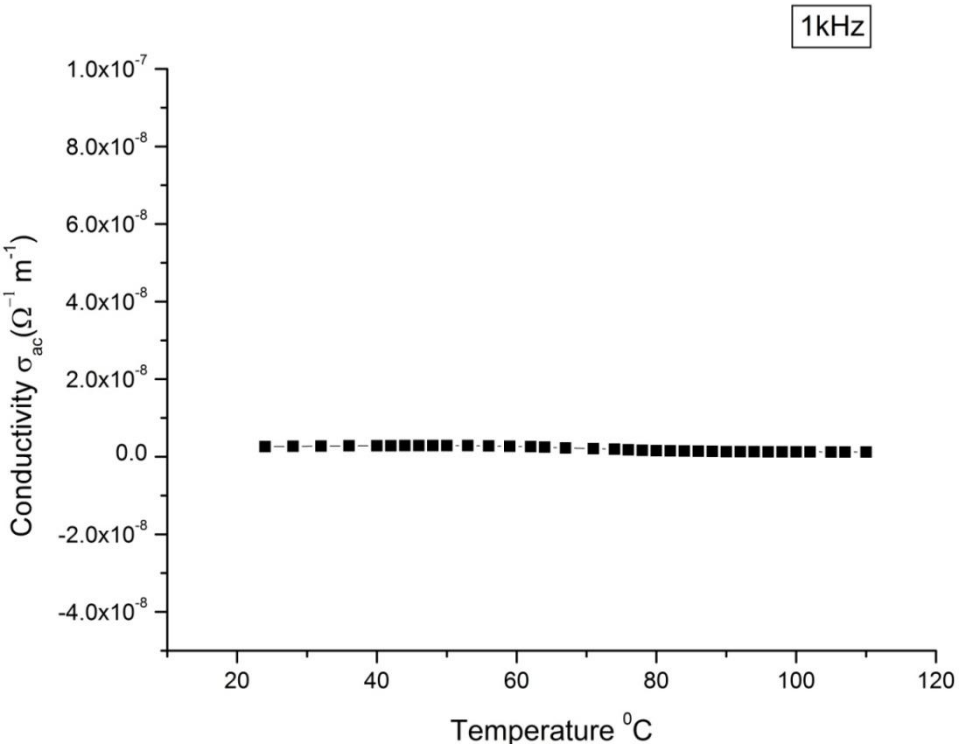

Figure 5.19: Variation of ac conductivity with temperature of the dehydrated sample of terbium fumarate at 1k Hz.

to the proton transfer in hydrogen bonded system, the sample was heated to 150 ^{o}C for about two hours and its ac conductivity was carried out. Fig. 5.19 shows very small conductivity of the dehydrated sample of terbium fumarate compound at 1 kHz which is $\approx 0.2\times 10^{-8}$ ohm^{-1} m^{-1} and remaining almost constant.

5.6.2. Frequency dependent ac conductivity

Fig. 5.20, Fig. 5.21 and Fig. 5.22 give a plot of ln $\sigma_{a.c}$ versus ln ω for terbium fumarate, gadolinium fumarate and mixed gadolinium terbium fumarate heptahydrate crystals kept at a temperature of 50 ^{o}C. The slope of these graphs determined the value of the exponents for each compound i.e for TFH, s= 0.46; for GFH, s= 0.35 and for GTFH, s= 0.9, which confirmed that for each compound, the value of 's' so obtained obeys Johnscher power law $\sigma(\omega)= \sigma_o + A\omega^s$ and its value lies in the range $0 < s < 1$. σ_o is the d.c conductivity which is the frequency-independent plateau in the low frequency region and can be obtained by fitting $\sigma(\omega)= \sigma_o + A\omega^s$ for both pure

fumarate crystals (TFH crystals) and mixed fumarate crystals (GTFH crystals) as shown in Fig. 5.23 and Fig. 5.24 and $\omega = 2\pi f$ is the angular frequency.

The trend of conductivity with frequency indicates hopping conduction of protons through hydrogen bonds [228]. Since the application of an electric field causes directional flow of charge carriers by hopping mechanism, therefore there occurs proton–phonon interaction. As such, when a proton tries to move, it has a strain field (a cloud of virtual thermal phonons) forming a quasi particle like polaron. The electrical conductivity $\sigma_{a.c}$ of many solids was shown by Johnscher [92] to consist of strongly frequency dependent components in glasses, polymers and crystals. In general, it was found that the a.c conductivity decreases with increasing frequency in case of band conduction and it increases with increasing frequency in case of hopping conduction.

The experimental results on the frequency dependence of a.c conductivity have shown that at a given temperature, the magnitude of conductivity is higher at higher frequencies, thereby supporting the small polaron hopping model [229]. But at extremely low frequencies, the ordered solids show no frequency dependence of their conductivity at frequencies below phonon frequencies. From the experimental data in a limited frequency region, it was noted that the electrical conductivity increases with frequency and follows the Johnscher's universal power law [92, 230]. The power law exponent 's' is a weak function of temperature, approaching unity at low temperature and zero at high temperature [231]. This power law is applicable for polymeric and semiconductor materials. At higher frequencies of applied a.c field, this quasi-particle disperses. When the cloud of phonons disperses, protons move and contribute to conductivity. That is why in the inset graphs (Figs. 5.14 and 5.16) of pure and mixed fumarate compounds, the magnitude of conductivity increases from 3.5×10^{-4} ohm^{-1} m^{-1} to 1.1×10^{-4} ohm^{-1} m^{-1} by increasing the frequency from 1 kHz to 3 MHz. Therefore, in the hopping conduction, it is possible to distinguish different characteristics regions of frequency.

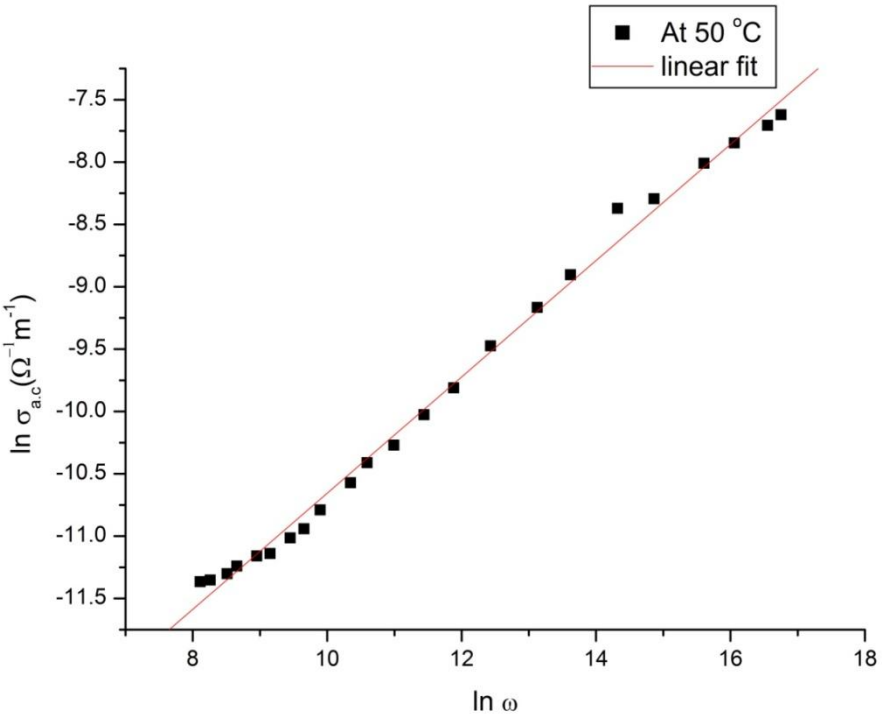

Figure 5.20: Variation of ac conductivity with frequency of TFH crystals at 50 °C.

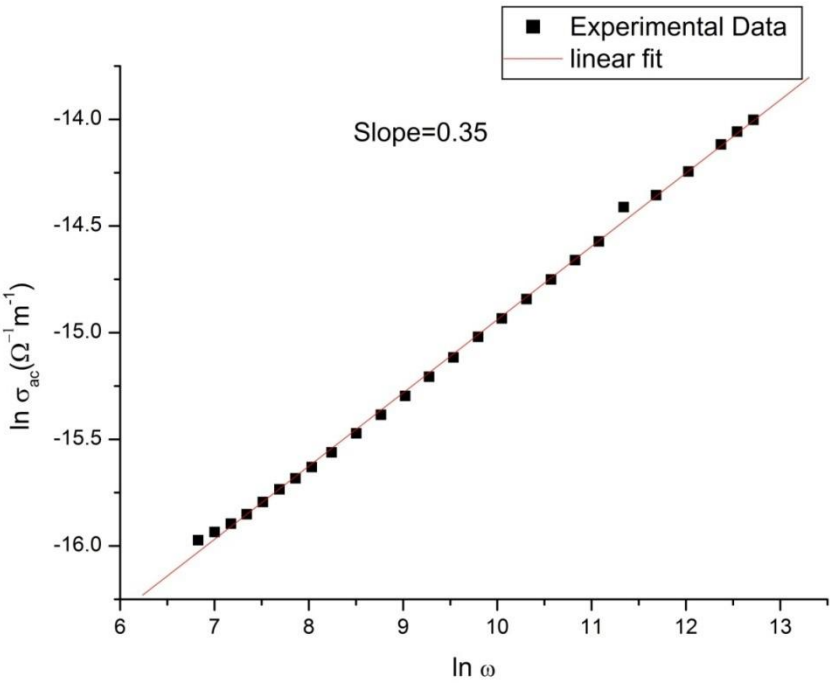

Figure

5.21: Variation of ac conductivity with frequency of GFH crystals at 50 °C.

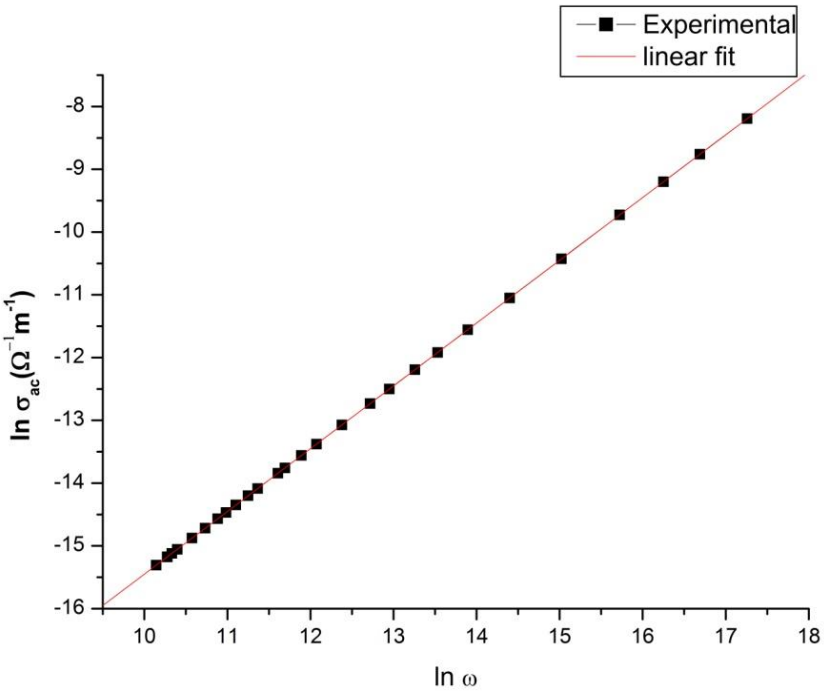

Figure 5.22: Variation of ac conductivity with frequency of GTFH at 50 ^{o}C**.**

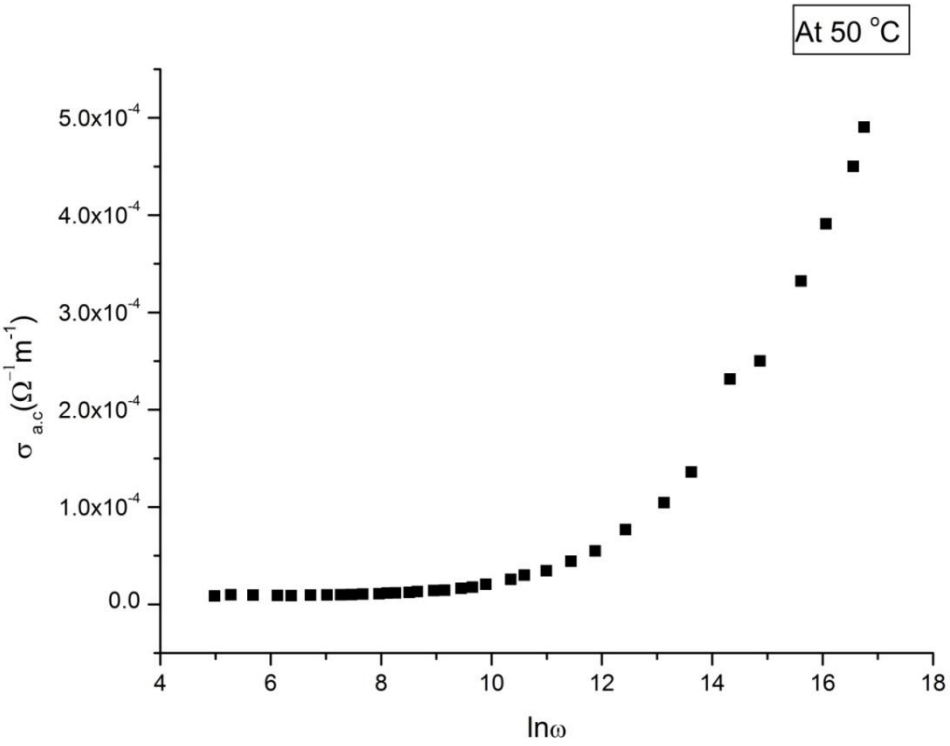

Figure 5.23: Variation of ac conductivity with frequency of TFH crystals at 50 ^{o}C showing frequency-independent plateau in the low frequency region.

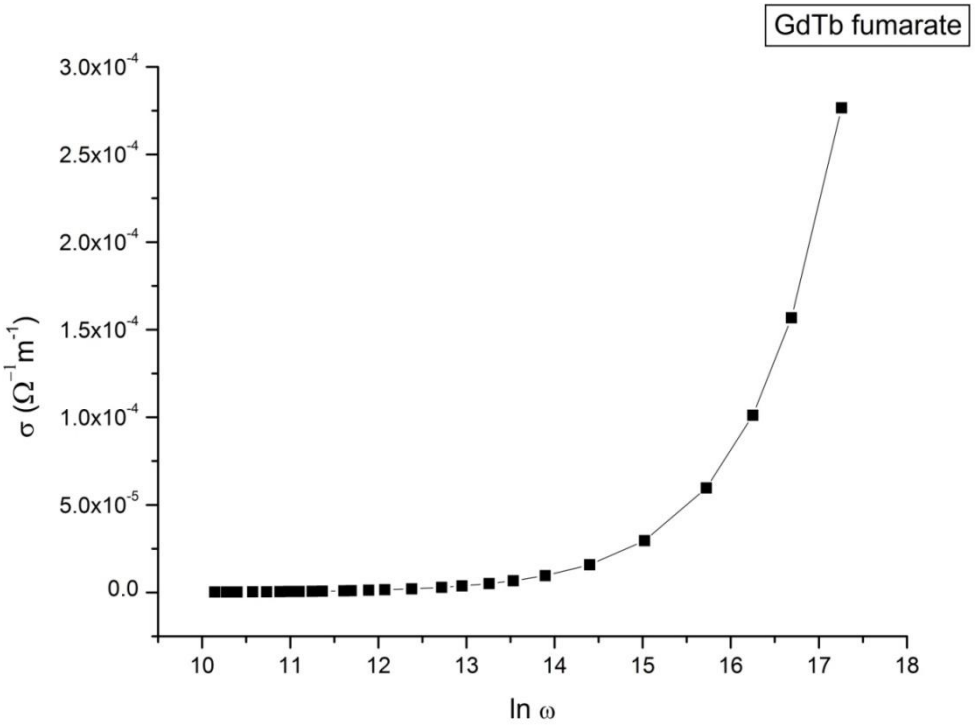

Figure 5.24: Variation of ac conductivity with frequency of mixed GTFH crystals at 50 ^{o}C showing frequency-independent plateau in the low frequency region.

Conclusions

1. The dielectric property and conductivity behaviour of TFH, GFH and mixed GTFH crystals have been discussed. The studies of the dielectric behaviour of these compounds show a strong dependence of dielectric constant on temperature and frequency of the applied electric field. The dielectric constant (ε) varies with the temperature and attains a peak value nearly at 85 ^{o}C for terbium fumarate and at 95 ^{o}C for gadolinium fumarate and mixed GdTb fumarate heptahydrates, thus establishing this temperature as the transition temperature.

2. It is worth to mention here that the dielectric anomaly found in the title compounds is attributed due to their dehydration and not due to the ferroelectric phase transition. The thermal decomposition substantiates that the dielectric anomaly taking place in the title compounds is due to the loss of water molecules and not due to any structural changes.

3. The ac conductivity σ_{ac} of the materials show a strong dependence on both the temperature and frequency of the applied ac field. The conductivity of the materials suggests that they are protonic conductors making protons to transfer through hydrogen bonds.

4. The ac conductivity of pure terbium fumarate compound is greater than that of pure gadolinium fumarate and mixed GdTb fumarate compounds. At 100kHz, the ac conductivity is 6×10^{-4} ohm^{-1} m^{-1} and 6×10^{-6} ohm^{-1} m^{-1} for terbium fumarate and gadolinium fumarate compounds respectively and for mixed fumarate compound the conductivity is 1.1×10^{-4} ohm^{-1} m^{-1}.

5. The ac conductivity of both terbium fumarate and mixed fumarate crystals is exactly same at 3MHz and is equal to 1.1×10^{-3} ohm^{-1} m^{-1}.

6. The activation energy of mixed fumarate crystals is greater than that of pure terbium fumarate crystals, thereby suggesting that the charge carriers in mixed fumarate crystals are more bound with the metal ions than that of pure terbium fumarate crystals.

7. The frequency dependent ac conductivity of both pure and mixed rare-earth fumarate crystals obeyed Johnscher power law equation.

CHAPTER-6

Thermal behaviour of terbium, gadolinium and mixed Gd-Tb fumarate heptahydrate single crystals

6.1 Introduction

Thermal methods, generally referred to as thermo-analytical techniques give a deeper insight into the mechanisms involved in changes in a given material besides leading to novel intermediate and end products in large number of cases. There has been some discussion on whether thermal analysis can really be regarded as an analytical method. It was concluded that thermal analysis could be fitted into general systems on theory model of chemical analysis [232] and is based on three elements i.e, the sample, the reagent and the signal, by considering heat as a reagent. Thermal studies are also very important to throw light on the thermal stability of the substances. Thermal analysis is the measurement of changes in physical properties of a substance as a function of temperature when the substance is subjected to a controlled temperature programme [233-235]. Important information regarding the phase transformations taking place in a material is also provided by the thermo-analytical techniques. Thermal methods of analysis are now being used in a very large range of scientific investigations. These techniques also provide a wide range application in materials like building materials, ceramics, cements, glass, minerals, soils, catalysts, explosives, plastics and rubber, textiles, oils, soaps, waxes, food, petroleum, and biological samples [236]**.** In this chapter, the comparative study of thermal behaviour of single crystals of terbium fumarate, gadolinium fumarate and mixed Gd-Tb fumarate heptahydrate crystals is reported. The non-isothermal decomposition kinetics of these compounds is also discussed.

6.2 Experimental Procedure

Single crystals of terbium fumarate, gadolinium fumarate and mixed GdTb fumarate heptahydrates were used for thermogravimetric and differential thermal analysis. For the single component rare-earth fumarate crystals of gadolinium fumarate and terbium fumarate heptahydrates simultaneous recording of TGA and DTA/DTG was performed from room temperature to 750 ^{o}C. And for mixed rare-earth fumarate crystals gadolinium-terbium fumarate heptahydrate crystals the thermal analysis was made from the room temperature up to 1000 ^{o}C, in the Nitrogen atmosphere at a heating rate of 10 ^{o}C/ min by using a Perkin-Elmer thermal analyser.

6.3 Results and discussions

6.3.1 Comparative study of the thermal behaviour of terbium fumarate, gadolinium fumarate and mixed gadolinium-terbium fumarate crystals

Thermal gravimetric analysis (TGA) is one of the techniques of thermal analysis in which changes in physical and chemical properties of materials are measured as a function of increasing temperature with constant heating rate, or as a function of time with constant temperature and/or constant mass loss. TGA/DTA can provide information about physical phenomena such as second order phase transitions, including vaporizations, sublimation, absorption, adsorption and desorption. Likewise, TGA can provide information about chemical phenomena including desolvation (especially dehydration), decomposition, and solid-gas reactions (e.g., oxidation or reduction). The TG curve can also give useful information for the thermal stability and composition of the sample under investigation. The recorded curve is first analyzed for obtaining the percentage weight loss of the compound in different steps of thermal decomposition at different temperatures. Thus, we are able to find the thermal stability and dissociation of the grown compounds.

Thermo grams shown in Fig. 4.23, Fig. 4.24 and Fig. 4.25 in chapter 4 show the thermal decomposition stages of terbium fumarate, gadolinium fumarate and mixed gadolinium-terbium fumarate heptahydrates respectively. The two pure rare-earth fumarate crystals i.e. terbium fumarate and gadolinium fumarate decompose completely in two stages till the formation of their oxides. But the mixed rare-earth fumarate, gadolinium-terbium fumarate crystals decompose in three steps till the

formation of its oxide $GdTbO_3$. In order to identify the final product of the thermal decomposition of terbium fumarate to be Tb_2O_3, its powder X-ray diffraction pattern was obtained and a phase matching search was carried out with the ICDD (International Centre for Diffraction Data) inorganic database, PDF2. The experimental pattern was found to be similar to that of PDF #00-043-1032, which belongs to Tb_2O_3. Fig. 6.1 shows the XRD pattern of Tb_2O_3 as the final product of thermal decomposition of terbium fumarate heptahydrate single crystals. Like wise, the oxide formation takes place for gadolinium fumarate and mixed gadolinium-terbium fumarate heptahydrate compounds as the final product, which are isomorphous to terbium fumarate heptahydrate as already discussed in chapter-4 of the thesis. Table 6.1 gives the comparative study of thermogravimetric analysis of pure and mixed rare-earth fumarate crystals. From this table, we come to know that

Table 6.1: Comparative study of temperature ranges, mass losses (%), and peak temperatures observed in thermal analysis of pure and mixed rare-earth fumarate crystals.

	Compound/ decomposition step	Step	Temp. range ^oC	Expt. mass loss %	Calcul. mass loss %	Loss of molecules in the step	Corresponding peak in DTG ^oC	Product
1.	$Tb_2(C_4O_4H_2)_3$ 7 H_2O	1	80-150	16.40	16.04	-7H_2O	132.63	$Tb_2(C_4O_4H_2)_3$
		2	410-650	37.33	37.42	- ($3H_2O$+6CO+6C)	481.5	Tb_2O_3
2.	$Gd_2(C_4O_4H_2)_3$ 7 H_2O	1	80-150	16.40	16.33	-7H_2O	133.63	$Gd_2(C_4O_4H_2)_3$
		2	420-650	37.33	38.10	- ($3H_2O$+6CO+6C)	484.59	Gd_2O_3
3	$GdTb(C_4O_4H_2)_3$ 7 H_2O	1	85-150	16.5	16.18	-7H_2O	149	$GdTb(C_4O_4H_2)_3$
		2	450-820	33.5	32.11	- ($3H_2O$+4CO+7C)	484	$GdTbO_2CO_3$
		3	820-1000	6	5.65	-CO_2	840	$GdTbO_3$

the endothermic peaks for pure rare-earth fumarate crystals (terbium fumarate and gadolinium fumarate) are nearly same respectively at 132.63 ^{o}C and 133.63 ^{o}C respectively and that of the mixed GdTb fumarate is at a higher temperature of 149 ^{o}C. It has also been observed that complete dehydration for both the single component rare-earth fumarates and the mixed rare-earth fumarate compounds takes place in the same temperature range of 80-150 ^{o}C but the thermal stability of anhydrous terbium fumarate, gadolinium fumarate and mixed Gd-Tb fumarate compounds is different and upto 410 ^{o}C, 420 ^{o}C and 450 ^{o}C respectively.

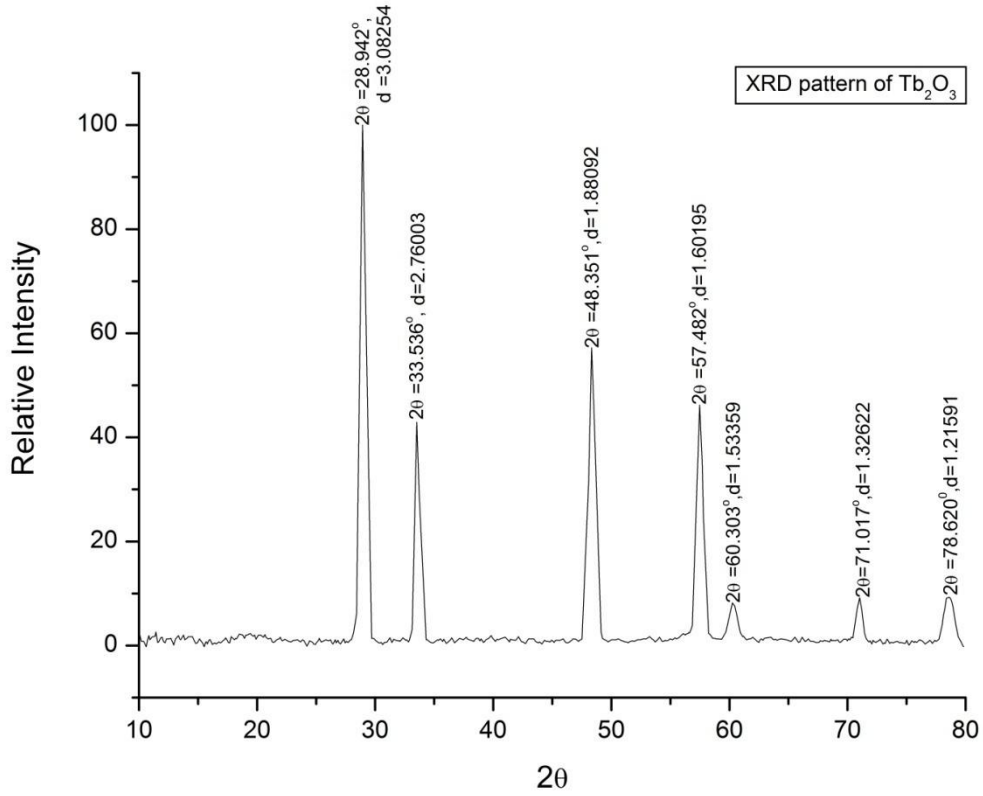

Figure 6.1: XRD pattern of terbium oxide (Tb_2O_3).

6.4 Non–isothermal decomposition kinetics

In most kinetic studies the variation in the concentration of reactants, or of products, with time, is followed under isothermal conditions, and rate coefficients 'k' are derived from the appropriate rate equations. Several experiments are then carried out at a series of different, but constant temperatures and from the temperature dependence of the rate coefficient , the Arrhenius parameters, i.e. the activation

energy, E, and the pre-exponential factor, A, can be estimated. The time taken for an adequate series of isothermal experiments is a considerable disadvantage and when the amount of reactant material available is also limited, it becomes most desirable to obtain maximum information from a single kinetic experiment where the reaction is carried out at a controlled temperature, continuously increasing according to some desired programme. In the present chapter non-isothermal kinetic methods have been used to determine activation energy E and pre-exponential factor A. Most kinetics start with the assumption that the rate of reaction is a function of degree of conversion and sample temperature.

The degree of conversion is given by

$$\frac{d\alpha}{dt} = k(T)\, f(\alpha) \qquad (6.1)$$

where, k (T) is the temperature dependent reaction rate constant, f(α) is the reaction model and α is the conversion fraction.

Integrating the above equation gives the integral rate law,

$$g(\alpha) = k\, t \qquad (6.2)$$

where g(α) is the integral reaction model. The temperature dependence of the rate constant is described by the Arrhenius equation [237].

$$k(T) = Ae^{-\frac{E}{RT}} \qquad (6.3)$$

where A is the pre-exponential (frequency) factor, E is the activation energy, T is the absolute temperature and R is the gas constant.

Substituting Eq. (6.3) in the above rate expressions gives,

$$\frac{d\alpha}{dt} = Ae^{--\frac{E}{RT}}\ f(\alpha) \qquad (6.4)$$

And $g(\alpha) = Ae^{--\frac{E}{RT}}\ t$ (6.5)

Several reaction models for the thermal decomposition of ionic solids [238], using f(α) or g(α) are listed in Table 6.2.

Kinetic parameters can be obtained from isothermal kinetic data by applying these rate laws or can be transformed into non-isothermal rate expressions describing reaction rate

as a function of temperature at a constant heating rate by utilizing the following,

$$\frac{d\alpha}{dT} = \frac{d\alpha}{dt}\frac{dt}{dT} \qquad (6.6)$$

where, *dα/dT* is the non-isothermal reaction rate, *dα/dt* is the isothermal reaction rate and *dt/dT* is the inverse heating rate (1/β).

Substituting Eq. (6.4) into Eq. (6.6) gives the differential form of the non-isothermal rate law,

$$\frac{d\alpha}{dT} = \frac{A}{\beta} e^{-\frac{E}{RT}} f(\alpha) \qquad (6.7)$$

Upon integration, Eq. (6.7) gives,

$$g(\alpha) = \frac{A}{\beta}\int_0^T e^{-\frac{E}{RT}}\, dT \qquad (6.8)$$

If, $\frac{E}{RT}$ is replaced by "*x*" and integration limits transformed, Eq. (6.8) becomes,

$$g(\alpha) = \frac{AE}{\beta R}\int_x^\infty \frac{e^{-x}}{\mathrm{x}^2}\, dx \qquad (6.9)$$

Eq. (6.9) can be written as,

$$g(\alpha) = \frac{AE}{\beta R}\, p(x) \qquad (6.10)$$

where, *p(x)* is the exponential integral.

Kinetic parameters can be obtained from non-isothermal rate laws by both model-fitting and iso-conversional (model-free) methods. There are several non-isothermal model-fitting methods, one of the most popular being the Coats and Redfern method [239, 240]. This method utilizes the asymptotic series expansion for approximating the exponential integral p(x) in Eq.(6.10), giving,

$$\ln\left[\frac{g(\alpha)}{T^2}\right] = \ln\left(\frac{AR}{E\beta}\left(1-\frac{2RT}{E}\right)\right) - \frac{E}{RT} \qquad (6.11)$$

Plotting the left-hand side of Eq. (6.11), which includes the model g(α), versus 1/T gives E and A from the slope and intercept, respectively. The model that gives the best linear fit is selected as the model of choice.

Table 6.2: Solid-state rate expressions for different reaction models.

Model	Differential form $f(\alpha) = \frac{1}{k}\frac{d\alpha}{dt}$	Integral form g(α) = kt
Nucleation models		
Avarami-Erofe'ev (A2)	$2(1-\alpha)[-\ln(1-\alpha)]^{1/2}$	$[-\ln(1-\alpha)]^{1/2}$
Avarami-Erofe'ev (A3)	$3(1-\alpha)[-\ln(1-\alpha)]^{2/3}$	$[-\ln(1-\alpha)]^{1/3}$
Geometrical contraction models		
Contracting area (R2)	$2(1-\alpha)^{1/2}$	$[1-(1-\alpha)^{1/2}]$
Contracting volume (R3)	$3(1-\alpha)^{2/3}$	$[1-(1-\alpha)^{1/3}]$
Diffusion models		
1D Diffusion (D1)	$1/2\alpha$	α^2
2D Diffusion (D2)	$[-\ln(1-\alpha)]^{-1}$	$[(1-\alpha)\ln(1-\alpha)] + \alpha$
3D Diffusion-Jander Eq. (D3)	$3(1-\alpha)^{2/3}/2(1-(1-\alpha)^{1/3})$	$[1-(1-\alpha)^{1/3}]^2$
Ginstling–Brounshtein (D4)	$(3/2((1-\alpha)^{-1/3}-1)$	$1-(2\alpha/3)-(1-\alpha)^{2/3}$

6.4.1 Non-Isothermal decomposition kinetics of terbium fumarate crystals

The non-isothermal kinetic parameters have been worked out for terbium fumarate heptahydrate single crystals for the complete stage 1 (100-150 ^{o}C) and stage 2 (410-650 ^{o}C) by using the integral method by applying the Coats – Redfern approximation [237, 238]. $\ln\left[\frac{g(\alpha)}{T^2}\right] = \ln\left(\frac{AR}{E\beta}\left(1-\frac{2RT}{E}\right)\right) - \frac{E}{RT}$

Table 6.3: Kinetic and statistical parameters values for the analysed models of terbium fumarate heptahydrate from TG experiment.

Stage	Model	| r |	E_α (kJmole^{-1})
1			
	D1	0.99382	211.35
	D2	0.9946	210.83
	D3	0.99474	49.493
	D4	0.99499	212.902
	A2	0.99588	51.064
	A3	0.99525	31.99
	R2	0.99485	103.8
	R3	0.99541	105.337
2			
	D1	0.85866	184.50
	D2	0.86237	187.83
	D3	0.84713	43.10
	D4	0.87292	195.46
	A2	0.89	50.25
	A3	0.85937	29.10
	R2	0.86378	93.38
	R3	0.88018	99.39

where α is the fraction of reactant used, g(α) is the conversion function which is dependent on the mechanism of the reaction, R the gas constant (= 8.314 J K^{-1} mol^{-1}) , E is the activation energy (kJ mol^{-1}),T the absolute temperature (K), β the linear heating rate (K s^{-1}) and A is the frequency factor (s^{-1}) .This equation is most often used to describe the kinetics of thermal decomposition of solids in general. A plot of $\ln\left[\frac{g(\alpha)}{T^2}\right]$ versus 1/T gives a straight line for the correct model. The statistical parameter such as the correlation coefficient 'r' was calculated to aid the selection of the g (α) function best describing the experimental results [241]. The values of the kinetic and statistical parameters for all analysed models are listed in Table 6.3, from which the best fitting expression for which the correlation coefficient for stage 1 and stage 2 is maximum is for 2D nucleation model D (A2) with activation energy of 51.064 kJ/mole and 50.25 kJ/mole respectively. The Arrhenius for the best fitting curve for the dehydration and the decomposition steps are shown in Fig. 6.2 and Fig. 6.3 respectively.

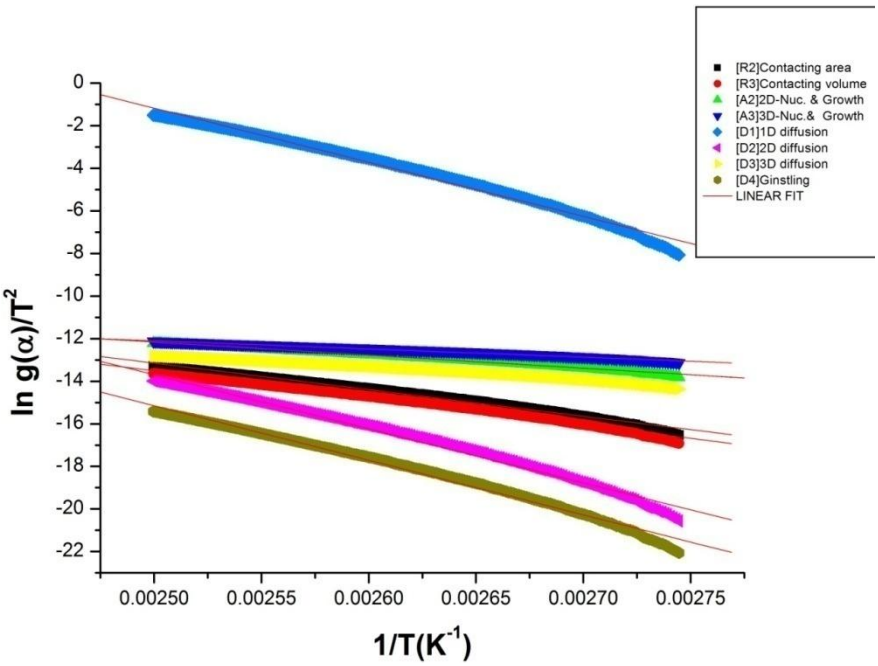

Figure 6.2: Arrhenius plot of the best fitting function g(α) for the dehydration step (100-150 ^{o}C) of TFH crystals.

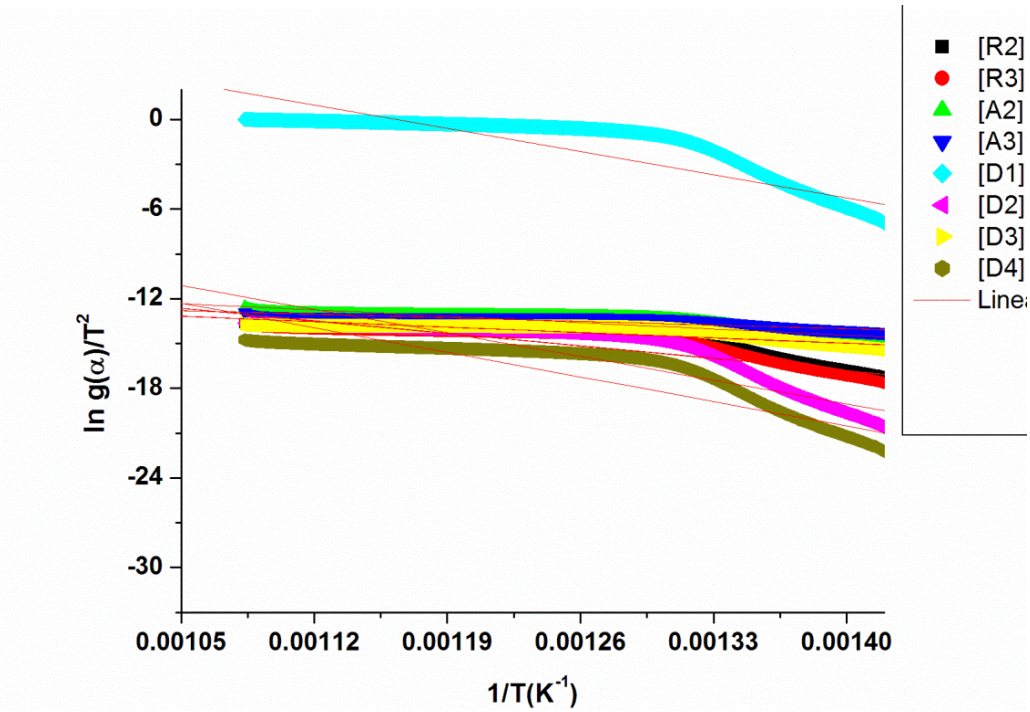

Figure 6.3: Arrhenius plot of the best fitting function g(α) for the decomposition step (410- 650 ^{o}C) of terbium fumarate crystals.

6.4.2 Non-isothermal decomposition kinetics of gadolinium fumarate crystals

Like terbium fumarate, the non-isothermal kinetic parameters of gadolinium fumarate have been worked out for the complete stage 1 (100-150 ^{o}C) and stage 2 (420-650 ^{o}C) using the integral method by applying the Coats – Redfern approximation as described in section 6.4.1. The values of the kinetic and statistical parameters for all analysed models are listed in Table 6.4. The Arrhenius plot for the best-fitting curve for the stage 1 and stage 2 of gadolinium fumarate heptahydrate is shown in Fig. 6.4 and Fig. 6.5 respectively. It is clear from the Table 6.4 that the best fitting expression for both the stage 1 and stage 2 is again for 2D nucleation model D (A2) with activation energy of 45.61 kJ/mol and 45.36 kJ/mole respectively.

Table 6.4: Kinetic and statistical parameters values for the analysed models of gadolinium fumarate heptahydrate from TG experiment.

Stage	Model	| r |	E_α (kJmole^{-1})
1			
	D1	0.97089	167.32
	D2	0.97635	171.53
	D3	0.9826	41.60
	D4	0.97929	175.97
	A2	0.98392	45.61
	A3	0.98138	28.26
	R2	0.97923	86.07
	R3	0.9826	89.63
2			
	D1	0.08608	171.49
	D2	0.86597	173.75
	D3	0.84839	39.01
	D4	0.87704	180.71
	A2	0.89182	45.36
	A3	0.85781	25.84
	R2	0.86708	85.78
	R3	0.884	91.22

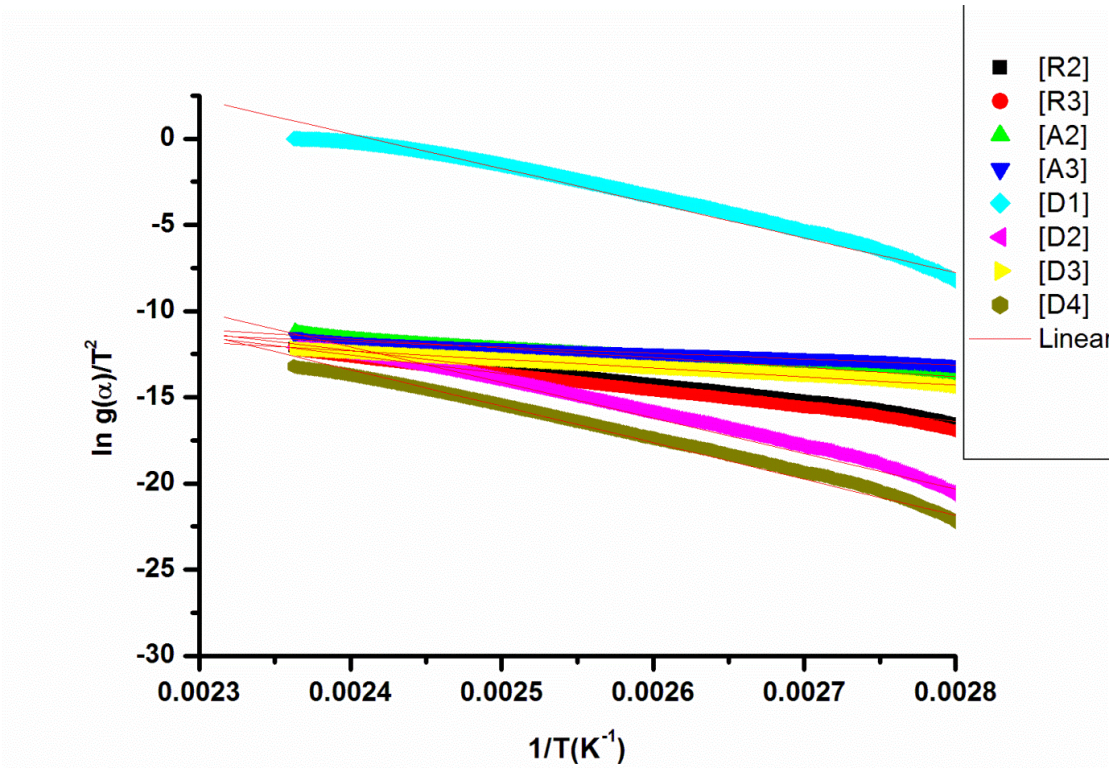

Figure 6.4: Arrhenius plot of the best fitting function g(α) for the dehydration step (100-150 ^{o}C) of gadolinium fumarate.

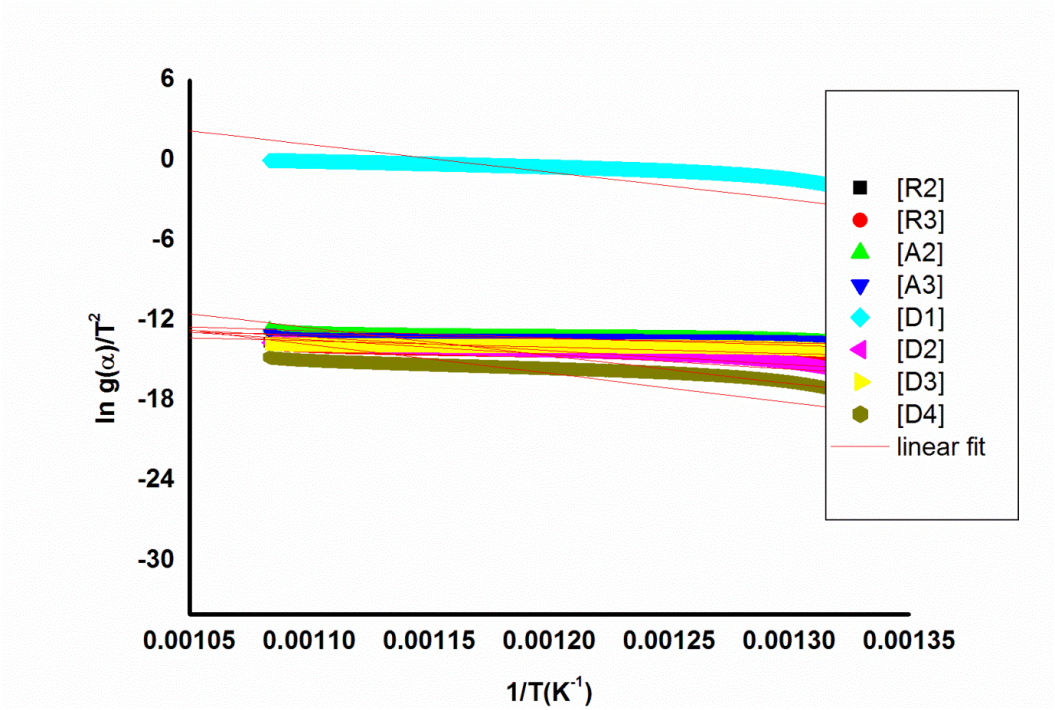

Figure 6.5: Arrhenius plot of the best fitting function g(α) for the thermal decomposition step (420- 650 ^{o}C) of GFH crystals.

6.4.3 Non-isothermal decomposition kinetics of mixed mixed Gd-Tb fumarate crystals

Like terbium fumarate and gadolinium fumarate heptahydrates, the non-isothermal kinetic parameters of mixed gadolinium terbium fumarate heptahydrate have been worked out for the thermal decomposition step 1 (100-150 ^{o}C) and step 2 (450-700 ^{o}C) using the integral method by applying the Coats – Redfern approximation as already described in section 6.4.1 and 6.4.2. The values of the kinetic and statistical

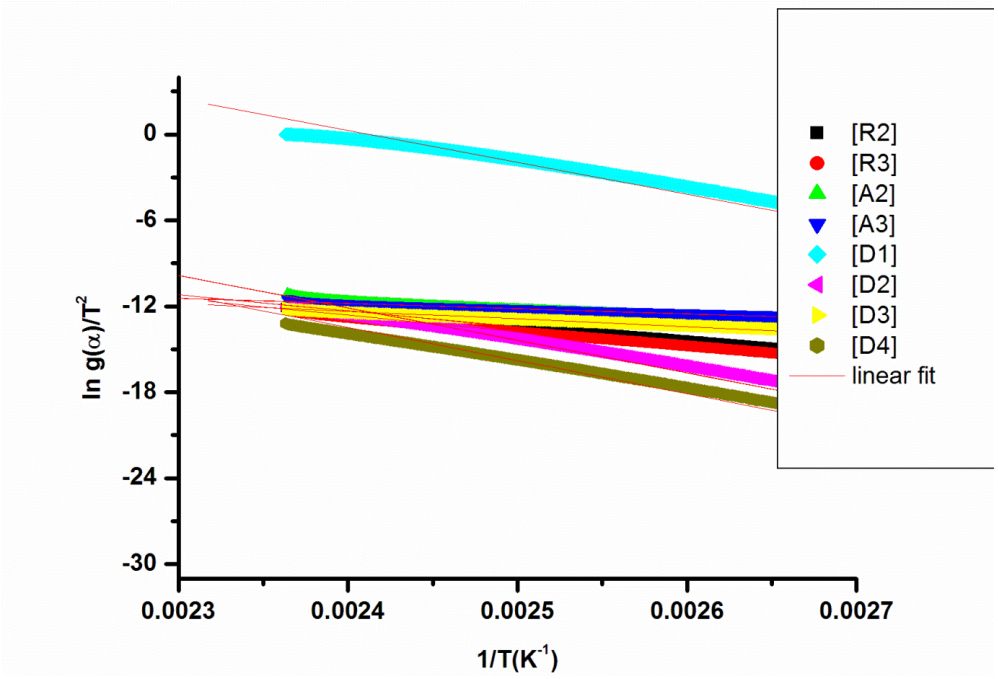

Figure 6.6: Arrhenius plot of the best fitting function g(α) for the dehydration step (100-150 ^{o}C) of mixed GdTb fumarate.

parameters for all analysed models are listed in Table 6.5.The Arrhenius plot for the best-fitting curve of mixed gadolinium-terbium fumarate heptahydrate for the stage 1 and stage 2 is shown in Fig. 6.6 and Fig. 6.7 respectively. It is clear from Table 6.5 that the best fitting expression for both the stage 1 and stage 2 for mixed fumarate complex is again for 2D nucleation model D (A2) with activation energy of 48.63 kJ/mol and 44.93 kJ/mole respectively.

Table 6.5: Kinetic and statistical parameters values for the analysed models of mixed Gd-Tb fumarate heptahydrate from TG experiment.

Stage	Model	| r |	E_α (kJmole^{-1})
1	D1	0.96828	185.46
	D2	0.97299	188.48
	D3	0.97528	45.31
	D4	0.97299	192.27
	A2	0.98031	48.63
	A3	0.97738	30.27
	R2	0.9753	94.02
	R3	0.97854	97.03
2			
	D1	0.7383	150.50
	D2	0.74335	155.63
	D3	0.71641	36.03
	D4	0.76227	164.77
	A2	0.79245	44.93
	A3	0.73922	25.42
	R2	0.74576	78.35
	R3	0.77499	85.64

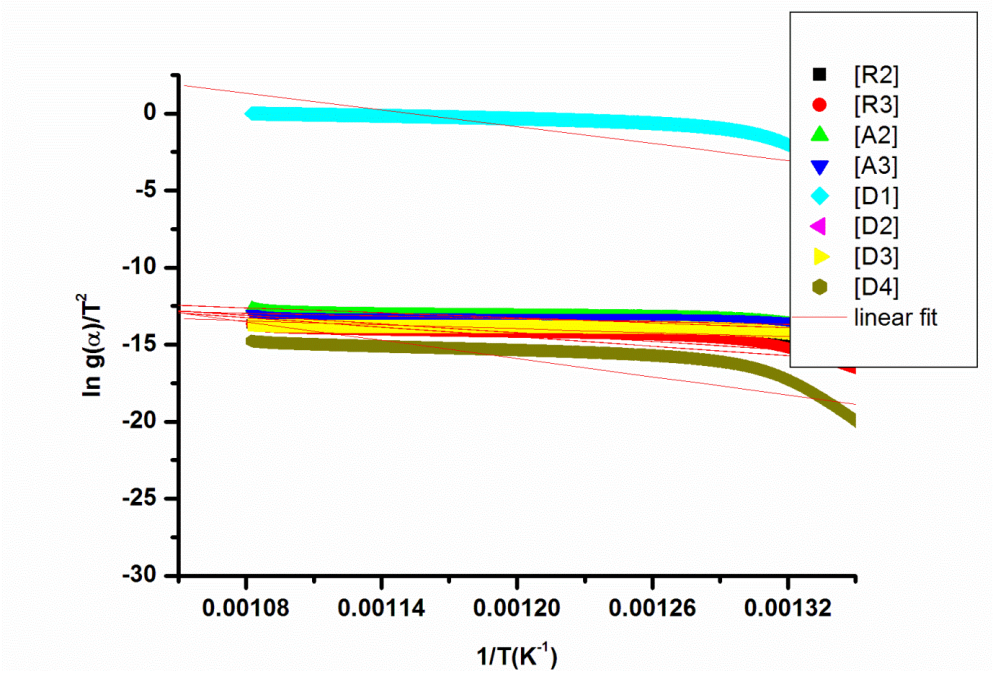

Figure 6.7: Arrhenius plot of the best fitting function g(α) for the thermal decomposition 2nd step (450-700 ^{o}C) of mixed GdTb fumarate.

Conclusions

1. From thermogravimetric analysis it is found that both the pure and mixed rare-earth fumarate crystals loose their both lattice and co-ordinated water molecules in the first step of thermal decomposition in the temperature range 80-150 ^{o}C.

2. The comparative study of thermogravimetric analysis of pure and mixed rare-earth fumarate crystals show that the anhydrous mixed Gd-Tb fumarate heptahydrate is thermally more stable than the pure rare-earth fumarate crystals.

3. Thermal decomposition of both pure rare-earth fumarate crystals (TFH, and GFH crystals) take place in only two steps ultimately leading to the formation of their corresponding oxides at a temperature of around 700 ^{o}C but the thermal decomposition of mixed terbium-gadolinium fumarate heptahydrate crystals takes place in three steps of thermal decomposition for the formation of its oxide and at a higher temperature of 840 ^{o}C.

4. The reactions corresponding to stages 1 and 2 in each of the three different compounds are governed by 2D nucleation model A2, as is also evidenced by Fig 4.8.(c) of SEM micrograph of chapter 4.

5. The activation energy for stage 1 and stage 2 is respectively given as 51.064 kJ/mol and 50.25 kJ/mol for terbium fumarate, 45.61 kJ/mol and 45.36 kJ/mol for gadolinium fumarate and 48.63 kJ/mol and 44.93 kJ/mol for mixed GdTb fumarate crystals.

CHAPTER-7

Luminescent properties of terbium and mixed Tb-Gd fumarate heptahydrate single crystals

7.1 Introduction

Luminescence is defined as the process in which light is produced by the absorption of energy. It consists of two basic forms, fluorescence and phosphorescence, depending on multiple spin state during the radiative relaxation process. Fluorescence refers to the emitting of light between energy states of the same spin multiplicity, and the process generally lasts no more than about 10 ns. However, phosphorescence refers to the emitting of light between states with difference spin multiplicity, and the process lasts a microsecond to seconds. In the past some inorganic and organic luminescent materials have been extensively explored and realized for their diverse functionalities and applications in lighting, display, sensing, and optical devices [242-245].

As far as the luminescence of rare-earth elements is concerned, they have unfilled 4f electron shells in their normal valence states and generally form trivalent ions in a crystal. These trivalent rare-earth ions have various energy levels of the $4f^n$ electronic configuration and these $4f^n$ energy levels are generally quite narrow, thus resulting sharp optical transitions and accompanying narrow emission lines. The unique functionalities of luminescence of rare-earth elements are due to the high color purity and narrow emission generated from these ions. The organic luminescent materials have developed their applications in organic light emitting diodes (OLEDs) by incorporating the luminescent organic material between two conductors as reported in the literature [246-248]. The Judd-Ofelt theory has been fruitful to characterize

radioactive transitions for rare-earth doped solids, as well as aqueous solutions. By applying this theory we can estimate the intensities of the transitions for rare-earth ions [249-252]. This theory defines a set of three intensity parameters, Ω_λ (λ = 2, 4, 6), that are sensitive to the environment of the rare-earth ions. These parameters can be determined experimentally from measurements of absorption spectra and the refractive index of matrix. From these parameters the important optical properties, including the radiative transition probability for spontaneous emission, the radiative lifetime of the excited states can be found. From this theory the absorption spectrum can be used to determine the oscillator strengths [253].

The hybrid materials of both inorganic and organic components in metal-organic coordination compounds are very promising for a multifunctional luminescent material [254-258]. For the energy transfer mechanism, the luminescent properties of materials are heavily dependent on the structure and intermolecular packing of the compounds, therefore, it is necessary to control the three-dimensional structure and intermolecular packing at the molecular level such as Van der Waals interactions, hydrogen bonding, and aromatic π-π interactions to control the 3D molecular packing [259]. In some metal organic frameworks the permanent porosities and collaborative luminescent properties are particularly useful to develop luminescent sensing materials. Infact, to make use of the pores within luminescent MOFs for their differential recognition of sensing substrates, a number of porous luminescent sensing MOFs have been fulfilled [260-263]. Luminescence can arise from direct organic ligands excitation (particularly from the highly conjugated ligands), metal-centered emission (widely observed in lanthanide MOFs through the so-called antenna effect), and charge-transfer such as ligand-to-metal charge transfer (LMCT) and metal-to-ligand charge transfer (MLCT). Furthermore, the guest molecules can also result in luminescence onto MOFs. Luminescent rare-earth compounds are interesting materials not only due to their academic importance but essentially due to a variety of potential technological applications, such as fluores- cence materials [264–266], electro luminescence devices [267-270] and as fluorescence probes and labels in a variety of biological systems [271–274]. Weissman and coworkers [73] first reported the light- emission characteristics of a rare-earth complex of β-diketone. Since then, much work has been carried out to obtain various rare-earth complexes with special structures and luminescence behavior. The main ligands include aromatic carboxylic

acid,1, 10- phenanthroline (phen), pyridine and b-diketon [275–277]. It is well known that the luminescent mechanism is an intra- molecular energy transfer from the ligands to the metal ions under excitation by near ultraviolet light, that is, ‘‘antenna effect’’ [278].

A group of particularly efficient light conversion molecular devices is formed by the compounds of Eu^{3+} and Tb^{3+} ions having one or more ligands. The function of these ligands is to absorb strongly in the near UV-region and non radiatively the energy is transferred to the rare-earth ion that may undergo a multiphonon relaxation and subsequently emit in the visible. Such a process of energy transfer was first invoked by Wiessman [73] to describe the strong luminescence of certain organo-europium compounds and was later observed and studied by several other authors [279-281]. The luminescence intensity, thus, depends on the balance between the absorption, non radiative decay, energy transfer and emission rates involved.

7.2 UV-Vis spectral analysis

7.2.1 UV-Vis spectral analysis of terbium fumarate

UV-Vis spectrum for both terbium fumarate heptahydrate (TFH) and gadolinium-terbium fumarate heptahydrate (GTFH) crystals was studied by Cary 5000 spectrometer in the range of 200-1000 nm. UV-Vis spectrum of TFH crystals is shown in Fig. 7.1. The spectrum showing maximum absorption in the near-UV range (200-350 nm) at 266 nm for which % reflectance is 14.426 was observed owing to $n \rightarrow \pi^*$ transition. This transition may be due to lone pair of electrons present on oxygen and antibonding π orbital of C=C of fumarate ligand. At 489 nm with % reflectance of 67.470, another dip is found in the UV-Visible spectrum. This wavelength is attributed to $\pi \rightarrow \pi^*$ transition and is because of C = C of fumarate part of terbium coordination complex. At 586 nm, UV-Visible spectrum shows another dip which may be due to d-f transition of terbium. From the spectrum, it has been inferred that TFH crystals have sufficient transmission nearly in the entire visible and IR region. The absorption coefficient is high at lower wavelength and the transparency in the visible part of the spectrum from 500 nm suggesting their suitability for laser and luminescent materials [279]. The band gap energy of terbium fumarate heptahydrate

crystals with the maximum wavelength of absorption (266 nm) is calculated by using the simple conversion equation, E= hc /λ_{max}= 4.65eV.

7.2.2 UV-Vis spectral analysis of gadolinium-terbium fumarate

The UV-Vis spectrum of GTFH crystals is shown in Fig 7.2. The spectrum showing maximum absorption in the near-UV range (200-350 nm) at 263 nm for which % reflectance is 6.057, was observed owing to n→π* transition. This transition may be due to the lone pair of electrons present on oxygen and antibonding π orbital of C=C of fumarate ligand. The absorption coefficient is high at lower wavelengths and the graph is more smooth for the compound and hence the transparency in the visible part of the spectrum from 540 nm is suggesting its much suitability for laser and luminescent materials [279]. For the maximum wavelength of absorption (263 nm), the band gap energy is calculated by using the simple conversion equation:

$$\text{Energy band gap, } E_g = hc/\lambda_{max}$$

$$E_g = 4.66\text{eV}.$$

Since both pure and mixed rare-earth fumarate compounds being isomorphous show the transparency in the visible part of the spectrum in the same range and also have the approximately the same energy gap.

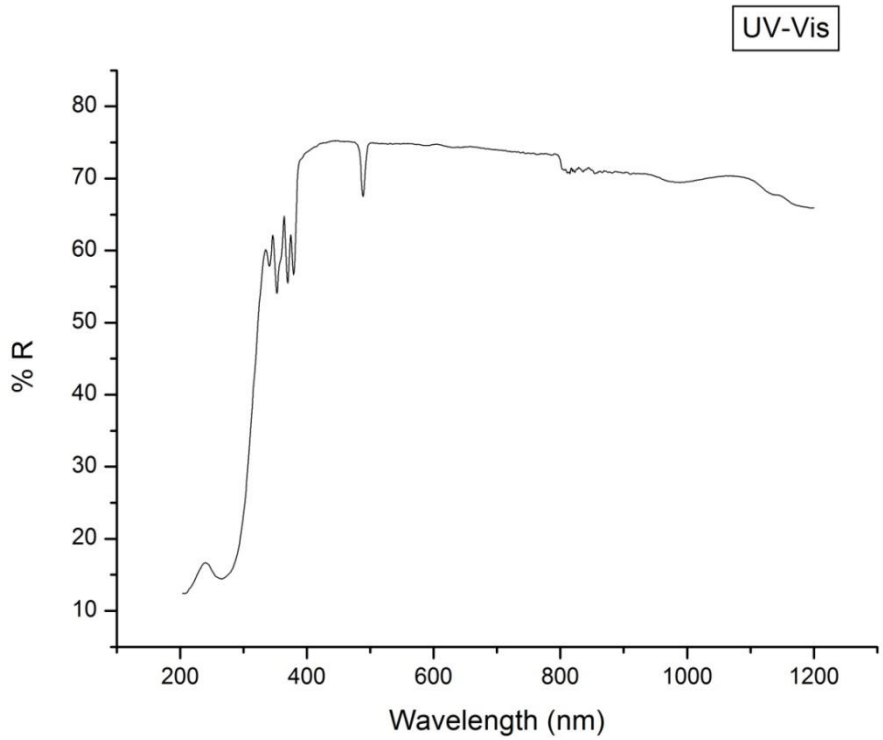

Figure 7.1: UV-Vis spectrum of terbium fumarate crystals.

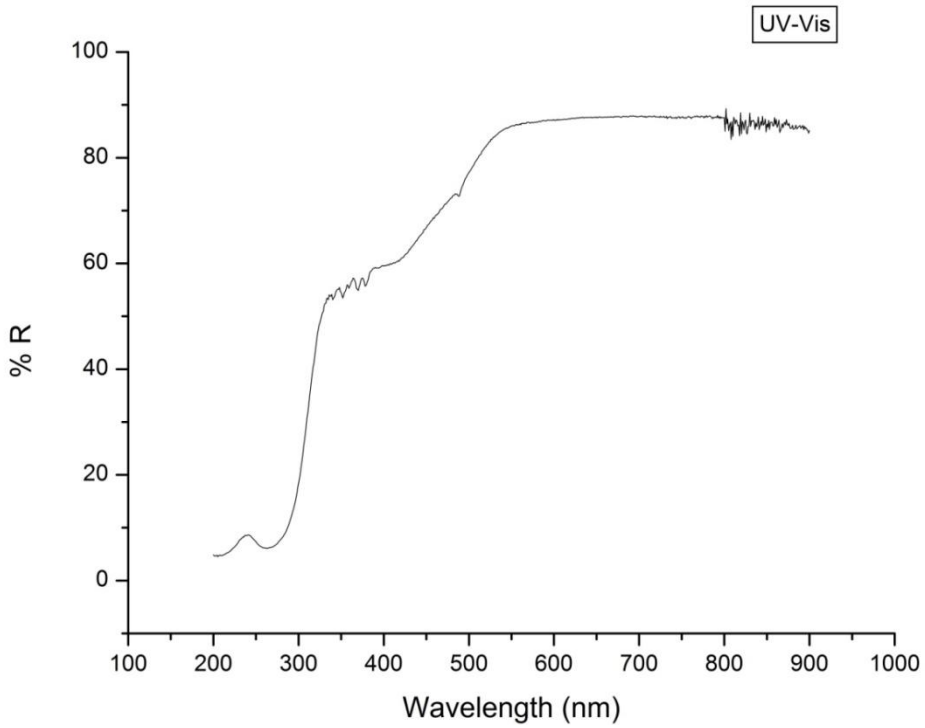

Figure 7.2: UV-Vis spectrum of mixed Gd-Tb fumarate crystals.

7.3 Photoluminescence spectroscopy

7.3.1 Photoluminescence spectrum of terbium fumarate crystals

The photo luminescence spectrum of these crystals was obtained by using Varian Cary-Eclipse spectrophotometer and recorded under the same experimental conditions. The lanthanide ions suffer from weak light absorption due to the forbidden f-f transitions, making the direct excitation of the metals very inefficient unless high-power laser excitation is utilized. This problem can be overcome by coupling species that can participate in energy transfer processes, known as "luminescence sensitization" or "antenna effect" [243, 282, 283]. Fig. 7.3 shows the emission spectrum of terbium fumarate heptahydrate single crystals recorded at room temperature. The emission spectrum of terbium fumarate complex exited at 339 nm, 350 nm or 368 nm reveals well resolved strong luminescence of the f-f transitions of Tb^{3+} ions.When terbium fumarate complex was exited at 339 nm,350 nm or 368 nm, the intense peaks at 491 nm, 546 nm, 587 nm, and 621 nm are ascribed to the $^5D_4$–^7F_J

(J= 6,5,4 and 3 respectively) are the characteristic 4f– 4f transitions of Tb^{3+} ions in the host lattice [65]. The luminescence spectrum of terbium fumarate is dominated at 546 nm in the green region, which is attributed to the $^5D_4 \rightarrow {}^7F_5$ transitions of Tb^{3+} ions. Because of the intense absorption bands of organic chromophores, much more light can be absorbed by the organic ligands than by the lanthanide ion itself. Therefore ligand to metal ion energy transfer can take place by the antenna effect and the energy absorbed by the ligand can effectively transfer to Tb^{3+}, thus the luminescence efficiency of Tb^{3+} ions is enhanced [284]. The four peaks of the Tb^{3+} ions with

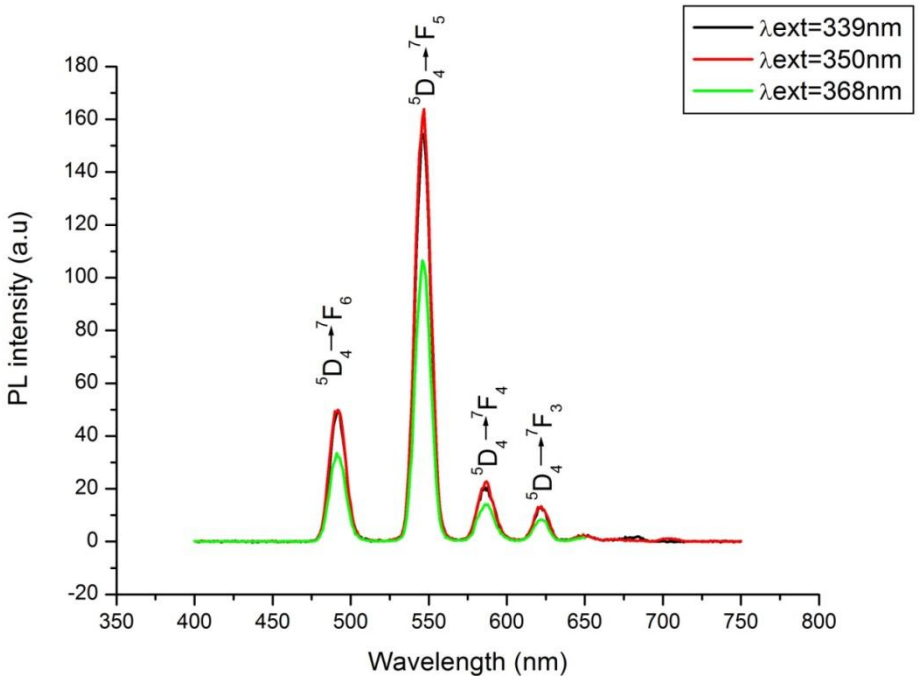

Figure 7.3: Photo luminescence spectra of terbium fumarate crystals.

different excitations are similar except for the emission intensities. However, the presence of water molecules in the grown crystals may quench the luminescence. Indeed, it has been reported that vibrations of water molecules could effectively remove the electronic energy of excited rare-earth ions, and the extent of the quenching was directly related to the number of the coordinated water molecules [285].

7.3.2 Photo luminescence spectrum of mixed GdTb fumarate

Energy transfers from one lanthanide to another lanthanide ion have also been observed to enhance the luminescence intensity in heterolanthanide MOFs. For instance, the Eu^{3+} emissions at 595 and 615 nm in the heterolanthanide MOF [(Eu, Tb)-$(C_6H_8O_4)_3(H_2O)_2]_3$ $(C_{10}H_8N_2)$ ($C_6H_8O_4$ = butane-1,4-dicarboxylate, $C_{10}H_8N_2$ = 4,40-bipyridine) are much stronger than those in $[Eu(C_6H_8O_4)_3(H_2O)_2]_3$ $(C_{10}H_8N_2)$, while the Tb^{3+} emission at 545 nm in the heterolanthanide MOF [(Eu, Tb)-$(C_6H_8O_4)_3(H_2O)_2]_3$ $(C_{10}H_8N_2)$ is completely quenched [286]. Within heterolanthanide MOF [(Eu, Tb)$(C_6H_8O_4)_3(H_2O)_2]_3$ $(C_{10}H_8N_2)$, the Tb^{3+} centers sensitize the $Eu^{3+,}$ leading to effectively enhanced Eu^{3+} emission.

As far as the luminescence of heteronuclear fumarate complex of Gd & Tb is concerned, there is no obvious shift in wavelength of luminescent emission peaks. However the luminous intensity in this mixed complex has unprecedently increased as shown in Fig. 7.4. When the rare-earth complexes composed of active rare-earth ions Tb^{3+} and inert rare-earth ions (La^{3+}, Y^{3+} and Gd^{3+}) were grown with some

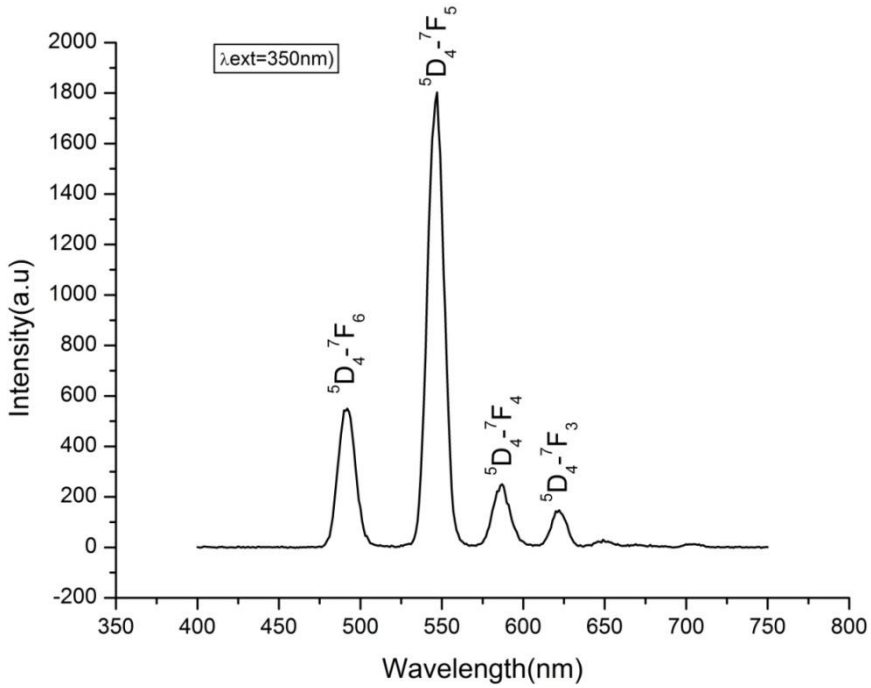

Figure 7.4: Photoluminescene spectra of mixed GTFH crystals.

organic ligand, the characteristic emission bands of active rare-earth ions Tb^{3+} were observed to get enhanced significantly. The reason may be concerned with both the

coordination structure of the compounds and the intra-molecular energy- transfer process. As reported in the literature [287], the exited states of other inert rare-earth ions La^{3+} and Y^{3+} are much greater than the triplet energy level of the ligands. Therefore, the absorbed energy of ligand also could not transfer to La^{3+} and Y^{3+}. However, the introduction of inert fluorescent rare-earth ions could reduce concentration quenching of Tb^{3+} ions, and more energy absorbed by the ligands could be transferred to Tb^{3+} ion in the mixed complex through the bridging ligands. Thus, the emission of mixed complexe is ascribed to direct excitation of the Tb^{3+} ion [288].

7.4. Energy transfer mechanism

The increase in luminous intensity of mixed Gd-Tb complex as compared to pure terbium fumarate complex may be because of the energy transfer probabilities of electric dipole transitions. Gadolinium may have transferred energy by means of intramolecular / intraionic energy transfer mechanism, accounts for the increase in the luminous intensity. Another factor may be the closer ionic radius of Gd to that of luminescent Tb due to lanthanide contraction. It can also favour intramolecular energy transfer. Closer the size of an ionic radius to that of luminescent ion, greater is the enhancement of luminous intensity [289]. Another reason may be attributed to the efficient packing of different moieties of hetreonuclear complex, thereby increasing the symmetry of co-ordination sphere. Two lanthanide ions (Gd & Tb) can bind the ligand fumarate molecules more firmly, making the complex rigid, compact and regularly oriented. The efficient packing may facilitate intramolecular and intra ionic energy transfer thereby increasing the luminous intensity.

The intra-molecular energy transfer takes place from the triplet level of ligand to the emissive level of Tb^{3+} ion. The triplet state energy level of the organic linkers such as fumaric acid (24034 cm^{-1}) is higher than the resonance energy levels of Tb^{3+} (20430 cm^{-1}), therefore the energy absorbed by the ligand can effectively transfer to Tb^{3+}, thus the luminescence efficiency of Tb^{3+} ions is enhanced [289]. When the rare earth compounds composed of active rare-earth ions Tb^{3+} and inert rare-earth ions (La^{3+}, Y^{3+} and Gd^{3+}) were grown with some organic ligand, the characteristic emission bands of active rare-earth ions Tb^{3+} were enhanced greatly. The reason may be concerned with both the coordination structure of the compounds and the intra-molecular energy- transfer process. In this co-luminescence system the lowest

excitation energy level of Gd (III) is 32200 cm^{-1}, which is higher than the lowest triplet level of the ligand. Therefore, the energy could not be transferred from ligand

to Gd (III) ions [287]. As reported in the literature [287], the exited states of other inert rare-earth ions La^{3+} and Y^{3+} are much greater than the triplet energy level of the ligands. Therefore, the absorbed energy of ligand also could not transfer to La^{3+} and Y^{3+}. However, the introduction of inert fluorescent rare-earth ions could reduce concentration quenching of Tb^{3+} ions, and more energy absorbed by the ligands could be transferred to Tb^{3+} ion in the mixed complex through the bridging ligands. Thus, the emission of mixed complexe is ascribed to direct excitation of the Tb^{3+} ion [288].

Conclusion

1. The study of UV-Vis spectra suggests the suitability of TFH and GTFH crystals for laser use and also from this study the band gap energy of the title compounds has been calculated.
2. The comparative study of photo luminescence spectra of TFH and GTFH crystals show that in case of mixed rare-earth complex (GTFH) the intensity was enhanced by Gd (III), which may be due to the intra-molecular energy transfer between inert rare-earth ions and active rare-earth ions.
3. The introduction of inert fluorescent rare-earth ions could reduce concentration quenching of the Tb^{3+} ions, and more energy absorbed by the ligands could be transferred to Tb^{3+} ion through the bridging ligands. Hence, based on these factors, the materials with more luminescent intensity could be obtained.

CHAPTER-8

Magnetic susceptibility measurements of pure and mixed rare-earth fumarate crystals

8.1 Introduction

The magnetic properties are very important to understand the fundamental structure of many solids, both metallic and non-metallic. Rare-earth compounds are interesting because of their magnetic properties. The rare-earth elements comprise 17 metals, starting from scandium (Sc) and yttrium (Y), to be complemented by the 15 lanthanoids ranging from lanthanum (La) to lutetium (Lu). Generally, the lanthanoids can be classified into two sections: the lighter lanthanoids include the atomic numbers from 57 to 64 from lanthanum to gadolinium and the heavier lanthanoids exhibiting atomic numbers from 65 to 71 from terbium to lutetium. It is obvious that the rare-earth elements have magnetically ordered structures and are associated with unpaired 4f electrons except for those elements for which the 4f shell is either empty or full. For example, for La, $4f^0$; for Yb and Lu, $4f^{14}$. Therefore, rare-earth compounds are the potential candidates for their magnetic properties as reported in the literature [290, 291]. The magnetic behaviour of many rare-earth compounds depend only on the nature of the rare-earth ions incorporated in the compound **[**292, 293]. The origin of magnetism of the trivalent rare-earths is in the angular momenta of the 4f level in the atoms. These magnetic electrons in the 4f levels are relatively little affected by the external influences. These 4f electrons which are responsible for the magnetism in rare-earth ions are deep in the atoms and are fairly well screened from intra-crystalline electric fields by a significant outer electron distribution. They include 5s and 5p closed shells and function as true ions. The diversity and the complexity of the magnetic behaviour of many rare-earth compounds depend only on

the nature of the rare-earth ions incorporated in them **[**292**].** The magnetic moments reported for many lanthatlide compounds confirm this phenomena [294-297]. The molar susceptibility and the magnetic moments of as-grown single crystals were determined for different external fields.

8.2 Experimental

The magnetic susceptibility of pure and mixed rare-earth fumarate single crystals (terbium fumarate, gadolinium fumarate and mixed gadolinium-terbium fumarate heptahydrates) were measured by using the Microsense EZ9 vibrating sample magnetometer (Make USA). Since the size of these crystals grown by gel diffusion method was small, therefore, the crystals were ground to a fine powder by adding 2-3 drops of acetone. The powder was then pressed into high density circular pellets of diameter 8 mm and thickness 1 mm at 10 MPa stress. Magnetic moment measurements were carried out on these pellets in a magnetic field of 5- 22k Oersted at a temperature of 20 ^{o}C.

8.3 Results and discussions

In the present study, the growth of rare-earth fumarates was undertaken which are basically the coordination compounds of rare-earth with fumarate ions. Since the unpaired electrons of rare-earth ions occupy the inner f-orbitals which are not influenced by the coordinating ligands, therefore, the rare-earth ions function as true ions even if they are coordinated to fumarate ions.

8.3.1 Theoritical magnetic moments of free tripositive rare-earth ions

In lanthanide ions, although the spin-orbit coupling is not negligible, however, the crystal field effects are very weak and can be ignored. The strong R-S coupling between the spin and orbital moments of the electrons in the unfilled 4f-shell produces a ground state multiplet. The spin orbit coupling constants are quite high so that L and S vectors couple effectively to produce J vector. The value of J in the ground-state multiplet is given by Hund's rule.

The value of J:

$$= | L-S | \text{ for filling } n < 1/2.$$

$$= S \text{ for filling } n = 1/2.$$

= L+S for filling n > 1/2

Therefore, the theoretical values of magnetic moment of Tb^{3+} and Gd^{3+} for which the ground states are $^7F_6$ and $^8S_{7/2}$ respectively have been calculated on the basis of following relation:

$$\mu_{eff} = g\sqrt{J(J+1)}\mu_B\,;\; g = 1 + \frac{J(J+1)+S(S+1)-L(L+1)}{2J(J+1)} \qquad (8.1)$$

where, g is Lande g factor and μ_B the Bohr magneton.

Table 8.1: Theoretical magnetic moment of tripositive rare-earth ions.

Ion	S	L	J	g	$\mu_{eff} = g\sqrt{J(J+1)}\,\mu_B$
La	0	0	0		0.00
Ce	½	3	5/2	6/7	2.54
Pr	1	5	4	4/5	3.58
Nd	3/2	6	9/2	8/11	3.62
Pm	2	6	4	4/5	2.68
Sm	5/2	5	15/2	4/3	0.85
Eu	3	3	0	-	0.00
Gd	7/2	0	7/2	2	7.94
Tb	3	3	6	3/2	9.72
Dy	5/2	5	15/2	4/3	10.65
Ho	2	6	8	5/4	10.61
Er	3/2	6	15/2	6/5	9.58
Tm	1	5	6	7/6	7.56
Yb	½	3	7/2	8/7	4.54
Lu	0	0	0	-	0.00

The theoretical values of magnetic moment of Tb^{3+} and Gd^{3+} are respectively 9.72 μ_B and 7.94 μ_B. For mixed gadolinium-terbium fumarate crystals the theoretical magnetic moment was taken as the average of the two rare-earth ions (Gd^{3+} and Tb^{3+}) and is equal to 8.83 μ_B. The magnetic moment of Tb^{3+} and Gd^{3+} ions in the grown crystals is well-described from the coupling of spin and orbital angular momenta ~ Russell-

Saunders coupling to give J vector. It reveals that 4f-orbital of Tb^{3+} in terbium fumarate and Gd^{3+} in gadolinium fumarate crystals remain unaffected by surrounding fumarate ligands. The theoretical values of the effective magnetic moment of free tripositive rare-earth ions by using equation (8.1) are reported in table 8.1.

8.3.2 Calculation of diamagnetic correction (in e.m.units)

Pascals constants are numbers which are used for calculating the magnetic susceptibility of coordination compounds [298, 299]. Some of these constants used for evaluating diamagnetic susceptibility of the title compounds are listed in table 8.2. On the basis of this table, evaluation of diamagnetic correction of the ligand and the title compounds has been calculated and are given below in table 8.3.

Table 8.2: Representative Pascal constants.

Ligand/Element/Bond-type	χ_{dia} (10^{-6} emu $mole^{-1}$)
H_2O	-13
H	-2.93
C	-6.00
O	-4.60
Tb^{3+}	-19
Gd^{3+}	-20
C=C	+5.5

Table 8.3: Diamagnetic corrections of grown compounds.

Ligand/ Compound	Formula	Diamagnetic Correction χ_{dia} (emu $mole^{-1}$)
Fumarate	$C_4H_2O_4$	-46.76×10^{-6}
Terbium fumarate heptahydrate	$Tb_2(C_4H_2O_4)_3 .7H_2O$	-2.57×10^{-4}
Gadolinium fumarate heptahydrate	$Gd_2(C_4H_2O_4)_3 .7H_2O$	-2.59×10^{-4}
Mixed Gd-Tb fumarate	$GdTb(C_4H_2O_4)_3 .7H_2O$	-2.58×10^{-4}

8.3.3 Experimental magnetic moments of pure and mixed Gd-Tb fumarate single crystals

The magnetic moment of terbium fumarate, gadolinium fumarate and mixed gadolinium-terbium fumarate heptahydrate single crystals was measured by using a vibrating sample magnetometer in a magnetic field of 5- 22 k Oersted at a temperature of 20 ^{o}C. Magnetic susceptibilities were corrected for diamagnetism of rare-earth ions, fumarate ions, and water by using the value as (-20×10^{-6} for Gd and -19×10^{-6} for Tb) [297], -42.76×10^{-6} for fumarate [298] and -13×10^{-6} for water [299] in cgs units, respectively. The experimental correction for the sample holder was carried out. The molar susceptibility χ_{mol} was obtained by using the following relation:

$$\chi_{mol} = \frac{\chi_{mass} M}{n}$$

where M is molar mass of the compound, n the number of rare-earth ions per molecule and χ_{mass} is their gram susceptibility.

The gram susceptibility, $\chi_{mass}=\frac{M}{H}$, where H is the magnetizing field and M is the magnetization per unit mass.

The susceptibility was corrected for the diamagnetism of the constituents by using the Pascal's tables [10, 11] and the corrected value of molar susceptibility was calculated by using the relation:

$$\chi_{mol}^{corr} = \chi_{mol} + \chi^{dia} \text{ (total diamagnetic correction)}$$

When a paramagnetic substance obeys the Curie law, the product of molar susceptibility and temperature is a constant. The effective magnetic moment, μ_{eff} is then defined as

$$\mu_{eff} = \sqrt{\frac{3k}{N\mu_B^2}}\sqrt{T\chi} \approx 2.82787\sqrt{T\chi}$$

Using χ_{mol}^{corr} for χ and T=293 K, the effective magnetic moments of the title compounds were calculated. The observed values of molar susceptibilities and

effective magnetic moments of terbium fumarate, gadolinium fumarate and mixed Gd-Tb fumarate heptahydrate crystals for a maximum magnetising field of 22 k Oersted are shown in Table 8.4. The results obtained as shown in the table reveal a good agreement between the observed and the theoretical values of effective magnetic moments of free rare-earth tripositive ions.This reveals that the diamagnetic behaviour

Table 8.4: Magnetic susceptibility measurements of pure and mixed rare-earth fumarates at 22 kOe.

Rare-earth compound	Experimental molar susceptibility, χ_M (in e.m.u)	Corrected (for diamagnetism of constituent atoms) molar susceptibility, $(\chi_M)_{corr.}$	Observed magnetic moment, $\mu_{eff} = 2.828[(\chi_M)_{corr.} T]^{1/2} \mu_B$	Theoretical effective magnetic moment of Rare-earth ions, $\mu eff = g[J(J+1)]^{1/2} \mu_B$
$Gd_2(C_4H_2O_4)_3.7H_2O$	2.20×10^{-2}	2.23×10^{-2}	7.23	7.94
$Tb_2(C_4H_2O_4)_3.7H_2O$	3.89×10^{-2}	3.91×10^{-2}	9.58	9.72
$GdTb(C_4H_2O_4)_3.7H_2O$	3.00×10^{-2}	3.02×10^{-2}	8.42	8.83

of the organic part of the crystal makes only a negligible contribution to the total magnetic moment of the compounds. Also, the experimental values of the effective magnetic moment of the double rare-earth fumarate crystal is in close agreement with the average value of the effective magnetic moments of the single component rare-earth fumarates. This shows that in mixed gadolinium-terbium crystals, the rare-earth ions coordinating the fumarate ligands are in the ratio of 1:1, which is also substantiated by EDAX analysis of section 4.5.5 of chapter 4. The comparative study of variation of molar susceptibility and the magnetic moments of the title compounds

for the magnetising field of 5-22 kOe is shown in table 8.5. And, the variation of their molar susceptibility in the magnetising field of range 5-22 kOe is shown in Fig. 8.1.

Table 8.5: Comparative study of molar susceptibility / magnetic moments of GFH, TFH and GTFH crystals

Field	Molar susceptibility			Magnetic moment (μ_B)		
in kOe	GFH	TFH	GTFH	GFH	TFH	GTFH
5	0.0226	0.0388	0.0304	7.26	9.53	8.44
6	0.0225	0.0389	0.0303	7.26	9.54	8.42
7	0.0224	0.0391	0.0303	7.24	9.57	8.42
8	0.0224	0.0393	0.0303	7.24	9.59	8.42
9	0.0223	0.0393	0.0302	7.23	9.59	8.41
10	0.0223	0.0393	0.0302	7.23	9.59	8.41
11	0.0223	0.0392	0.0302	7.23	9.58	8.41
12	0.0223	0.0392	0.0301	7.21	9.58	8.39
13	0.0222	0.0391	0.0301	7.21	9.57	8.39
14	0.0222	0.0391	0.0301	7.21	9.57	8.39
15	0.0222	0.039	0.03	7.21	9.56	8.38
16	0.0222	0.039	0.03	7.21	9.56	8.38
17	0.0221	0.0389	0.03	7.19	9.54	8.38
18	0.0221	0.0388	0.0299	7.19	9.53	8.37
19	0.0221	0.0388	0.0299	7.19	9.53	8.37
20	0.0221	0.0389	0.03	7.19	9.54	8.38
21	0.0222	0.0391	0.0301	7.21	9.57	8.39
22	0.0223	0.0392	0.0302	7.21	9.58	8.41

GFH= gadolinium fumarate heptahydrate; TFH= terbium fumarate heptahydrate; GTFH= gadolinium-terbium fumarate heptahydrate.

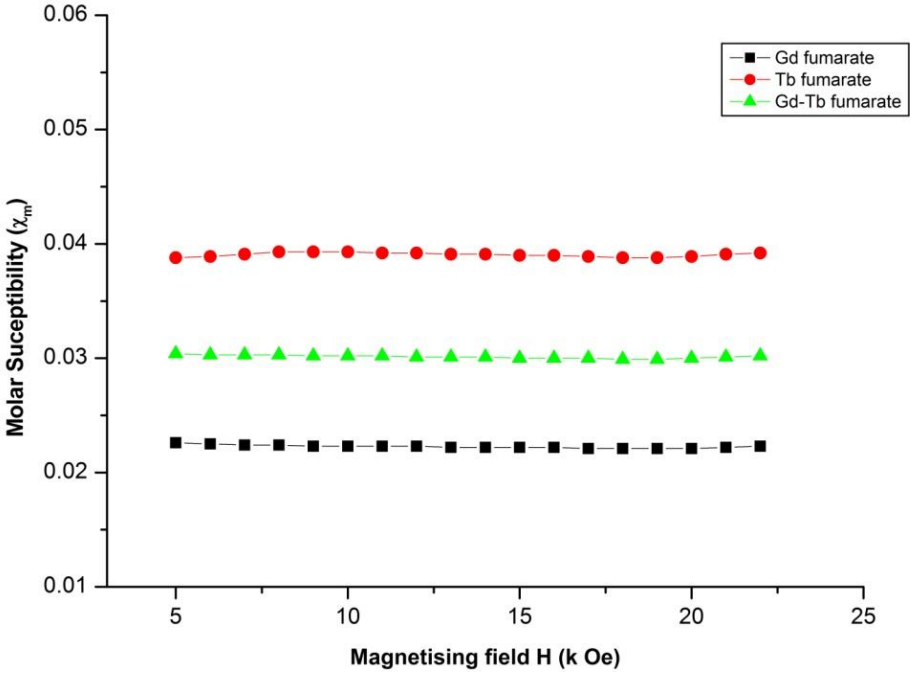

Figure 8.1: Graph between molar susceptibility and magnetizing field of GFH, TFH and GTFH single crystals.

Conclusions

It may be concluded that the experimental values of magnetic moments for $Gd_2(C_4H_2O_4).7H_2O$, $Tb_2(C_4H_2O_4).7H_2O$ and $GdTb(C_4H_2O_4).7H_2O$ are in good agreement with the theoretical magnetic moments of the tripositive rare-earth ions. Moreover, the magnetic moment of mixed fumarate complex is equal to the average of the magnetic moments of single component rare-earth fumarate crystals. As such, it substantiates the EDAX analysis that the mixed fumarate complex consists of Gd and Tb coordinating the ligand in the ratio of 1:1.

CHAPTER-9

Summary and Future Scope

9.1 Summary

In the present work, the growth of terbium fumarate, gadolinium fumarate and mixed Gd-Tb fumarate heptahydrate single crystals was accomplished by an inexpensive silica gel diffusion technique. The effect of various growth parameters, such as gel concentration, gel age, gel pH, upper reactant concentration, lower reactant concentration and gel temperature on the nucleation rate of these crystals was studied. The results found thereof, were in good conformity with the classical nucleation theory. The optimized gel pH for the growth of well faceted crystals was found to be of the range $5.0 \leq pH < 6.0$.

The qualitative and quantitative elemental analysis, employing EDAX and CHN techniques, confirm the presence of heavier and lighter elements of the compounds. From CHN analyses, a molecular formula for terbium fumarate, gadolinium fumarate and mixed gadolinium-terbium fumarate could be established respectively as $Tb_2(C_4O_4H_2)_3.7H_2O$, $Gd_2(C_4O_4H_2)_3.7H_2O$ and $GdTb(C_4O_4H_2)_3.7H_2O$. The crystallinity of these materials was confirmed by their X-ray diffraction analyses. The presence of all the functional groups associated with the fumarate ligand was confirmed by the FT-IR spectrum. Scanning electron microscopy suggested the monoclinic morphology of the crystals with two- dimensional spreading and piling up of layers. From single crystal XRD analysis, the crystal structure of terbium fumarate heptahydrate was found to be monoclinic bearing a space group $P2_1/n$, with the cell parameters: a=9.4495 Å, b=14.6561 Å, c=14.7272 Å and $\alpha = \gamma = 90^o$ and $\beta = 91.318^o$. The cell parameters of gadolinium fumarate heptahydrate and mixed GdTb fumarate heptahydrate were found by using Crysfire software programme. For gadolinium

fumarate heptahydrate, a= 9.491 Å, b= 14.772Å, c= 14.813Å and α= γ= 90^o and β= 91.26^o and for mixed GdTb fumarate heptahydrate, a = 9.2705 Å , b = 14.3701 Å, c = 14.3602 Å and α = 90 ^{o}, β = 91.41^o and γ = 90^o. The cell parameters of gadolinium fumarate and mixed gadolinium-terbium fumarate heptahydrates were seen to be nearly equal to the cell parameters of terbium fumarate heptahydrate as obtained from its single crystal X-ray diffraction. As such, the three compounds grown in the present work are isomorphous to each other. A phase matching search was also followed, which showed that samarium fumarate heptahydrate crystals are isomorphous to terbium fumarate heptahydrate and hence isomorphous to gadolinium fumarate heptahydrate and mixed GdTb heptahydrate. The molecular formula for each of the compounds was substantiated by their thermogravimetric analyses. The thermal stability of terbium fumarate and gadolinium fumarate crystals was found to be 110 ^{o}C and that of the mixed GdTb fumarate crystals was 120 ^{o}C. DTA/DTG peaks for each of the compounds corresponding to nearly the same temperature suggest an isomorphic phase transition. The dehydration of coordinated water molecules of these compounds correspond to the DTA peaks respectively at 132.63 ^{o}C, 133.63 ^{o}C and 149 ^{o}C for terbium fumarate, gadolinium fumarate and mixed terbium-gadolinium fumarate heptahydrates. The pure rare-earth fumarate crystals decompose in two steps of thermal decomposition with the formation of their corresponding oxides, while as the mixed rare-earth fumarate decomposes in three steps till the formation of its oxide. The decomposition peaks of the dehydrated compounds correspond to 481.5 ^{o}C, 484.59 ^{o}C and 493.45 ^{o}C respectively for terbium fumarate, gadolinium fumarate and mixed gadolinium-terbium fumarate. This suggests that the molecular structure of these pure and mixed compounds could be same with the exemption that the mixed compound could be a bit harder than the pure fumarate crystals.

The non-isothermal kinetic parameters have been worked out for the two stages of thermal decomposition of terbium fumarate, gadolinium fumarate and mixed GdTb fumarate crystals by using the integral method by applying the Coats – Redfern approximation. The reactions corresponding to stages 1 and 2 in each of the three different compounds are governed by 2D nucleation and growth model A_2, as is also evidenced by Fig 4.8.(c) of SEM micrograph of chapter 4. The activation energy for stage 1 and stage 2 is 51.064 kJ/mol and 50.25 kJ/mol respectively for terbium

fumarate, 45.61 kJ/mol and 45.36 kJ/mol respectively for gadolinium fumarate and 48.63 kJ/mol and 44.93 kJ/mol respectively for mixed GdTb fumarate crystals.

The dielectric constant (ε) for each of the grown compounds slowly increases with temperature and attains a maximum value and then decreases with further increase in temperature. The dielectric anomaly for terbium fumarate heptahydrate was found to be at 85 ^{o}C and that of the gadolinium fumarate and mixed gadolinium-terbium fumarate was found to be at 95 ^{o}C. Since all the three rare-earth based fumarate compounds belong to centro-symmetric space group, therefore, the anomalous behaviour of dielectric constant found in the title compounds may be due to their dehydration of lattice and coordinated water molecules and not due to the ferroelectric phase transition. The conduction behaviour of the materials showed that with increase in frequency of the applied field the conductivity increases, thus suggesting a hopping conduction due to protons transferring through hydrogen bonds. Therefore, these materials behave as protonic conductors. Though, the magnitude of ac conductivity for gadolinium fumarate compound was low but the conductivity of terbium fumarate and mixed Gd-Tb fumarate single crystals increased from 10^{-4} to 10^{-3} ohm^{-1} m^{-1}, when the frequency was increased from 100 kHz to 3 MHz.

From the UV-Vis spectra it has been inferred that both terbium fumarate and mixed GdTb fumarate heptahydrate crystals have sufficient transmission nearly in the entire visible region and IR region. The high absorption coefficient at lower wavelength and the transparency in the visible part of the spectrum suggests their suitability for laser and luminescent materials. The study of luminescent properties of terbium fumarate revealed that the compound exhibiting strong luminescent emissions of Tb^{3+} ions may come from the sensitizing effect of the fumarate ligand. Mean while, in case of mixed rare-earth compound, the intensity was found to get enhanced by Gd (III) which may be due to the intra-molecular energy transfer between inert rare-earth ions and active rare-earth ions.

The magnetic susceptibility measurements show that the experimental values of magnetic moments for pure and mixed rare-earth fumarates are in good agreement with the theoretical magnetic moments of the tripositive rare-earth ions. The magnetic moment of Tb^{3+} and Gd^{3+} ions in the grown crystals is well-described from the coupling of spin and orbital angular momenta ~ Russell-Saunders coupling to give J

vector. Moreover, the magnetic moment of mixed fumarate complex was found to be equal to the average of the magnetic moments of single component rare-earth fumarate crystals (terbium fumarate and gadolinium fumarate), thus suggesting that in mixed gadolinium-terbium fumarate compound both Gd and Tb are coordinating the fumarate ligands in the ratio of 1:1. This is in conformity with the EDAX analysis carried on mixed fumarate complex.

Almost whole of the work carried out in the present thesis has been published in different international journals of well repute.

9.2 Future scope of the work

The ultimate aim of the present day technology is to work out an appropriate method for getting good quality crystals by probing into the field of crystal growth. In the present work attempts have been successfully made to grow pure and mixed rare-earth fumarate crystals by a simple silica gel diffusion technique. These crystals have shown dielectric, ac conductivity, thermal, optical and magnetic properties as already discussed in different chapters of the thesis. An extensive research has been performed in the growth of rare-earth fumarate single crystals. Since, the size of as-grown single crystals was small, therefore, their dielectric study was performed on pellets rather than on the single crystals. The density of pellet sample is oftenly less than the density of single crystals, therefore, the porosity in the pellets could play its role for decreasing the dielectric constant of the sample. It is, therefore, suggested that there is a future scope of the work to increase the size of the single crystals so that dielectric measurements could be more accurately done directly on the single crystals rather than on the pellets. This may increase the dielectric constant of the compounds, which substantiately may increase their ac conductivity and may lead their use for technological importance. There is also the possibility of long range magnetic order in mixed rare-earth fumarate crystals at low temperature. Since, the title compounds grown in the present work belong to centrosummetric space group, which are non-ferroelectrics and in case of solids most of the properties are structure dependent. Therefore, for future research in growing substituted rare-earth fumarate crystals rather than the mixed ones, the new compounds could be non-centrosymmetric and may also exhibit ferroelectric and NLO properties.

Bibliography

[1] T. J. Kane and R. L. Byer, Optics Letters, **10**, 65 (1985).

[2] C. R. Ronda, T. Jstel and J. Nikol, J. Alloys Compd. **275**, 669(1998).

[3] H.J. Scheel, Historical introduction in *Handbook of Crystal Growth*, Vol. 1a, ed. by D.T.J. Hurle ,Elsevier, Amsterdam (1993) pp. 1–41.

[4] D. Elwell and H.J. Scheel, *Crystal Growth from High Temperature Solution,* Academic, London (1975).

[5] J. L. C. Rowsell and O. M. Yaghi, *Micropor. Mesopor. Mat.*, **73**, 3 (2004).

[6] B. Moulton and M. J. Zaworotko, *Chem. Rev.* **101**, 1629 (2001).

[7] G. B. Gardner, D. Venkataraman, J. S. Moore and S. Lee, *Nature* **374**, 792 (1995).

[8] O.M. Yaghi, G.M. Li and H.L. Li, *Nature* **378**, 703 (1995).

[9] S. Subramanian and M. J. Zaworotko, *Angew. Chem., Int. Ed. Engl* **34**, 2127 (1995).

[10] T.C.Shehee, R.E.Sykora, K.M.Ok, P.S.Halasyamani and T.E. Albrecht-Schmitt, J.Inorg .chem **42,** 457(2003).

[11] D.S.Chemla, J.Zyss, Nonlinear Optical Properties of Organic Molecules and Crystals, Academic Press, New York, (1987).

[12] H.B.Cui, B.Zhou, L.S.Long, Y.Okano, H. Kobayashi and A. Angew. Chem., Int.Ed. **47**, 3376 (2008).

[13] B.Zhou, A.Kobayashi, H.B.Cui, L.S.Long, H.Fujimori and H.Kobayashi, J. Am.Chem.Soc. **133**, 5736 (2011).

[14] G.C.Xu, W.Zhang, X.M.Ma, Y.H.Chen, L.Zhang, H.L.Cai, Z.M.Wang, R.G.Xiong and S.Gao,J. Am. Chem. Soc.**133**, 14948 (2011).

[15] P.Jain, V.Ramachandran, R.J.Clark, H.D.Zhou, B.H.Toby, N.S.Dalal, H.W.Krotoand and A.K.Cheetham,J. Am. Chem. Soc. **131**, 13625 (2009).

[16] K.D. Kreuer, S.J. Paddison, E. Spohr and M. Schuster, Chem. Rev. **104**, 4637 *(*2004).

[17] B.C. Wood and N. Marzari, Phys. Rev. B **76**, 134301 *(*2007).

[18] K. Liua, G. Jia, Y. Zheng, Y. Song, M. Yang, Y. Huang, L. Zhang and H. You, Inorg.Chem.Commun. **121**, 1246 (2009).

[19] B. Ji, D. Deng, X. He, B. Liu, S. Miao, N. Ma and W. Wang, Inorg.Chem. **51**, 2170 (2012).

[20] S. Jana& R. K. Mukherjee, *Solid State Communications* **116**, 581 (2000).

[21] M. Gasginer, *J. Mater. Sci* **26**,1989 (1991).

[22] M. A. Ahmed, E. Ateia, S. I. El-Dek, and F.M Salem, J. Mater. Sci. **38**, 1087 (2003).

[23] J.C.G. Bunzli, Lanthanide Probes in Life, Chemical and Earth Sciences: Theory and Practice; Elsevier: Amsterdam (1989).

[24] A. J. Kenyon, Prog. Quantum Electron. **26**, 225 (2002).

[25] G. Blasse and B. C. Grabmaier, Luminescent Materials; Spinger-Verlag: Berlin, (1994).

[26] G. Blasse, Prog. Solid State Chem. **18**, 79 (1998).

[27] M. Elbanowski and B. Makowsaka, J. Photochem. Photobiol. A **99**, 85 (1996).

[28] J. B. Yu, L. Zhou, H. J. Zhang, et al. Inorgnic Chemistry **44**, 1611 (2005).

[29] Z. R. Hong, W. L. Li, D. X. Zhao, et al. Synthetic Metals **104**, 165 (1999).

[30] Z. Kin, H. Kajii, Y. Hasegawa, et al. Thin Solid Films **516**, 2735 (2008).

[31] Z. R. Hong, W. L. Li, D. X. Zhao, et al. **111**, 43 (2000).

[32] R. G. Sun, Y. Z. Wang, B. Q. Zheng, et al. J. Appl. Phy. **87**, 7589 (2000).

[33] Y. Kawamura, Y. Wada and Y. Hasegawa, et al. Appl. Phy. Lett. **74**, 3245 (1999).

[34] Z. R. Hong, C. J. Liang and R. G. Li, et al. Thin Solid Films **391**, 122 (2001).

[35] N. Sabbatini, M. Guardigli & J. M. Lehn, Coord. Chem. Rev. **123**, 201(1993).

[36] M. Elhabiri, R. Scopelliti, J. C. G. Bunzli & C. Piguet, J. Am. Chem. Soc. **121**, 10747 (1999).

[37] D. Kustaryono, N. Kerbellec, G. Calvez, S. Freslon, C. Daiguebonne and O. Guillou, cryst. growth and design. **10**, 780 (2010).

[38] J. C. G. Bunzli, S. Comby, A. S. Chauvin and C. D. B. Vandevyver, J. Rare Earths **25**, 257 (2007).

[39] Y. Hasegawa, Y. Wada and S. Yanagida, J. Photochemistry and Photobiology C: Photochemis. Rev. **5**, 183 (2004).

[40] J. Kido and Y. Okamoto, Chem. Rev. **102**, 2357 (2002).

[41] S. Faulkner, S.J.A. Pope and B.P. Burton-Pye, Appl. Spectroscopy Rev. **40**, 1 (2005).

[42] T. Gunnlaugsson and F. Stomeo, Organic and Biomolecular Chemistry **5**, 1999 (2007).

[43] H. Tsukube, S. Shinoda and H. Tamiaki, Coord. Chem. Rev. **226**, 227 (2002).

[44] M. P. Rosynek, *Catalysis Reviews: Science & Engineering* **16**, 111(1977).

[45] R. Bazzi, M. A. Flores- Gonzalez, C. Louis, K. Lebbou, C. Dujardin, A. Brenier, W. Zhang, O. Tillement, E. Bernstein, P.Pessiat, J. Luminescence **102**, 445(2003).

[46] J. Blanusa, N . Jovic, T.Dzomic, B. Antic, A. Kremenovic, M. Mitric & V. Spasojevic, *Opt. Mater*. **30**,1153 (2008).

[47] S. Sato, R. Takahashi, M. Kobune, H. Gotoh,*Applied Catalysis A: General* **356,** 57 (2009).

[48] M. S'roda, J. Therm. Anal. Calorim. **97**, 239 (2009).

[49] P. Mele, C. Artini, R. Masini, G. A. Costa, A. Hu, N. Chikumoto and M. Murakami, Physica C. **391,** 49 (2003).

[50] C. Peng and Z. Zhang, Ceram. Int. **33**, 1133 (2007).

[51] D. Y. Chung and E. H. Lee, J. Alloy. Compd. **374**, 69 (2004).

[52] T.C. Tseng, C. Lin, X. Shi, S.L. Tait, X. Liu, U. Starke, N. Lin, R. Zhang, C. Mint, M.A. VanHore, J.I. Cerda and K. Kern, Phys.Rev.B **80**, 155458 (2009).

[53] W. Zhou and T. Yildirim, Phys.Rev.B **74**, 180301(R) (2006).

[54] P.C. Rusu, G.Gianluca, C. Weijtens, R. Coehoorn and G. Brocks, Phys. Rev. B **81**, 125403 (2010).

[55] S.H. Liang, D.P.Liu, L.L.Tao, X.F.Han and H.Guo, Phys.Rev.B **86**, 224419 (2012).

[56] P. Capena, Y.J Chabal and T. Thonhauser, Phy. Rev. B **87**, 094407 (2013).

[57] M. Pratzer, H. J. Elmers, M. Bode, O. Pietzsch, A. Kubetzka, and R. Wiesendanger, Phys. Rev. Lett. **87**, 127201 (2001).

[58] R. Cl´erac, H. Miyasaka, M. Yamashita, and C. Coulon, J. Am. Chem. Soc. **124**, 12837 (2002).

[59] P. Gambardella, A. Dallmeyer, K. Maiti, M. C. Malagoli, W. Eberhardt, K. Kern, and C. Carbone, Nature **416**, 301 (2002).

[60] C.N.R. Rao, S. Natarajan and R. Vaidhyanathan, Angew. Chem. Int. Ed. **43,**1466 (2004).

[61] N. C. Jeong , B. Samanta , C. Y. Lee , O. K. Farha and J. T. Hupp, J. Am. Chem. Soc. **134 (1),** 51 (2012).

[62] T. Yamada, M, Sadakiyo and H Kitagawa, J. Am. Chem. Soc. **131(9)**, 3144 **(**2009).

[63] V.Aleksandrovic and J.Djonlagic, J Serb Chem Soc. **66**, 139 (2001).

[64] M.Ohnishi, T.Uno, M.Kubo and T.Itoh, J Polym Sci A Polym Chem. **47**, 420 (2009).

[65] W.H.Zhu, Z.M.Wang and S.Gao, InorgChem.**46**, 1337 (2007).

[66] W.H .Zhu, Z.M.Wang and S.Gao, Dalton Trans. **6**, 765 (2006).

[67] S.C.Manna,E.Zangrando, J.Ribas and N.R.Chaudhuri, Polyhedron **25**, 1779 (2006).

[68] Sonja, Skuban, T. Dzomic and A.Kapor, AIP conference **899**, 652 (2007).

[69] C. Mathoniere , C. J. Nuttall , S. G. Carling and P. Day , Inorg. Chem. **35 (5),** 1201 (1996).

[70] B. Gil-Hernandez , S. Savvin , G. Makhloufi , P. Nunez , C. Janiak , and J. Sanchiz , Inorg. Chem. **54 (4)**, 1597 (2015).

[71] T. Endo , K. Kubo, M. Yoshitake , S. Noro , N. Hoshino , T. Akutagawa , and T. Nakamura, *Cryst. Growth Des.* DOI**:** 10.1021/cg501560z, (2015).

[72] K. M. Wong, C. Hui, K. Yu and V.W. Yam **229**,123 (2002).

[73] S.I.Weissman, J.Chem.Phys.**10**, 214 (1942).

[74] GA. Crosby, Mol. Cryst. **1**, 37 (1966).

[75] W. De, W. Horrocks, Jr. and M. Albin, Prog. Inorg. Chem. **31**, 9 (1984).

[76] G.F. Buono-Core, H. Li and B. Marciniak, Coord. Chem.Rev. **99**, 55 (1990).

[77] R.E. Whan,G.A.Crosby, J.Mol.Spectrosc. **8,** 315 (1962).

[78] M.E.Torres,T. Lo'pez, J. Peraza, J. Stockel, A.C.Yanes, C. Gonz´alez-silgo,C. Ruiz-perez and P.A. Lorenzo-luis, J. Appl. Phys. **84**, 5729 (1998).

[79] G.C. Xu, X.M. Ma, L. Zhang, Z.M. wang and S. gao, J.Am.Chem.Soc. **132**, 9588 (2010).

[80] H. Cui, B. Zhou, L.S. Long, Y.Okano, H.Kobayashi and A.Kobayashi, Angew.Chem. Int.Ed. **47**,3376 (2008)

[81] A H Scott, D L: Curtis, A L L Auritzenandj, D. J. Res. Nalt. Bur. Stand, Soc A. **66**, 269 (1962)

[82] D. Gulcking and H.J .Suss ;Z Angew Phys (Germany) **28,** 238 (1970).

[83] A. Tanaka, A. Uemura and Y. Ishida , J. Polymer Sci. **A8,** 1585 (1970).

[84] C. R. Ashcraft and R. H. Boya, J.Poly. Phy. Ed.(USA) **14,** 2153 (1976).

[85] S.K. Srivastave and A.P. Srivastave, Indian J. Pure. Appl. Phys. **19**, 953 (1981).

[86] Y. K. Kulshreshtha and A. P. Srivartave, Thin Solid Films **71**, 41 (1980).

[87] I. M. Stalwart, H. C. Sinha and A. P. Srivastave, Mat. Sci. Lett. **4**, 448 (1985).

[88] R. Sathyamoorthy, S. K. Narayandass, C. Balasubramanian and D. Magalaraj, *Proc. Solid State Phys. Symp*. **33C,** 409 (1991).

[89] Byung-Moon Jin, A. S. Bhalla, Byung-Chun Choi and Jung-Nam Kim, *Phys. Stat. Sol*. **140,** 239 (1993).

[90] S. C. Raghvendra, R. L. Raibagkar, A. B. kulkarni, *Bull. Mater. Sci.* **25,** 37 (2002).

[91] C.R. Mariappan, G. Govindaraj, S.V. Rathan and G.V. Prakash, Mater. Sci. Engng B**123,** 63 (2005).

[92] A.K. Jonscher, Nature **267**, 673 (1977).

[93] T.Yamada, S. Morikawa and H. Kitagawa, Bull. Chem. Soc. Jpn.**83**, 42 (2010).

[94] J. Bruinink, J. Appl. Electrochem. **2**, 239 (1972).

[95] Energy Transfer with Special Reference to Biological Systems, Discuss. Faraday SOC. **No. 27**, 134 (1959).

[96] M. Eigen, Discuss. Faraday Soc. **No. 39**, 7 (1965).

[97] Electrical Conduction in Organic Solids, Discuss. Faraday SOC., **51** (1971): (a) D. D. Eley, p 116.

[98] D.K. Deb Ray, E. Ryba and L.N. Muley, J. Appl Phys. **38**, 3459 (1967).

[99] G. Bush, J. Appl. Phys., **3** (1967) 1386.

[100] W.M. Mc Call, K.S.V.L.Narasimhan, and R.A. Butera, J. Appl. Phys.. **44**, 4224 (1973).

[101] N. Nelson, J. Appl. Phys. **44**, 4327 (1973).

[102] H. E. BucWey, Crystal Growth, John Wiley and Sons, Inc. NY (1951).

[103] R. A. Laudire, The Growth of Single Crystals, kentice Hall, Inc., NJ (1970).

[104] B. R. Pamplin, (Ed.), Crystal Growth, Pergamen Press, Oxford (1975).

[105] C. S Barrat, and T. B Massalski, Structure of Metals, McGraw-Hills, New York, 3rd edn., (1966).

[106] D.T.J. Hurle (Ed.): Handbook of Crystal Growth, North Holland, Am-sterdam (1994).

[107] A. Verneuil and C. R. Paris, **135**, 791(1902).

[108] J. Czochralski, Z. Phys. Chem., **92**, 219 (1971).

[109] H. K. Henisch, Crystal Growth in Gels, The Pennsylvania State Univ. Press, University Park (1973).

[110] H. K. Henisch, Crystals in Gels and Liesegang Rings, Cambridge Univ. Press, Cambridge (1988).

[111] S. K. Arora, A review, Prog. Cryst.Growth Charact.**4**, 345 (1981).

[112] A. R. Patel and A.VenkateswaraRao, Bull. Mater.Sci. **4**, 527 (1982).

[113] F.Lefaucheux and M.C. Robert, Handbook of Crystal Growth, ed. by D. T. J. Hurle, Elsevier Science, Amsterdam (1994).

[114] W. A. Tiller; *Acta. Met*., **5,** 565 (1957).

[115] J. P. van der Eerden; " *Fundamentals of Crystal Growth*", World Scientific Publishing, (1993).

[116] B. Chalmers; "Principles of Solidification", John Wiley, New York (1964).

[117] N. Bardsley, D.T.J.Hurle and J. B. Mullin; Crystal Growth: A Tutorial Approch", North- Holland Series in Crystal Growth, Vol-2, Amstredam (1979).

[118] A.V. Shubnikov, A.A. Cherhov, N.N. Sheftal; "Growth of Crystals", Kluwar Academic, (1979).

[119] A. Majchrowski; *"*Single Crystal Growth, Characterization and Applications*",* Ed. J. Zielinski, SPIE-International Society for Optical Engineering (1999).

[120] K. Byrappa and T. Ohachi, Eds.; "Crystal Growth Technology*: Characterization and Applications",* Noyes Publication, (2001).

[121] K. Nishioka, J. Harda, A. Sasaki, H. Teiki; "Advaces in Understanding of Crystal Growth Mechanism", Elsevier Science, (1997).

[122] D.T. J. Hurle; Handbook of Crystal Growth, Vols: 1 to 3, Elsevier Science, 1999 - 2000.

[123] A. Holden and P. S. Morison; "Crystal and Crystals Growing*",* Amazon.

[124] L. W. Fisher and F. L. Simons; *Amer. Mineralogist*, **11,** 124 (1926).

[125] R. E. Liesegang; Z. Phys. Chem. **88,** 1 (1914).

[126] S. C. Bradford; "Colloidal Chemistry", Ed. J. Alexander, (1926).

[127] H. N. Holmes; " Colloidal Chemistry", Ed. J. Alexander, (1926).

[128] W. Ostwald; Z. Phys. Chem. **27,** 365 (1897).

[129] L. Rayleigh; Phil. Mag. **38,** 738 (1919).

[130] E. Hatschek; Kolloid Z. **8,** 709 (1911).

[131] H. K. Henisch, J. Dennis and J. I. Hanoka, *J. Phys. Chem. Solids*, **26,** 493 (1965).

[132] H. K. Henisch; "Crystal Growth in Gels," Dover Publication, New York (1996).

[133] S. N. Kalkura, S. Devnarayanan, *J. Cryst. Growth*, **110**, 265 (1991).

[134] K. Ambujan; *Ph. D. thesis,* University of Madras (2005).

[135] H.K Henisch. Crystal growth in gels. University Park: Pennsylvania State University Press (1970).

[136] X.S Shajan and C. Mahadevan Bull Mater Sci. **27(4)**, 327 (2004).

[137] I. Quasim, A. Firdous, B. Want, S.K Khosa and P.N Kotru. J. Cryst Growth. **310**, 5357 (2008).

[138] A. Firdous , I. Quasim, M.M Ahmad and P.N Kotru. J Cryst Growth. **310**, 3855 (2009).

[139] B.S. Kumar, M.H.Rahim Kutty, M.R.Sudarsana Kumar and K.R. Babu, Bull Mater Sci. **30(4)**, 349 (2007).

[140] M Volmer, and A Weber, Z. Phys. Chem. **119**, 127 (1925).

[141] A. R Patel and A.V. Rao, *J. Cryst. Growth,* **47**, 213 (1979).

[142] T. Bandyopadhyay and De Asok, *Indian J. Earth Sci*., **4,** 95 (1977).

[143] J. W. McCauley and H. M. Gehrhardt; Report, AMMRC TR-70-13 (AD-710236),25 (1970).

[144] A. R. Patel and H. L. Bhatt, *J. Cryst. Growth,* **18,** 288 (1973).

[145] A. R. Patel and A. V. Rao; *J. Cryst. Growth.,* **43,** 351 (1978).

[146] A. E. Alexander and P. Johnson; "*Colloid Science",* Vol.2; Clarendon Press, Oxford (1949).

[147] S. K. Arora, Prog.*Cryst. Growth and Charact.,Pergmon Press Ltd., UK,* **4, (**1961)

[148] A. R. Patel and S.K Arora, *J. Cryst. Growth,* **18**, 199 (1973).

[149] S. NarayanaKalkura, V. K. Vaidyan, M. Kanakavel and P. Ramasamy, J. Cryst. Growth, **132**, 617 (1993).

[150] E. K. Girija, S. NarayanaKalkura, P. Ramasamy, J. Mater. Sci. Mater. Med. **6**, 617 (1995).

[151] S. NarayanaKalkura and S. Devanarayanan, J. Cryst. Growth, **94**, 810 (1989).

[152] M. T. George and V. K. Vaidyan; *Crystal Res. Technol*., **15,** 653 (1980).

[153] M. T. George and V. K. Vaidyan; *J. Crystal Growth*, **53,** 300 (1981).

[154] Z. Blank and W. Brenner, *Nature*, **222,** 79 (1969).

[155] M. Staniforth, J. Goldstein, P. Echlin, E. Lifschin, and D. Newbury, Scanning Electron Microscopy and X-Ray Microanalysis, Springer-Verlag, New York, 2003.

[156] W. L Bragg, *The Crystalline State ,Macmillan*, New York (1933).

[157] B . Wunderlich, *Thermal Analysis, Academic Press* (1990) .

[158] M. E. Brown, Introduction to Thermal Analysis: Techniques and Applications, 2nd edition, Springer-Verlag, New York (2001).

[159] N.B. Colthup, L.H. Daly, S.E. Wiberley, Introduction to Infrared and Raman Spectroscopy; 2nd Ed. Academic Press: New York, NY, USA (1975).

[160] Skoog, et al. Principles of Instrumental Analysis. 6th ed. Thomson Books, 349, (2007).

[161] P. J. Dean, Prog. Cryst. Growth Charact. **5**, 89 (1982).

[162] D.O.Smith, Rev.sci.instrum. **27**, 261 (1956).

[163] A. Kennelly, Impedance AIEE, 1893.

[164] M.R.Shedam and V.Rao, Bull.Mater.Sci. **16,** 309 (1993).

[165] S.L.Garud and K.B.Saraf, Bull. Mater.Sci.**31**, 639 (2008).

[166] A. Michaelides, V.Kiritsis, S.Skoulika and A.Aubry, Angew. Chem., Int. Ed.Engl.s **32**, 1495 (1993).

[167] M.Edgar, R.Mitchell,A. Slawin, M.Z. Lightfoot, and P.A. Wright, J. Chem. Eur. **23**, 5168 (2001).

[168] G.Zhang, G.Yang and J.S. Ma, Cryst Growth Des. **2**, 3 (2006).

[169] V.P.Sevost0yanov and L.M.Dvornikova, Izv Vyss Uchebn zaved khim khim tekhnol. **14**, 1771 (1971).

[170] V.P.Sevost0yanov and L.M.Dvornikova, Zhur Neorg Khim. **17**, 2884 (1972).

[171] P.S. Bassi, B.S. Randhawa, C.M. Khajuria and S.Kaur, J Therm Anal. **32**, 567 (1987).

[172] N.J. Carr and A.K.Galwey, J Chem Soc Faraday Trans. **84**, 1357 (1998).

[173] B. Want, F. Ahmad and P.N. Kotru, J. Mater.Sci.**42**, 9324 (2007).

[174] B.Want, F.Ahmad and P.N.Kotru, Mater. Sci. and Engg: **A.443**, 270 (2007).

[175] S.Gits , M.C.Robert and L.Lefaucheuse , *J. Cryst. Growth* **71,** 203(1985).

[176] G.S.Belikova and I.M.Belyaev, *Growth of crystals* (eds) A V Shubnikov and N N Sheftal (New York: Consultants Bureau) 3 p. 228 (1962)

[177] X.S. Shajan & C. Mahadevan, *Bull. Mater. Sci.* **27**, 327(2004).

[178] W. Chuan-De, Z. XiaPing, L. Can-Zong, Z. Hong-Hui and H. Jin-Shun, *Acta Crystallogr.* **E 58,** 228 (2002).

[179] S. Mondal, M. Mukherjee,S. Chakerborty and A. Mukherjee, *Cryst. Growth Des*.**6**, 940 (2006).

[180] E.Y.Ionashiro, F.J.Caires, A.B.Siqueira, L.S.Lima and C.T.Carvalho, J. Therm. Anal. Calorim. **108**, 1183 (2012).

[181] G.zhang, G.Yang and J.S.Ma, Cryst. Growth Des. **6**, 933 (2006).

[182] F.S.Alves,L.H.Bembo, F.J.Caires and E.Y.Ionashiro, J.Therm. Anal.Calorim., **113**, 739 (2013).

[183] M. Jianfang, W. Gecheng and N. Jiazuan, J. ActaPhysico-ChimicaSinica **06** (1993).

[184] A.Michaelides, S.Skoulika, E.G.Bakalbassis and J.Mrozinski, Cryst. Growth Des. **3**, 487 (2003).

[185] J.W. Mullin, Crystallization,Fourth Edition , Butter worth Heinemann, pp. 185 (2001).

[186] R.A. judge, R.S. Jacobs, T. Frazier, E.H. Snell, and M.L. Pusey, J.Biophys.**77**, 1585 (1999)

[187] A.F. Arimington and J.I. O'Connor, Mater. Res. Bull. **2**, 907 (1967).

[188] H.K. Henisch, Helv. Phys. Acta.**41**, 888 (1968).

[189] V. Alexeyev, Quantitative Analysis, MirPublishsers, Moscow, pp. 84 (1969).

[190] R.A. Laudise, The Growth of Single Crystals, Prentice-Hall, Inc.,Englewood Cliffs, NJ, pp. 272 (1970).

[191] B. Want, F. Ahmad and P.N. Kotru, J. Crystal Growth, **299**, 336 (2007).

[192] S.K. Arora, V. Patel, A. Kothari and B. Amin, Cryst. Growth Des., **4**, 343 (2004).

[193] M.V. Massa and K.D. Veress , Phy. Rev. Lett. **92**, 255509 (2004).

[194] S.Grazulis, A.Daskevic, A.Merkys, D.Chateigner, L.Lutterotti, M.Quiros, N. R.Serebryanaya, P. Moeck, R.T. Downs and A. Le Bail, Nucleic Acids Research, **40 D(1)**, 420 (2012).

[195] M. A. Neumann, J. Appl. Crystallogr., **36**, 356 (2003).

[196] R. Shirley (1999), The CRYSFIRE System for Automatic Powder Indexing: User's Manual, The Lattice Press, 41 Guildford Park Avenue,Guildford, Surrey GU2 5NL, England.

[197] I.Korah, C.Joseph, M.A.Ittayachen, J Minerals and Materials characterization and Engineering **9**, 1081 (2010).

[198] P. Müller, R. Herbst-Irmer, A.L.Spek, T.R. Schneider and M. Sawaya, Crystal Structure Refinement, Oxford University Press (2005).

[199] G.M. Sheldrick, SHELXS97 and SHELXL97, University of Go¨ ttingen, Germany,1997.

[200] M.D. Shah and B. Want, Current Appl. Phys. **15**, 64 (2015).

[201] H.M. Patil, D.K. Sawant and D.S. Bhavsar, J. Therm. Anal. Calorim., **107**, 1031 (2012).

[202] K. Nakamoto, Infra red and Raman Spectra of Inorganic and Coordination Compounds, Part B, 5th ed., Wiley, New York (1997) 60.

[203] J. Fujita, A.E. Martell, K. Nakamoto, J. Chem. Phys. **36,** 324 (1962).

[204] S. Pandita, R. Tickoo, K.K. Bamzai and P.N. Kotru, Mater. Sci.Engng.B **87**,122 (2001).

[205] K. Liua, G. Jia, Y. Zheng, Y. Song, M. Yang, Y. Huang, L. Zhang and H. You, Inorg. Chem. Commun, **121**,1246 (2009).

[206] S. Bhat, S.K. Khosa, P.N. Kotru and R.P. Tandon, Mater. Sci.Engng.B **30**, 7 (1995).

[207] S. Bhat, S.K. Khosa, P.N. Kotru and R.P. Tandon, Cryst. Res.Technol. **30**, 267 (1995).

[208] A.M. Farid and A.E. Bekheet, Vacuum **59**, 932 (2000).

[209] Q.Ye, X.S.Wang, H. Zhao and R.G.Xiong. Chem.Soc. Rev. **34**, 208 (2005).

[210] M.A. Omar, Elementary Solid State Physics, Pearson education, Inc; 381 & 410-412, (2007).

[211] P. Debye, "Polar Molecules." Dover, New York, (1929).

[212] A. R. Blythe, "Electrical Properties of Polymers." Cambridge Univ. Press, Cambridge, (1979).

[213] K. S. Cole and R. H. Cole, Chem. Phys. **10**, 341 (1941).

[214] D. W. Davidson and R. H. Cole, J. Chem. Phys. **19**, 1484 (1951).

[215] S. Havriliak and S. Negami, Polymer **8**, 161 (1967).

[216] A. K. Jonscher, "Dielectric Relaxation in Solids" Chelsea Dielectric Press, London, (1983).

[217] A.K. Jonscher, IEEE Trans Electron Insul. **27**, 407 (1992).

[218] A. Soukiassian, A. Tagantsev and N. Setter, Appl. Phys. Lett. **97,** 192903 (2010).

[219] M.M. Ahmad, S.A. Makhlouf and K.M.S. Khalil, J. Appl. Phys. **100**, 094323 (2006).

[220] J. Sjostrom, J. Mattsson, R. Bergman, E. Johansson, K. Josefsson and D. Svantesson, J. Swenson, Phys. Chem. Chem. Phys. **12**, 10452 (2010).

[221] B. Tareev, Physics of Dielectric Materials, Mir Publishers, Moscow, p. 155 (1975).

[222] A.K. Jonscher, Colloid Polym. Sci. **253**, 231 (1975).

[223] I.G. Austin and N.F. Mott, Adv. Phys. **18**, 41 (1969).

[224] P.Dutta, S.Biswas, M.Ghosh, S.K.De and S. Chatterjee. 2000. Synth. Met., **122**, 455 (2000).

[225] T.Higuchi, T.Tsukamoto, S.Yamaguchi, N.Sata, K.Hiramoto, M. Ishigame and S.Shin, J.Appl.Phys. **41**, 6440 (2002).

[226] H.Mahamoud, B.Louati, F.Hlel and K.Guidara, Bull. Mater.Sci. **34**, 1069 (2011).

[227] K. Pogorzelec-Glaser, J. Garbarczyk, C.Z. Pawlaczyk and E. Markiewicz, Mater. Sci.Poland **24**, 245 (2006).

[228] R.Vuilleumier, D.Borgis Nature chemistry, **(4) D**, 432 (2012).

[229] R.M.Hill and A.K. Jonscher J. Non- Cryst. Solids. **32**, 53 (1979).

[230] A.K. Jonscher, J. Mater. Sci. **16,** 2037 (1981).

[231] M.D. Ingram, J. Phys. Chem. Glas. **28**, 215 (1987).

[232] T.Meisel, J Thermal Anal; **29**, 1379 (1984).

[233] H.J.Borchardt and F.J.Daniels, J. Am. Chem. Soc. **79**,41(1957)

[234] A. Broido, J. Polym. Sci. **7A(2)**, 1761(1969).

[235] W.W.Wendlandt, Thermal Methods of Analysis, Interscience, New York (1964)

[236] R.C. Mackenzie , Differential Thermal Analysis , Academic Press London, Vol 2 chap 44 ,p 500 (1972).

[237] K.J.Laidler, J.Chem.Educ. **61,** 494(1984).

[238] A.K. Galwey, M.E.Brown, (999)Thermal Decomposition of Ionic Solids: Chemical Properties and Reactivities of Ionic Crystalline Phases, second ed., Elsevier,Amsterdam, 1, p.75.

[239] A.W. Coats, J.P. Redfern, Nature **201**, 68 (1964).

[240] A.W.Coats, J.P. Redfern, J. Polym. Sci. B: Polym. Lett. **3**, 917 (1965).

[241] J.Straszko, M. Olszak-Humienik and J.Mozejko J. Therm.Anal. **39,** 935 (2000).

[242] S.V.Eliseeva and J.C.G. Bunzli, Chem. Soc. Rev. **39,** 189 (2010).

[243] K. Binnemans, Chem. Rev. **109**, 4283 (2009).

[244] S.H.Hwang, C.N. Moorefield and G.R. Newkome, Chem. Soc.Rev. **37**, 2543 (2008).

[245] L.D.Carlos, R.A.S. Ferreira, V.de Zea Bermudez, B.Juli_an-L_opez and P. Escribano, Chem. Soc. Rev. **40**, 536 (2011).

[246] S.C.Lo and P.L. Burn, Chem. Rev. **107**, 1097 (2007).

[247] A.C.Grimsdale, K. Leok Chan, R.E. Martin, P.G. Jokisz and A.B. Holmes, Chem. Rev. **109**, 897 (2009).

[248] J.C.G.Veinot and T.J. Marks, Acc. Chem. Res. **38**, 632 (2005).

[249] P. A. Azeem, S. Balaji and R. R. Reddy, Spectrochim. Acta, Part **A 69**, 183 (2008) .

[250] Q. Su, H. Lang, C. Li, H. He, Y. Lu, J. Li and Y. Tao, J. Lumin. **122**, 927 (2007).

[251] H. Lang, H. Hanzawa and K.-I. Machida, Opt. Mater. **29**, 1789 (2007).

[252] N. Wada and K. Koima, J. Lumin. **126**, 53 (2007).

[253] P. Babu and C. K. Jayasankar, Opt. Mater. **15**, 65 (2000).

[254] C. Janiak, Dalton Trans. 2781 (2003).

[255] C.L.Cahill, D.T. de Lill and M.Frisch, CrystEngComm. **9**, 15 (2007).

[256] M.Suh, Y. Cheon and E. Lee, Coord. Chem. Rev. **252**, 1007 (2008).

[257] D. Maspoch, D. Ruiz-Molina and J. Veciana, Chem. Soc. Rev. **36**, 770 (2007).

[258] J.Rocha, L.D. Carlos, F.A.A. Paz and D. Ananias, Chem. Soc. Rev. **40**, 926 (2011).

[259] A.D. Buckingham and P.W. Fowler, J. Chem. Phys. **79**, 6426 (1983).

[260] B.V.Harbuzaru, A. Corma, F. Rey, P. Atienzar, J.L.Jord a, H.Garc_ia, D.Ananias, L.D.Carlos and Rocha, J. Angew. Chem., Int. Ed. **47**, 1080 (2008).

[261] B.Chen, Y. Yang, F. Zapata, G. Lin, G. Qian and E.B. Lobkovsky, Adv. Mater. **19**, 1693 (2007).

[262] H.-L Jiang, Y. Tatsu, Z.-H Lu and Q. Xu, J. Am. Chem. Soc.**132**, 5586 (2010).

[263] Y.Takashima, V.M. Mart_inez, S. Furukawa, M. Kondo, S. Shimomura, H. Uehara, M.Nakahama, K. Sugimoto and S. Kitagawa, Nat. Comms. **2**, 168 (2011).

[264] G.E.Buono-core, H.Li and B.Marciniak, Coord.Chem.Rev.**90**, 55 (1990).

[265] W.N.Wu, N.Tang and L.Yan, J.Fluoresc.**18**, 101 (2008).

[266] Q.M.Wang and B.Yan, J.Mater.Chem.**14**, 2450 (2004).

[267] A.Edward, T.Y.Chu, C.Claude, I.Sokolik, Y.Okamoto and R.Dorsinville, Synth.Met. **84**, 433 (1997).

[268] J.Kido, K.Nagai and Y.Okamoto, J.AlloysCompd.**192**, 30 (1993).

[269] J.B.Yu, L.Zhou, H.J.Zhang, Y.X.Zheng, H.R.Li, R.P.Deng, Z.P.Peng and Z.F.Li, Inorg. Chem. **44**, 1611 (2005).

[270] A.Kukhta, E.Kolesnik and I.Grabchev, J.Fluoresc.**16**, 375 (2006).

[271] C.F.Meares and T.G.Wensel, Acc.Chem.Res.**17**, 202 (1984).

[272] F.B.Wu and C.Zhang, Anal.Biochem. **311**, 57 (2002) .

[273]T.Nishioka, J.L.Yuan, Y.J.Yamamoto, K.Sumitomo, Z.Wang, K.Hashino, C.Hosoya, K.Ikawa, G.L.Wang and K.Matsumoto, Inorg.Chem.**45**, 4088 (2006).

[274] L.K.Scott and W.D.Horrocks, J.Inorg.Biochem.**46**, 193 (1992).

[275] B.L.An, M.L.Gong, M.X.Li, J.M.Zhang and Z.X.Cheng, J.Fluoresc.**15**, 613 (2005).

[276]Y.G.Lv, J.C.Zhang, W.L.Cao, J.C.Juan, F.J.Zhang and Z.Xu, J. Photochem. Photobiol. A **188**, 155 (2007).

[277] S.B.Meshkova, J.Fluoresc.**10**, 333 (2000).

[278] J.-M. Lehn, Angew. Chem. Int. Ed. Engl. **29**, 1304 (1990).

[279] G.A. Crosby, Mol. Cryst**. 1**, 37 (1966).

[280] W. De W. Horrocks, Jr. and M. Albin, Prog. Inorg. Chem.**31**, 9 (1984).

[281] G.F. Buono-Core, H. Li and B. Marciniak, Coord. Chem.Rev. **99**, 55 (1990).

[282] E.G.Moore, A.P.S. Samuel and K.N. Raymond, Acc. Chem. Res. **42**, 542 (2009).

[283] N.Sabbatini, M. Guardigli and J.-M. Lehn, Coord. Chem. Rev. **123**, 201 (1993).

[284] R. E.Whan and G. A. Crosby, J. Mol. Spectrosc. **8**, 315 (1962).

[285] G.R. Choppin and D.R. Peterman; Coord. Chem. Rev. **174**, 283 (1998).

[286] D.T.de Lill, A. de Bettencourt-Dias and C.L. Cahill, Inorg. Chem. **46**, 3960 (2007).

[287] K. Kong, H. Zhang, R. Ma , Y. Chen, H. Chu and Y. Zhao, J. of rare earths **31**, 32 (2013).

[288] L. Guo, X. Wen, Y. Xiao, J.Xiao and L. Xue; Journal of Luminescence **129,** 639 (2009).

[289] Y.X.Ci and Z.H. Lan, Analyst **113**, 1453 (1988).

[290] E. Talik, M. Klimczak, R. Troc, J.Kusz, W. Hofmeister and A. Damm, J. Alloys Compd. **427**, 30 (2007).

[291] Y.O. Tokaychuk, O.I. Bodak, Y.K. Gorelenko and K. Yvon, J. Alloys Compd. **415**, 8 (2006).

[292] S.P.Mc Alister, J. Phys. **14**, 2167 (1984).

[293] S.P.Mc Alister, J. Appl. Phys., **55**, 2343 (1984)

[294] D.K. Deb Ray, Earle Ryba and Muley and L. N., J. Appl Phys. **38**, 3459 (1967).

[295] G.J. Bush, J. Appl. Phys. **3**, 1386 (1967).

[296] W.M.Mc Call, K.S.V.L. Narasimhan, and R.A. Butera, J. Appl. Phys. **44**, 4224 (1973).

[297] N. Nelson, J. Appl. Phys. **44**, 4327 (1973).

[298] G.A. Bain, J.F. Berry, J. Chem. Educ; **85**, 532 (2008).

[299] Pascal, P. Ann. Chim. Phys. **19**, 5 (1910).